HEPARAN SULFATE IS REQUIRED FOR PROSTATE CANCER INITIATION AND PROGRESSION

by XUANYANG LI

(Under the Direction of Lianchun Wang)

ABSTRACT

Prostate cancer (PCa) is one of the most prevalent forms of malignancy and the second most common cause of cancer-related death in men. The failure in treatment of this disease is our inability to prevent and control PCa growth and metastasis. A better understanding of the mechanisms underlying PCa pathogenesis will greatly enhance our effort to cure this life-threatening disease. Heparan sulfate (HS) is a linear, sulfated polysaccharide, and expresses abundantly in prostate and PCa tissues. Intriguingly, the HS content and sulfation modifications appear to increase when the prostate becomes malignance, suggesting that HS may critically modulate PCa pathogenesis. In current study, we specifically ablated Ext1, the enzyme that initiates HS biosynthesis, in mouse prostate at late development stage. The Ext1 ablation does not affect prostate development and function; instead, it protects the mice from tumorigenesis and invasion in a spontaneous PCa mouse model. Tissue staining showed that the Ext1 deficiency attenuated PCa cell proliferation, increased apoptosis, and blocked PCa stem/progenitor cell differentiation and epithelial-mesenchymal transition. The Ext1 deficiency PCa tissues also showed significant attenuation of fibrinosis, inflammation, MMP-9 activity and hypoxia. In summary, our studies demonstrate that HS functions via multiple mechanisms to promote PCa tumorigenesis and invasion, and also reveal that targeting HS may represent a novel and effective approach to cure PCa.

INDEX WORDS: Prostate Cancer, Heparan Sulfate, Pten Conditional Knockout Mouse Model, Differentiation, Tumorigenesis, Invasion

HEPARAN SULFATE IS REQUIRED FOR PROSTATE CANCER INITIATION AND PROGRESSION

by

XUANYANG LI

MS, Fudan University, China, 2007

BS, Harbin Institute of Technology, China, 2004

A Dissertation Submitted to the Graduate Faculty of The University of Georgia in Partial Fulfillment of the Requirements for the Degree

DOCTOR OF PHILOSOPHY

ATHENS, GEORGIA

2013

HEPARAN SULFATE IS REQUIRED FOR PROSTATE CANCER INITIATION AND PROGRESSION

by

XUANYANG LI

Major Professor:	Lianchun Wang
Committee:	Michael Tiemeyer
	Tamas Nagy
	Michael Pierce

Electronic Version Approved:

Maureen Grasso
Dean of the Graduate School
The University of Georgia
May 2013

DEDICATION

This work is dedicated to my parents, Wenqing and Zhufen, who always supported and encouraged my choice. I have never been able to complete the degree without your love and support.

Feng, Peng and Hanhui, our friendship keeps me going and always reminds me where I’m belonging to.

Thanks to my friends Qiang and Chang, who used to enthusiastically discuss future life and career with me, your encouragements and supports make me stronger.

ACKNOWLEDGEMENTS

I wish to acknowledge and thank all those who have offered me their support and assistance to complete my Ph.D. degree. In particular, thanks to Dr. Lianchun Wang, my advisor and mentor, your continuous support, mentorship and enthusiasm have made tremendous contributions to my development as a scientist.

I would like to extend my heartfelt gratitude and appreciation to the past and present Wang lab members: Bing, Cathy, Eduard, Fang, Hong, Hongying, QinJun, Jyoti, Kiran, Siyuan, Sumit, Wenyuan, and Xiang.

I am truly grateful to my committee members, Dr. Tamas Nagy, Dr. Michael Pirece, and Dr. Michael Tiemeyer for great guidance and advice on my project and the thesis.

I would like to thank Dr. Huabei Guo, Zhifeng Zheng, Kelley Moremen, and Alison Nairn for useful discussions, collaboration, and equipment access.

To Yong, thank you for let me join your everyday workout. It has been a real privilege to live a healthy lifestyle in the last year of graduate student.

Finally, I want to thank my family and friends, whose emotional and mental support and trust provide with the encouragement and boost my motivation to achieve this goal.

TABLE OF CONTENTS

Page

LIST OF TABLES

Page

LIST OF FIGURES

Page

CHAPTER 1 LITERATURE REVIEW AND INTRODUCTION

Introduction to mouse prostate cancer tumorigenesis

Prostate cancer (PCa) continues to be a leading health problem for men. The American Cancer Society estimates that during 2013, about 238, 590 new cases of PCa will occur in the United States, and 29, 720 men will die of it. PCa is the most common cancer in men and the second leading cause of cancer death in men [1]. Early diagnosis by prostate specific antigen (PSA) tests and improved treatment methods such as surgical, radiation and Hormone deprivation therapy have significantly lessened the number of deaths. However, there is still no effective treatment for men with advanced disease.

Risk factors of prostate cancer

Most prostate tumors are adenocarcinomas with characteristics of pathology, progression, and invasive behavior similar to other epithelial cancers, such as colon and breast cancer. The following characteristics for PCa are relevant for investigation of the disease.

1. Correlation with aging

One of the characteristic features of PCa is its close association with aging. It is believed that aging is the most significant factor for PCa. For example, the chance of being diagnosed with PCa for each age group is 1 in 8,499 for men younger than 40 years, 1 in 38 for men aged 40 through 59 years, 1 in 15 for men aged 60 through 69 years, and 1 in 8 for men aged 70 years and older respectively. The overall lifetime risk of developing PCa is of 1 in 6 men. Besides, the

overall lifetime risk for precancerous lesions is significantly more prevalent, around 1 in 3 men, than the incidence of PCa [1]. Therefore, although the morphological changes, such as hyperplasia, associated with initiation of PCa are common and occur early in life, progression to invasive carcinoma is a less common event that associates with aging.

2. Race

PCa is common in North America and northwestern Europe, but less common in Asia and South America. African-American men have among the highest documented PCa incidence rates in the world. From 2004 to 2008, the average incidence rates each year are significantly higher in African-Americans (230.8 per 100,000 men) than among whites (142.8 per 100,000). Meanwhile, the rates for whites in turn, are higher than those for Hispanic (126.7 per 100,000) and Asians/ Pacific Islander (79.7 per 100,000). Also, form 2004 to 2008, the mortality rate for African-Americans was 2.4 times higher than for whites, 3.0 times higher than for Hispanics and 5.2 times higher than for Asians or Pacific Islanders [1].

3. Family History

Hereditary factors account for a small portion (~10%) of PCa and are associated with early onset disease [2-4]. Epidemiological studies point out that men with a positive family history are diagnosed at an earlier age on average 6 to 7 years earlier than those without [3]. These studies estimate that 5% to 10% of all PCa cases and around 40% of those occurring at less than 55 years old may have a genetic background that susceptible to PCa. Other than being diagnosed at an earlier age, hereditary PCa does not clinically differ from diseases of sporadic incidences [5]. The family clustering of PCa may result from the inheritance of a susceptibility gene. In recent studies, at least nine loci on chromosomes 3, 6, 7, 8, 10, 11, 17, 19 and X associated with PCa were identified, and candidate susceptibility genes are CPNE3, IL16, CDH13, MSMB, LMTK2 and KLK3 [6, 7].

4. Steroid hormones

Steroid hormone receptor signaling plays a vital role in all stages of prostate carcinogenesis. Men who underwent castration before puberty and those with congenital abnormalities in androgen metabolism do not develop PCa [8]. Besides, androgen ablations either by surgery or luteinizing hormone-releasing hormone (LH-RH) agonists are effective tactics in treating advanced PCa. However, plasma testosterone or dihydrotestosterone concentration has not been certainly associated with increased risk of PCa [9]. In addition, the transition to androgen independence a sign of advanced PCa, has been a focus of numerous investigations.

5. Inflammation

Chronic inflammation causes proliferative inflammatory atrophy (PIA) [10], which in 30% of cases progresses to prostatic intraepithelial neoplasia (PIN) the precursor of PCa [11]. PIA is believed to be a clear correlation between inflammation and PCa. Therefore, SNPs (single nucleotide polymorphisms) in genes involved in inflammation such as cyclooxygenase (COX-2) [12, 13], interleukin-1 (IL-1), IL-6, IL-8, and IL-10, tumor necrosis factor-α (TNF-α), and toll-like receptor-4 (TLR4) [12, 14-16] displayed an association with PCa risk.

6. Heterogeneity and multifocality

The heterogeneous and multifocal nature of PCa lesions makes the disease difficult for researchers to study. Histological inspection of PCa tissue typically reveals adjacent benign glands, preneoplastic (Prostate Intraepithelial Neoplasia, PIN) foci, and neoplastic foci of varying severity.

Multifocal tumor is one of the most typical features of human PCa. Individual neoplastic lesions within a given section of PCa tissue have been described as genetically distinct (nonclonal) [17, 18]. This observation suggests that different neoplastic foci may originate and develop independently, which has implication for the molecular mechanisms of PCa progression. The

heterogeneity and multifocality of PCa make it difficult to obtain sufficient quantities of homogeneous material. The recently developed microdissection, laser-capture microscopy and cell-sorting approaches that facilitate tissue sample analysis have partially overcome these difficulties [18-20].

The Architecture of the Normal Prostate Gland

1. Anatomy of the human and the mouse prostate

The prostate is a compound tubuloalveolar exocrine secretary gland which is part of the male reproductive system in both human and mouse [21]. In human, the prostate is a walnut-sized gland under the bladder and secrets a slightly acidic fluid which usually constitutes 20–30% of the volume of the semen. There are three distinctive regions in the human prostate, including the peripheral zone, the transition zone, and the central zone (Fig. 1.1A). Benign prostatic hyperplasia (BPH) is usually found in the transition zone, and prostate carcinoma occurs mainly in the peripheral zone. Malignant prostatic tumors are among the most common neoplasia in men. However, cancers are rarely observed in other ductal organs of the male urogenital system such as the seminal vesicles and bulbourethral glands [22].

By contrast to human, the mouse prostate consists of four lobes, anterior, dorsal, lateral, and ventral lobes which have branching morphology and secretory protein (Fig. 1.1B) [23, 24]. The corresponding mouse prostate lobes for human prostate zones are still unknown. Some studies claim the dorsolateral lobes of mouse prostate are most similar to the human peripheral zone. However, the prostate gland in the murine dorsal lobe is most histologically different from the human prostate as epithelial cells often fill up the lumen of prostate acini.

2. Prostatic epithelial cell types and their correlations to carcinogenesis

Both human and murine prostates consist of two tissue compartments: epithelial and stromal (Fig. 1.2). Stromal and epithelial compartments are separated by the basement membrane a thin sheet of fibers that underlies the epithelium containing various extracellular matrix proteins, such as laminin and collagen [25, 26]. The prostate epithelium contains two types of epithelial cells, the basal epithelial cells located on the on the basal cell layer along the basement membrane and the luminal epithelial cells located on the luminal layer. The luminal cell layer is consisting of secretory luminal epithelial cells. The basal cell layer contains the epithelial stem cells [19, 27].

At the molecular level, luminal cells are characterized by expression of many cell-type-specific protein markers, including high levels of AR, cytokeratins 8 and 18, CD57, and Nkx3.1, a prostate-specific homeodomain-containing transcription factor. By comparison, basal cells express cytokeratins 5 and 14, p63, CD44, and low levels of AR. Both human and mouse prostate epithelium contains a subpopulation of transiently amplifying/ intermediate cells, which initiate a differentiation program and are in the process of becoming luminal cells, express markers of both basal and luminal epithelial cells [28, 29]. These cells are enriched in proliferative inflammatory atrophy (PIA), express the c-MET receptor, low-level of AR, and represent the progenies of the basal cells [30].

Epithelial cells are not the only cell type in prostate epithelium; there also contains rare neuroendocrine cells, which produce and secrete various neuropeptides and growth factors necessary for growth of luminal cells [25, 31].

Development and Maintenance of the Prostate Gland

The mouse prostate starts to develop at embryonic day 17.5 in the late stage of embryogenesis. At the beginning of the development, the prostates are just epithelial buds in the urogenital sinus

[32]. Androgen promotes rapid extension and branching morphogenesis of these buds. The early prostate development continues afterbirth until reaching sexual maturity, around 8-9 weeks of age in mice. The developing prostate has many proliferative cells at the tips of growing prostatic ducts; however, in the adult prostate the epithelial cells are largely quiescent, only few cells undergoing either cell divisions or apoptosis [33].

Androgen receptor (AR) signaling is critical in both epithelial and stromal cell compartments. AR signaling plays a critical role in the mesenchyme during early prostate morphogenesis. In tissue recombination experiments, epithelial and mesenchymal cells from the embryonic urogenital sinus were mixed and transplanted under the capsule of a recipient adult nude mouse. Tissue recombination experiments with mesenchymal cells lacking the AR and wild-type epithelial cells failed to produce prostate tissue[34]. Tissue recombination experiment of wild-type mesenchymal cells and epithelial cells with AR deficiency resulted in prostate tissue formation suggesting that AR signaling is also crucial in epithelial cells. [35].

Luminal epithelial cells need androgen to survive in adult prostate. The androgen deprivation on castration causes the prostate gland regression and luminal epithelial cell death except a fraction of cells at the proximal region of the prostate [36, 37]. Implantation of testosterone to the abdomens of these castrated animals results in rapid regrowth of the prostate gland [23].

Morphological and cytological changes that take place during PCa initiation and progression

Technically, prostate carcinoma involves an accumulation of cancerous epithelial cells; however, nonepithelial cell types also play an significant role in PCa initiation and progression. In general, significant changes in both epithelial and stromal cell compartments take place during PCa

initiation and progression. The PCa is developed from normal prostatic tissue, and the cancer development also goes through different stages, which includes: 1.Normal prostate epithelial, 2. Prostate intraepithelial neoplasia, 3. Invasive adenocarcinoma. Androgen ablation therapy is effective in androgen-dependent cancer, the early stage of PCa, but these cancers eventually become androgen independent, and go on to progress and metastasize, 4. Metastasis. Metastatic PCa is usually developed from androgen-independent PCa [38]. Only a small portion of PCa does not relapse from androgen ablation therapy and become nonaggressive disease, which do not progress to metastasis (Fig.1.3).

1. Benign prostatic hyperplasia

Benign prostatic hyperplasia (BPH) is usually found in older men with a hyperplastic prostate epithelium [39]. In BPH, the number of luminal epithelial cells is increased, but the branch morphology and nuclear cytology remain normal. Prostate hyperplasia is developed in around 25% of men in their 50s and 90% in their 80s; however, only 10% of the cases becomes symptomatic and requires treatment [40]. Drugs that attenuating dihydrotestosterone synthesis block the prostate enlargement. Alpha adrenergic inhibitors which cause relaxation of smooth muscle are an alternative treatment [41].

2. Prostatic intraepithelial neoplasia

Prostatic intraepithelial neoplasia (PIN) is believed to be early precursor of invasive adenocarcinoma. Although PINs were initially divided into high- and low-grade lesions, low-grade PIN is not a precursor for carcinoma. PINs usually appear in the peripheral regions of the prostate gland where luminal epithelial cells accumulate with enlarged nuclei [42]. In PIN, basal cells are discontinuously presented along the basement membrane. Cancer cells from high-grade PIN lesions can invade and generate prostate carcinoma.

3. Prostate adenocarcinoma

Adenocarcinoma is the main type of tumors in the prostate. Histological analysis reveals that, the transition from PIN lesions to adenocarcinomas is characterized by several histological changes. Invasive PCa has several luminal characteristics: excessive branching morphogenesis, loss of the basal cell layer, and cytologic atypia with enlargement of nuclei and nucleoli (Fig. 1.3). PCa is diagnosed based on digital rectal examination, ultrasound, and increased levels of PSA in blood plasma. The prostate adenocarcinomas are multifocal and common in the peripheral zone of the human prostate gland.

4. Cellular origin of PCa

The origin of PCa initiating cells is still unknown; however, several lines of evidences suggest that particular genetic, epigenetic changes or aberrations in stem, progenitor, and differentiated cells could cause distinct biological and clinical phenotypes. There are two leading hypotheses for answering where the cellular origin of PCa is. One is that transformation of terminally differentiated luminal cells results in partial dedifferentiation and acquisition of immortality. An alternative hypothesis is that oncogenic transformation takes place in the prostate stem cells, which are believed to be residing among the basal cells (Fig. 1.4). The transformed stem cells then, through partial and incomplete differentiation of their daughters, would produce proliferative cells with a luminal phenotype, making up most of the tumor. For example, Patrawala et al found a hierarchical order in the tumorigenic potential of human prostate xenograft tumors. One subpopulation of prostate stem cells ($CD44^{+}/\alpha2\beta1^{+)}$ was enriched with tumor-initiating cells. So the tumorigenic potential of human xenograft tumors was dependent on their cellular origins. They found that the tumorigenic potential is higher in $CD44^{+}/\alpha2\beta1^{+/high}$ and $CD44^{+}/\alpha2\beta1^{-/low}$ prostate stem cells, but the tumorigenic potential is lower in $CD44^{-}/\alpha2\beta1^{+/high}$ cells and much lower in $CD44^{-}/\alpha2\beta1^{-/low}$ cells [43].

Mulholland et al isolated LSC ($Lin^{-}/Sca\text{-}1^{+}/CD49f^{high}$) stem/progenitor cells, by using $Sca\text{-}1^{+}/CD49f^{high}$ enrichment, as well as hematopoietic and endothelial lineage ($CD45^{+}CD31^{+}Ter119^{+}$) depletion and FACS cell sorting in the Pten null PCa prostate epithelial cells. They also performed in vivo regeneration assays using cells derived from in vitro prostate spheres cultures or from primary tumors. The results suggest that the LSC subpopulation (as opposed to the more differentiated luminal subpopulation) is composed of basal-like cells that recapitulate the pathologic process of primary Pten-/- prostate tumors and elicit a tumor-initiating activity [44]. By introducing various oncogenic stimuli (fibroblast growth factor activation, ERG1 expression, PI3K signaling) into distinct subpopulations of prostate basal stem cells, luminal cells, and stromal cells. Lawson et al demonstrated that prostate basal stem cells have a greater efficiency for cancer initiation than luminal cells and could produce luminal-like disease [45]. Oncogenic stem cell population was also found in other solid tumor types such as intestinal cancer. Oncogenic stimuli targeted to these cells results in accelerated and effective tumor formation, while tumor growth is much more attenuated when the same oncogenic stimuli are targeted to more differentiated cell population [46].

A recent study found another possible cellular origin of PCa other than the stem cells in the basal compartment. In this study, a subpopulation of stem cells called “CARNs” (castration-resistant Nkx3.1-expressing cells) was identified in the luminal compartment. CARN cells specific knockout of Pten in the mouse prostate, resulted in PCa development [47]. Because CARN cells are from luminal compartment, the CARN-cell origin of PCa is an attractive possibility that tumorigenic events can take place in luminal compartment and thus can better explain luminal phenotype of PCa cells. The CARN cells may be the intermediate cells progenitor cells which exist in the suprabasal and luminal layers of the prostate epithelium. Korsten et al also showed

in PSA-driven Pten null mouse model that the $Clu^{+}Tacstd2^{+}Sca\text{-}1^{+}$ luminal progenitor cells are candidate tumor initiating cells (Fig. 1.5) [48].

Further experiments to characterize the differentiation mechanism and defining lineage stem/progenitor cells in the prostate epithelium will be necessary for identification of the cellular origin of PCa.

Malignant transformation of prostatic stem/progenitor cells during prostate carcinogenesis and metastases

Genetic aberrations are gradually accumulated in prostatic stem/progenitor cells and their progenies during aging. These aberrations lead to mutations in tumor suppressor genes and these mutations usually inactivate tumor suppressor genes such as Pten and p53. Pten acts as a tumor suppressor gene through its phosphatase protein product, which is involved in the regulation of the cell cycle, and negatively regulate Akt/PKB signaling pathway. Conditional inactivation of Pten in prostate epithelium results in development of high-grade PCa which occasionally develops metastatic lesions in the distant organs [49]. The development of primary tumors is even more significant in mice with prostate-specific inactivating mutations of both Pten and p53 tumor-suppressor genes [50]. Those mutations sustained activate diverse oncogenic products which are frequently associated with PCa initiation and disease development.

The mutations in different tumor suppressor genes are also necessary to prevent the cellular senescence and apoptosis induced by particular tumor-initiating events, therefore, promoting the malignant transformed stem/progenitor cells in to tumorigenic PCa stem/progenitor cells[50, 51].

Invasive tumor cell phenotype is characterized by epithelial-mesenchymal transition (EMT), which indicates loss of cell adhesion, increased cell motility and repression of E-cadherin

expression. During EMT program, the tumorigenic PCa stem/progenitor cells obtain more malignant behaviors including increased cell motility and changes in their local tumor microenvironment and may cause malignant transformation into migrating PCa stem/progenitor cells. A recent study using the Pten-/-; p53-/- PCa mouse model, have derived lineage-specific cell lines with $CK8^+$ cells and a variable percentage of double positive $CK8^+/CK5^+$ cells. These cells can induce several of tumors including basal/squamous carcinomas, sarcomatoid carcinomas and adenocarcinomas when orthotopically injected to nude mice. These evidences suggest that mutation on tumor suppressor genes is necessary for tumor initiation from multipotential progenitors [50, 52, 53]. Recently, Mulholland et al using a Pten-null; K-ras activated model to accelerated PCa progression caused by Pten loss significantly, with EMT and macrometastasis. They also identified a novel stem/progenitor subpopulation, the Lin^- $EpCAM^{low}CD24^{low}$ cells, with mesenchymal characteristics isolated from the compound mutant prostates, which was metastatic upon orthotopic transplantation [54]. Therefore, the tumorigenic and migrating PCa stem/progenitor cells can undergo invasion and dissemination through the peripheral circulation, hence facilitate the progression to metastases at adjacent organs and distant sites including bones [52].

Recent studies have identified a subpopulation of highly tumorigenic PCa stem/progenitor cells expressing the stem cell-like markers in malignant prostatic adenocarcinomas and metastatic neoplasms and PCa cell lines. For example, Mulholland et al found that LSC^{high} (Lin^- $Sca1^+CD49f^{high}$) stem/progenitor cells have high sphere-forming activity and are both necessary and sufficient for initiating Pten-null PCa [44]. Korsten et al insist that a lineage progenitor subpopulation, the $Clu^+Tacstd2^+Sca\text{-}1^+$ luminal progenitor cells are capable to initiate hypoplasia

in a PSA-driven Pten null mouse model, thus, can be consider as candidate tumor initiating cells [48].

The up-regulation of stemness genes, such as Oct3/4, Sox2, Nanog and Bmi-1 which contribute to self-renewal, increases migratory abilities and enhances tumorigenic PCa stem/progenitor cells aggressive behavior and treatment resistance under tumor hypoxic conditions [55-58]. For instance, interleukin-6 (IL-6) secreted by PCa cells can activate the cancer-associated fibroblasts, which in turn may secrete MMPs to induce the EMT program, and elicit an increased expression of stem cell-like markers in PCa cells, formation of prostate spheres and self-renewal, thus promote their metastatic spread [59, 60].

Changes in prostate stroma during PCa initiation and progression

The stromal cell compartment of the prostate gland is comprised of many cell types, such as fibroblasts, smooth muscle cells, endothelial cells, and neuroendocrine cells. Smooth muscle cells represent the most abundant cell type in the normal stroma [61] and form a surrounding cell layer around glands. Scattered between the mesenchymal cells are endothelial cells, lymphatic cells, and inflammatory cells. Like other glandular organs, the prostate epithelial cells require support from the stromal cells and blood vessels for their survival. In response to androgen, stromal cells secrete andromedins, growth and survival factors such as fibroblast growth factor-7 (FGF-7), FGF-10 and insulin-like growth factor-I (IGF-1), to promote the proliferation, survival, and differentiation of epithelial cells. Androgen deprivation or inflammation elicit stromal fibrosis which in turn cause the atrophy of epithelial cells [62].

Although PCa is an epithelial neoplasm, cells in the prostate stroma also play a critical role in cancer initiation and progression. One of the most significant changes that take place early in PCa initiation is the formation of regions of proliferative inflammatory atrophy (PIA) in prostate epithelium, which are associated with inflammation events found in the stromal compartment [63]. Inflammation might influence the pathogenesis of cancers by causing cell and genome damage, activating cell proliferation to replace damaged cells, and inducing the secretion of cytokines that stimulate cell replication, angiogenesis and tissue repair [64]. PIA and high-grade PIN and carcinoma are often concurrent events in the same region of the prostate. Therefore, PIA might be a precursor to prostate neoplasia [10]. Lymphocytic inflammation and other types of infiltrating immune cells are crucial parts of the tumor microenvironment. For instance, tumor-infiltrating events activate the inflammation-responsive IkappaB kinase (IKK)-α in PCa cells, and IKK-α inhibits the metastasis suppressor MASPIN and thus stimulates tumor metastasis [65, 66]. Inflammation is also important at the final stages of PCa as it is found in castration-resistant tumors. B lymphocytes infiltration in tumor was also found to be associated with the initial death of cancer cells during androgen ablation therapy. B lymphocytes produce lymphotoxin which can activate IKK-α and STAT3 to promote the formation of castration-resistant tumors [65].

A collection of host stromal cells, called “reactive stroma”, are believed to influence the growth and invasive potential of carcinoma cells [67-69]. Fibroblasts are reported to be the main source in the stroma for secretion of growth factors, inflammatory cytokines, extracellular matrix proteins and their proteases [68, 70]. These secretions help create a microenvironment to promote motility of cancer cells.

Cancer cell proliferation and invasion through the basement membrane into the stromal compartment will stimulate a potential stromal cells phenotypic switching, that is fibroblasts and

smooth muscle cells switching into the myofibroblast (MF) phenotype which is induced by transforming growth factor-β (TGF-β) [68]. Fibroblasts in the adjacent stroma of tumor express several mesenchymal markers such as α-smooth muscle actin (α-SMA), fibroblast-activating protein (FAP), and vimentin [71].

Not only can the activated fibroblasts stimulate cancer progress to invasive stage, but also the tumor cells in turn stimulate activated stromal cells including fibroblasts to release molecules promoting their growth and dissemination [72]. There seems exists some interactions between stromal cells and tumor cells. Indeed, it is reported that prostate cancer epithelium stimulates cancer associated fibroblasts (CAFs) to express specific markers for the MF phenotype, and CAFs coinoculated with initiated but nontumorigenic epithelial cells promoted their tumor growth in vivo[73, 74].

Prostate Cancer in Mouse Models

Several transgenic mouse models have been developed by modifying genes involved in tumor initiation and progression. Methods such as engineering the tumor suppressor genes, oncogenes, steroid hormone and growth factors receptors, and cell cycle and apoptosis regulatory proteins have been employed in mouse models establishment. PCa mouse models have contributed significantly to the understanding of the molecular and pathological aspects of PCa [75].

Both TRAMP and LADY (LPB-Tag) mouse lines, and their derivatives are models utilizing prostate-specific expression of SV40 large T antigen. The TRAMP transgenic mouse line contains a prostate specific probasin promoter to drive the expression of both SV40 large T and small t antigens. They develop high-grade PIN and/or prostate cancer within 12 weeks of age and finally develop metastases by 30 weeks. The ‘LADY model’ lacks small t antigen and develops

lower-grade PIN and/or prostate cancer than in TRAMP mice, but still display reproducible rates of tumor formation, ranging from 12 weeks to over 20 weeks of age [76, 77]. However, tumor in the above lines of animals displays neuroendocrine characteristics that resemble human AR- and PSA-negative small cell carcinoma [78-80]. It is still unclear whether the neuroendocrine tumors in the various SV40-based transgenic models reflect higher sensitivity of neuroendocrine cells to SV40 viral oncogenes or some inherent difference in neuroendocrine tumor susceptibility between mice and humans.

There are several PCa mouse models utilize genetic changes that are confirmed in human PCa, among these models, Pten conditional knockout model is widely used recently. Pten is known as a tumor suppressor gene which encodes a phosphatase protein product. This phosphatase functions as an inhibitor of the PI3 kinase/Akt pathway and regulates the cell cycle. PTEN undergoes Loss of heterozygosity (LOH) at advanced stages in many cancers, including prostate, and represent an excellent model for studying prostate cancer progression. The Cre-loxP is widely used in mouse models for cell type and tissue specific genetic alterations. To establish a prostate epithelium Pten conditional knockout model, Mice that express the Cre recombinase under the control of a prostate epithelium specific probasin (PB) promoter are crossed with mice that express Pten gene flanked by loxP genetic region. Cre recombinase recognizes and binds to the loxP sites and excises the DNA fragment between the sites. Cre expression in PB-Cre4 strain is postnatal and is specific to prostate epithelium, avoids the neuroendocrine phenotype. Therefore, the Pten gene is tissue-specifically knockout in prostate epithelium [81]. Conditional knockout of PTEN using PB-Cre4; Pten $^{loxP/loxP}$ model recapitulates the human prostate cancer progressions. PCa is initiated with PIN, followed by developing invasive adenocarcinoma, and then progressing to metastasis. Moreover, although PCa regresses after androgen ablation, many

PCa patients finally progress to an androgen independent state [49]. Conditional deletions of PTEN and overexpression of c-Myc in the prostate epithelium are two models that most faithfully replicate the development of human adenocarcinoma [49, 82].

Besides the loss of PTEN and overexpression of Myc, the sustained activation of FGF signaling pathway in mouse prostate epithelial cells can also cause development of PCa which exhibit significant epithelial-to-mesenchymal transition (EMT) and generate sarcomatoid carcinomas. Rare metastatic lesions were found in these mice, contain spindle-shaped cells, which originated from prostate epithelial and lost the epithelial morphology, because of dedifferentiation [83].

Androgen signaling plays a vital role in human PCa. An androgen receptor (AR) overexpression mouse model has been established to study the role of androgen in prostate carcinogenesis. These transgenic mice, which express androgen receptor (AR) under the control of the probasin promoter, develop hyperplasia at 50 weeks of age and PIN in mice older than one year [84].

Although there are multiple similarities between human and mouse PCa, some differences still exist. One of the most significant differences is a universal loss of basal cells in human PCa, but the presence of the basal cell populations in some mouse cancers [29]. In general, while tumor pathology and metastatic potential in mouse models significantly differ from human tumors, it is still unclear whether these differences are because of inherent differences between mice and humans, or the failure of mouse models to recapitulate the PCa tumorigenesis in human.

Oncogenic pathways involved in the malignant transformation of PCa stem/progenitor cells and their progenies during PCa progression and metastases.

Prostate stem cells generate a pool of pluripotent committed progenitor cells, which finally develop into terminally differentiated cells. In PCa, dysregulation of the proliferation for

progenitor cells results in significant clonal expansion and loss of differentiation. The activation of extracellular growth factor signaling pathways may contribute to the sustained growth, survival and migration of PCa stem/progenitor cells and their progenies (Fig 1.6). It was reported that the hedgehog signaling pathway elements, Patched 1 (PTCH1) and glioma-associated oncogene homolog 1(GLI-1), were commonly colocalized with a p63 basal marker in CD44/CK8/14-expression prostatic hyperplasia basal cells, but PCa cells were rarely detected in normal basal cells. These results indicate that hedgehog signaling involves in generating basal cell hyperplasia and its progressing towards cancer. The hedgehog signaling induces a transitory differentiation of prostatic stem/progenitor cells into $CD44^{+}/p63^{-/+}$ hyperplasia basal cells with an intermediate phenotype (CK8/14), and increases PTCH1 and GLI-1 expressions in $CD44^{+}$ PCa cells [85, 86].

TGF-β1 has a growth inhibitory effect in the early stages of PCa, but promotes PCa angiogenesis and metastasis in the late stages. TGF-β1 might involve in PCa progression through angiogenesis and change of the tumor microenvironments. TGF-β1 activates VEGF expression via multiple signaling pathways including Smad3, HIF-2a and mRNA-stabilizing factor HuR; indicating that TGF-β1 might contribute to angiogenesis under non-hypoxic conditions [87]. Elevated TGF-β1 expression could induce VEGF, and metalloproteinase-2/9 expression in prostate basal epithelial cells, suggesting that TGF- β1 is involved in phenotype changes associated with malignant behavior [88].

The enhanced expression and activation of epidermal growth factor receptor (EGFR) may lead to the sustained activation of mitogen-activated protein kinases, phosphatidylinositol 3'-kinase (PI3K)/Akt, NF-κB and MIC-1 in PCa stem/progenitor cells and their progenies [57, 89]. Recent studies demonstrated that the CD133(+)/CD44(high)/AR(-/low) side population (SP) cell

fraction, which is isolated from tumorigenic and invasive WPE1-NB26 cells, has a high self-renewal potential. Prostasphere-forming assays results have revealed that the SP cells were able to generate dense and large prostaspheres in culture after 7 days without the addition of exogenous EGF. Moreover, EGF stimulation increased the number and size of prostaspheres indicating EGF-EGFR signaling is essential for the self-renewal of these PCa stem/progenitor cells. Inhibiting EGFR by using gefitinib significantly reduced the EGF-promoted prostasphere formation in $CD133^+$ SP WPE1-NB26 cells [90].

It was reported that production of reactive oxygen species in PC3 cells is mediated through a sustained activation of 5-lipoxygenase which in turn promotes the oxidation and activation of Src to activate pro-survival signals and degrade the pro-apoptotic protein Bim [91].

It is believed that the Wnt signaling pathway regulates self-renewal of PCa cells with stem cell characteristics which is AR independent. The Wnt signaling pathway stimulates stem/ progenitor cells proliferation [92]. Immunohistochemical analysis of rat prostate organ cultures showed that modulation of Wnt signaling can affect differentiation of stem/ progenitor cells into luminal cells. In this organ culture experiment, lots of p63 positive cells were observed in the ductal region of Wnt3a-treated cultures while fewer p63 positive cells were present in Wnt inhibitor Dickkopf-related protein-1(DKK1) treated cultures[93]. Blocking canonical Wnt/ β-catenin pathway by using inhibitors such as DKK1 or secreted Frizzled related protein-2 (sFRP2), lessened the number and reduced the size of self-renewing prostaspheres derived from metastatic LNCaP and C4-2B PCa cell lines [94].

The CXC chemokine receptor 4 (CXCR4) and its ligand stromal cell-derived factor-1 (SDF-1) can regulate the migration and metastatic spread of PCa through a chemoattractant gradient of

SDF-1. Recent studies showed that binding of SDF-1 to CXCR4 leads to high expression of α5 and β3 integrins. Integrin expression is a salient characteristic for Disseminated PCa cells. α5β3 integrins are crucial in regulating the growth and metastasis of PCa cells in the bone, and overexpression of α5 subunits increased the adhesion of the PC-3 cells to collagen type I, fibronectin, and laminin [95]. It is also reported that treatment with an anti-CXCR4 antibody of $CD133^{+}/CD44^{+}$ PCa cells which are immature and has stem cell-like characteristics, inhibited the SDF-1 dependent migration [96].

Heparan Sulfate and Heparan Sulfate Proteoglycans

Glycosaminoglycans

Glycosaminoglycans (GAGs) can be defined as unbranched polysaccharides that consist of an N-acetyl-hexosamine, the N-acetylglucose amine or N-acetylgalactose amine, and a hexuronic acid (glucuronic acid or iduronic acid) or galactose disaccharide repeat unit. Different GAGs have distinct disaccharide repeats. Heparin/Heparan sulfate (HS), keratan sulfate and hyaluronic acid (HA) contain N-Acetylglucosamine (GlcNAc) residues while chondroitin sulfate and dermatan sulfate contain N-acetylgalactosamines (GalNAc) (Table 1.1). The biosynthesis of GAGs needs six precursor molecules: UDP-GlcNAc, UDP-GalNAc, UDP-Gal, UDP-GlcA, UDP-Xyl and 3'-phosphoadenosine 5'-phosphosulfate (PAPS), the provider of sulfate moieties for sulfation of GAG chains [97-99]. All GAGs except HA are heavily sulfated and carry an overall negative charge. GAGs usually attach to a core protein with the exception of HA and are found mainly at the cell surface and in the extracellular matrix. GAGs have a high degree of diversity with regard to molecular weight, types and number of GAG chains attached and sulfation. This reflects the

multiple functions of proteoglycans perform, most of which are highly dependent on the GAG chains.

Heparan Sulfate Proteoglycans (HSPGs)

Heparan sulfate proteoglycans (HSPGs) are glycoconjugates composed of a core protein and one or more heparan sulfate (HS) glycosaminoglycan (GAG) chains (Fig.1.7) [100-102]. HSPGs present abundantly on the cell surface (including syndecans and glypicans) and in the ECM (including perlecan, agrin and others) where they interact with numerous growth factors, extracellular matrix proteins, morphogens, tissue remodeling factors, adhesion molecules and chemokines [100-103] (Table 1.2).

Heparan sulfate proteoglycans (HSPGs) are composed of a core protein and one or more heparan sulfate (HS) glycosaminoglycan (GAG) chains. There are mainly three families of HSPGs: the membrane-spanning syndecans, the glycophosphatidylinositol (GPI)-linked glypicans, and the secreted extracellular matrix (ECM) agrin and perlecan. The HS chains at the cell surface are mostly attached to syndecan and glypican core proteins (Fig. 1.7). Syndecans are transmembrane proteins that bear HS chains distal from the plasma membrane [104]. There are four vertebrate syndecans designated as syndecan 1-4. Syndecans carry primarily HS chains but syndecan 1 and 4 may also carry CS [105]. Glypicans are glycosylphosphatidyl (GPI) - anchored proteoglycans comprise a family of six members in mammals (GPC 1-6). They share many common sequences including an N-terminal signal sequence, a characteristic pattern of 14 conserved cysteine residues, a presumably GAG attachment sequences near the plasma membrane, and a C-terminal sequence involved in formation of a glycosyl phosphatidyl inositol (GPI) linkage to the plasma membrane [100]. It has been suggested that attachment of glypicans via the GPI anchor may

target them to lipid rafts. Localization of glypicans to lipid rafts may facilitate their interaction with specific signaling molecules. It has also been proposed that GPI anchors may regulate non-proteolytic cleavage of glypicans from the cell surface by phospholipases [106].

The perlecan and agrin mainly exist in the ECM. They are involved in maintaining basement membrane structure as well as modulating various signaling transduction events. Perlecan is a large multidomain proteoglycan that is expressed in basement membranes, mesenchymal and connective tissues. Perlecan contains attachment sites for both HS and CS at its N-terminal domains. It is involved in blood vessel development and inhibits smooth muscle cell proliferation and then facilitates maintaining of the vascular homeostasis. HS of perlecan has been implicated in sequestering and storing of growth factors as well as serving as co-receptors for growth factor receptors to stimulate endothelial growth and re-generation [107].

Heparan Sulfate Biosynthesis

Heparan sulfate (HS) is a linear polysaccharide that is synthesized as an alternating copolymer of uronic acid and glucosamine with various sulfation modifications, and is typically 50-200 disaccharides in length. HS synthesis initiates with the transfer of xylose from UDP-xylose by xylosyltransferase 1 and 2 to serine residues of the core protein. The formation of a core protein linkage tetrasaccharide primer GlcAβ1-3Galβ1-3Galβ1-4Xylβ1-O- is completed by attaching two galactose (Gal) residues by galactosyltransferases 1 and 2 and glucuronic acid (GlcA) by glucuronosyltransferase 1 (Fig 1.9).

The EXTL3, EXT1/EXT2 co-polymerize adding of the first N-acetylglucosamine (GlcNAc) residue to the linkage tetrasaccharide primer. After this chain elongation of HS is carried out by members of the EXT gene family, which alternately add GlcNAc and GlcA residues [97].

Following chain elongation, N-deacetylase/N-sulfotransferases (Ndsts) act on discrete regions of the HS precursor, replacing N-acetyl groups with N-sulfates [108]. Regions of N-sulfation (NS-domain) then act as the substrate for additional modifications, including epimerization, and 2-O, 6-O and 3-O-sulfation [101, 109]. The second polymer modification is epimerization and 2-O-sulfation. HS glucuronyl C5 epimerase (HSGLCE) catalyzes epimerization of GlcA to IdoA. HS2ST sulfates the resulting IdoA residues at C2. 6-O-sulphation is catalyzed by HS6ST1-3 adding sulfation at C6. The last modification is 3-O-sulphation, which is catalyzed by HS3ST 1-6. The modifications are incomplete, and the enzymes involved have substrate specificities, which result in IdoA and O-sulfate residues occurring predominantly in the NS-domains. The pattern of negatively charged sulfates and uronic acids, as well as their length and spacing, contribute to the structural heterogeneity of HS and create binding sites for many proteins ligands [110-112]. The distribution, length, and modification of such domains tightly regulated in a tissue- or cell-specific fashion [113], suggesting that the regulatory role of HS occurs spatio-temporally by interacting with protein ligands in different tissues and at different developmental/pathological stages [113, 114].

Heparan Sulfate and PCa

The structural diversity of tumor cell HS (both at the cell surface and ECM) enables them to modulate several aspects of tumor cell phenotype, including tumor cell growth, invasiveness and metastatic potential [115]. Depends on where the HS or HSPG locate, anchors at the cell surface or presents in the ECM, and the HS sequence a given tumor-derived HS or HSPG can be tumor-promoting or anti-tumorigenic. The studies on HS or HSPGs have suggested that HS critically modulates multiple aspects of cancer biology [100, 116-121].

Recent evidence reveals that, during the transformation to malignant phenotypes, cells alter their cell-surface HSPG profile, including both the proteoglycan protein cores and HS fine structures [122-125]. For example, syndecan is required to maintain the differentiated morphology and localization of epithelial cells. Syndecan-1 expression is down regulated in various malignant tumors, including uterine carcinoma and multiple myeloma [126]. The expression of syndecan-1 decreases as in situ carcinoma progresses to invasive carcinoma [127]. Similarly, glypican-1 expression is up-regulated in pancreatic cancer cells [128]. On the other hand, glypican-3 is down-regulated in breast cancer, ovarian carcinomas and mesotheliomas [128-130]. HS structural changes were noted during the malignant transformation of colon cancer cells from adenoma to carcinoma [123]. The association between mutations in glypican-3 gene and Simpson-Golabi-Behmel syndrome, an inherited syndrome that increase cancer risk, directly link HSPGs to tumorigenesis [131]. Hereditary multiple exostosis (HME) is an autosomal dominant disorder characterized by suffering benign bone tumors on the active bone growth areas. Genetic studies observed that HS biosynthetic gene Ext1 or Ext2 heterozygous mutant patients developed HME with at least 2% of the exostoses undergoing malignant transformation into chondrosarcoma or osteosarcoma, suggesting that Ext1 and Ext2 are a putative tumor suppressor gene [132-136]. Down-regulated Ext1 in HL-60 cells demonstrate tumor-suppressing activity with a marked reduction of 54% in colony formation; xenograft implantation of these cells in nude mice indicate that EXT1 knockdown HL-60 cells had much lower tumorigenicity than control [137]. These results demonstrate that EXT1 may suppress or promote the growth of cancer cells depend on the tissue and cell types.

In addition to play roles in malignant transformation, tumor cell surface HS is an pivotal regulator of tumor growth and progression [115, 138, 139]. The diverse structural characteristics

of HS allow them to act either as inhibitors or potentiators of these tumor growth and progression related signaling pathways, depending on the HS sequence location or ligands binding. For example, In vitro studies have suggested that tumor cell surface HS binds to FGF2 with a short N-and 2-O-sulfated sequence, facilitating intracellular signaling and tumor cell growth[140-143]. The same functional model has been shared by other growth factors and morphogens, such as vascular endothelial growth factor, hedgehog and bone morphogen [100, 140, 144]. It is also reported that HS-deficient CHO cells were incapable of forming tumors in nude mice, demonstrating that self-made HS is essentially required for tumor growth [145]. On the other hand, cell surface HSPGs can serve as a "trap" to inhibit these signaling pathways. A recent “catch or present” model for QSulf1 a HS-specific 6-O endosulfatase, regulates Wnt signaling by removing 6-O sulfates from HS chains to promote the formation of low affinity HS-Wnt complexes that interact with Frizzled receptors and then initiate Wnt signaling (Fig 1.10). Therefore, under certain circumstances HS can exert a function to promote or disrupt tumor growth and progression.

By mediating interactions between cancer cells and platelets, endothelial cells and host organ cells, HS regulate tumor metastasis to distant organs. In human cancer cells, results from recent experiments have shown that HS participates in the cell–cell and cell–ECM adhesion processes that are required for tumor metastasis [146, 147]. A few studies suggested that tumor cell surface HS interacts with molecules related to leukocyte recruitment to participate tumor cell vascular dissemination during metastasis. During the dissemination, circulating tumor cells share a molecular mechanism of leukocyte recruitment in inflammation to initial tumor cell attachment. It may also act as a co-receptor to facilitate chemokines binding to their receptors that are co-

expressed on the tumor cell surface. This may promote tumor cell migration and invasion [138, 148-150].

In addition to the roles of HS in mediating tumor invasion, HS in the ECM, along with structural proteins such as collagen and laminin, forms a barrier to constrain tumor cells. However, during the invasion and metastasis, tumor cells secrete enzymes that degrade both the protein (e.g. matrix metalloproteinases) and polysaccharide (e.g. heparanases) components of the basement-membrane barrier. Heparanase expression by several human tumor types, including colorectal and pancreatic carcinomas, has been shown to increase during a tumor's transition, from benign to malignant and onto invasive carcinoma. In addition, transfection of the gene that encodes heparanase into a nonmetastatic cell type results in a marked phenotypic change and enhanced metastatic potential. Heparanases have also been shown to promote tumor growth by releasing growth factors that are normally sequestered by HS proteoglycans in the ECM [115, 151].

A recent study has showed that Heparan sulfate 2-O-sulfotransferase (2OST) expression correlates with increasing metastatic potential in the LNCaP models, and the SHH, FGF and TGFβ pathways all require 2OST for optimal signaling in metastatic LNCaP-C4-2B cells. This evidence suggesting that increased sulfation of HS chains on HSPG allows for increased growth factor-HSPG binding and is essential for proliferation and invasion of PCa cells[152].

Summary

HS has been implicated in regulating various tumorigenesis and cancer progression through their ability to interact with many proteins that include growth factors, chemokines, morphogens, and adhesive proteins. PCa tumorigenesis and progression are controlled by various heparan sulfate-

binding growth factors, therefore, may be an critical component to modulate PCa cell growth, invasion and metastasis.

References

1. American-Cancer-Society., *Cancer Facts and Figures 2013,* 2013, American Cancer Society: Atlanta.
2. Cannon, L., et al., *Genetic epidemiology of prostate cancer in the Utah Mormon genealogy.* Cancer Surv, 1982. **1**(1): p. 47-69.
3. Carter, B.S., et al., *Mendelian inheritance of familial prostate cancer.* Proceedings of the National Academy of Sciences, 1992. **89**(8): p. 3367-3371.
4. Carter, B.S., et al., *HEREDITARY PROSTATE-CANCER - EPIDEMIOLOGIC AND CLINICAL-FEATURES.* Journal of Urology, 1993. **150**(3): p. 797-802.
5. Bratt, O., *Hereditary prostate cancer: clinical aspects.* The Journal of Urology, 2002. **168**(3): p. 906-913.
6. Thomas, G., et al., *Multiple loci identified in a genome-wide association study of prostate cancer.* Nat Genet, 2008. **40**(3): p. 310-315.
7. Eeles, R.A., et al., *Multiple newly identified loci associated with prostate cancer susceptibility.* Nat Genet, 2008. **40**(3): p. 316-321.
8. Crawford, E.D., *Epidemiology of prostate cancer.* Urology, 2003. **62**(6, Supplement 1): p. 3-12.
9. Hsing, A.W., *Hormones and prostate cancer: what's next?* Epidemiologic reviews, 2001. **23**(1): p. 42-58.
10. De Marzo, A.M., et al., *Inflammation in prostate carcinogenesis.* Nat Rev Cancer, 2007. **7**(4): p. 256-269.
11. De Marzo, A.M., et al., *Human prostate cancer precursors and pathobiology.* Urology, 2003. **62**(5, Supplement 1): p. 55-62.
12. Danforth, K.N., et al., *Polymorphic variants in PTGS2 and prostate cancer risk: results from two large nested case–control studies.* Carcinogenesis, 2008. **29**(3): p. 568-572.
13. Fernandez, P., et al., *COX-2 promoter polymorphisms and the association with prostate cancer risk in South African men.* Carcinogenesis, 2008. **29**(12): p. 2347-2350.
14. Zabaleta, J., et al., *Cytokine genetic polymorphisms and prostate cancer aggressiveness.* Carcinogenesis, 2009. **30**(8): p. 1358-1362.
15. Wang, M.-H., et al., *Association of IL10 and Other immune response- and obesity-related genes with prostate cancer in CLUE II.* The Prostate, 2009. **69**(8): p. 874-885.
16. Pierce, B., et al., *C-reactive protein, interleukin-6, and prostate cancer risk in men aged 65 years and older.* Cancer Causes and Control, 2009. **20**(7): p. 1193-1203.
17. Bostwick, D.G., et al., *Independent origin of multiple foci of prostatic intraepithelial neoplasia - Comparison with matched foci of prostate carcinoma.* Cancer, 1998. **83**(9): p. 1995-2002.
18. Macintosh, C.A., et al., *Precise Microdissection of Human Prostate Cancers Reveals Genotypic Heterogeneity.* Cancer Research, 1998. **58**(1): p. 23-28.
19. Liu, A.Y., et al., *Cell–cell interaction in prostate gene regulation and cytodifferentiation.* Proceedings of the National Academy of Sciences, 1997. **94**(20): p. 10705-10710.
20. Liu, A.Y., et al., *Analysis and sorting of prostate cancer cell types by flow cytometry.* The Prostate, 1999. **40**(3): p. 192-199.
21. Tsukise, A. and K. Yamada, *Complex carbohydrates in the secretory epithelium of the goat prostate.* The Histochemical Journal, 1984. **16**(3): p. 311-319.

22. McNeal, J.E., *ORIGIN AND DEVELOPMENT OF CARCINOMA IN PROSTATE.* Cancer, 1969. **23**(1): p. 24-&.
23. Sugimura, Y., G.R. Cunha, and A.A. Donjacour, *Morphogenesis of ductal networks in the mouse prostate.* Biology of Reproduction, 1986. **34**(5): p. 961-971.
24. Hayashi, N., et al., *Morphological and functional heterogeneity in the rat prostatic gland.* Biology of Reproduction, 1991. **45**(2): p. 308-321.
25. Bonkhoff, H., et al., *Basement membranes in fetal, adult normal, hyperplastic and neoplastic human prostate.* Virchows Archiv, 1991. **418**(5): p. 375-381.
26. Bonkhoff, H., et al., *Distribution of basement membranes in primary and metastatic carcinomas of the prostate.* Human Pathology, 1992. **23**(8): p. 934-939.
27. van Leenders, G.J.L.H. and J.A. Schalken, *Epithelial cell differentiation in the human prostate epithelium: Implications for the pathogenesis and therapy of prostate cancer.* Critical Reviews in Oncology/Hematology, 2003. **46, Supplement**(0): p. 3-10.
28. Verhagen, A.P.M., et al., *Differential expression of keratins in the basal and luminal compartments of rat prostatic epithelium during degeneration and regeneration.* The Prostate, 1988. **13**(1): p. 25-38.
29. Wang, S., et al., *Pten deletion leads to the expansion of a prostatic stem/progenitor cell subpopulation and tumor initiation.* Proceedings of the National Academy of Sciences of the United States of America, 2006. **103**(5): p. 1480-1485.
30. van Leenders, G., et al., *Demonstration of Intermediate Cells during Human Prostate Epithelial Differentiation In Situ and In Vitro Using Triple-Staining Confocal Scanning Microscopy.* Lab Invest, 2000. **80**(8): p. 1251-1258.
31. Bonkhoff, H. and T. Fixemer, *Neuroendocrine differentiation in prostate cancer: an unrecognized and therapy resistant phenotype.* Pathologe, 2005. **26**(6): p. 453 - 460.
32. Prins, G.S. and O. Putz, *Molecular signaling pathways that regulate prostate gland development.* Differentiation, 2008. **76**(6): p. 641-659.
33. Bhatia-Gaur, R., et al., *Roles for Nkx3.1 in prostate development and cancer.* Genes & Development, 1999. **13**(8): p. 966-977.
34. Cunha, G.R., et al., *Growth factors as mediators of androgen action during the development of the male urogenital tract.* World Journal of Urology, 1995. **13**(5): p. 264-276.
35. CUNHA, G.R. and P. YOUNG, *Inability of Tfm (Testicular Feminization) Epithelial Cells to Express Androgen-Dependent Seminal Vesicle Secretory Proteins in Chimeric Tissue Recombinants.* Endocrinology, 1991. **128**(6): p. 3293-3298.
36. English, H.F., R.J. Santen, and J.T. Lsaacs, *Response of glandular versus basal rat ventral prostatic epithelial cells to androgen withdrawal and replacement.* The Prostate, 1987. **11**(3): p. 229-242.
37. Evans, G.S. and J.A. Chandler, *Cell proliferation studies in the rat prostate: II. The effects of castration and androgen-induced regeneration upon basal and secretory cell proliferation.* The Prostate, 1987. **11**(4): p. 339-351.
38. Feldman, B.J. and D. Feldman, *THE DEVELOPMENT OF ANDROGEN-INDEPENDENT PROSTATE CANCER.* Nature Reviews Cancer, 2001. **1**(1): p. 34.
39. Kristal, A.R., et al., *Androgen receptor CAG repeat length is not associated with the risk of incident symptomatic benign prostatic hyperplasia: Results from the prostate cancer prevention trial.* The Prostate, 2010. **70**(6): p. 584-590.
40. Bushman, W., *Etiology, epidemiology, and natural history of benign prostatic hyperplasia.* The Urologic clinics of North America, 2009. **36**(4): p. 403-15, v.

41. Auffenberg, G.B., B.T. Helfand, and K.T. McVary, *Established Medical Therapy for Benign Prostatic Hyperplasia.* Urologic Clinics of North America, 2009. **36**(4): p. 443-459.
42. Ayala, A.G. and J.Y. Ro, *Prostatic Intraepithelial Neoplasia: Recent Advances.* Archives of Pathology & Laboratory Medicine, 2007. **131**(8): p. 1257-1266.
43. Patrawala, L., et al., *Hierarchical Organization of Prostate Cancer Cells in Xenograft Tumors: The CD44+α2β1+ Cell Population Is Enriched in Tumor-Initiating Cells.* Cancer Research, 2007. **67**(14): p. 6796-6805.
44. Mulholland, D.J., et al., *Lin−Sca-1+CD49fhigh Stem/Progenitors Are Tumor-Initiating Cells in the Pten-Null Prostate Cancer Model.* Cancer Research, 2009. **69**(22): p. 8555-8562.
45. Lawson, D.A., et al., *Basal epithelial stem cells are efficient targets for prostate cancer initiation.* Proceedings of the National Academy of Sciences, 2010. **107**(6): p. 2610-2615.
46. Barker, N., et al., *Crypt stem cells as the cells-of-origin of intestinal cancer.* Nature, 2009. **457**(7229): p. 608-611.
47. Wang, X., et al., *A luminal epithelial stem cell that is a cell of origin for prostate cancer.* Nature, 2009. **461**(7263): p. 495-500.
48. Korsten, H., et al., *Accumulating Progenitor Cells in the Luminal Epithelial Cell Layer Are Candidate Tumor Initiating Cells in a <italic>Pten</italic> Knockout Mouse Prostate Cancer Model.* PLoS ONE, 2009. **4**(5): p. e5662.
49. Wang, S., et al., *Prostate-specific deletion of the murine Pten tumor suppressor gene leads to metastatic prostate cancer.* Cancer Cell, 2003. **4**(3): p. 209-221.
50. Chen, Z., et al., *Crucial role of p53-dependent cellular senescence in suppression of Pten-deficient tumorigenesis.* Nature, 2005. **436**(7051): p. 725-730.
51. Zenzmaier, C., G. Untergasser, and P. Berger, *Aging of the prostate epithelial stem/progenitor cell.* Experimental Gerontology, 2008. **43**(11): p. 981-985.
52. Mimeault, M., et al., *Functions of Normal and Malignant Prostatic Stem/Progenitor Cells in Tissue Regeneration and Cancer Progression and Novel Targeting Therapies.* Endocrine Reviews, 2008. **29**(2): p. 234-252.
53. Martin, P., et al., *Prostate Epithelial Pten/TP53 Loss Leads to Transformation of Multipotential Progenitors and Epithelial to Mesenchymal Transition.* The American Journal of Pathology, 2011. **179**(1): p. 422-435.
54. Mulholland, D.J., et al., *Pten Loss and RAS/MAPK Activation Cooperate to Promote EMT and Metastasis Initiated from Prostate Cancer Stem/Progenitor Cells.* Cancer Research, 2012. **72**(7): p. 1878-1889.
55. Liu, T., et al., *Establishment and characterization of multi-drug resistant, prostate carcinoma-initiating stem-like cells from human prostate cancer cell lines 22RV1.* Molecular and Cellular Biochemistry, 2010. **340**(1): p. 265-273.
56. Fan, X., et al., *Effective enrichment of prostate cancer stem cells from spheres in a suspension culture system.* Urologic Oncology: Seminars and Original Investigations, 2012. **30**(3): p. 314-318.
57. Mimeault, M., et al., *Cytotoxic Effects Induced by Docetaxel, Gefitinib, and Cyclopamine on Side Population and Nonside Population Cell Fractions from Human Invasive Prostate Cancer Cells.* Molecular Cancer Therapeutics, 2010. **9**(3): p. 617-630.
58. Klarmann, G., et al., *Invasive prostate cancer cells are tumor initiating cells that have a stem cell-like genomic signature.* Clinical and Experimental Metastasis, 2009. **26**(5): p. 433-446.

59. Giannoni, E., et al., *Reciprocal Activation of Prostate Cancer Cells and Cancer-Associated Fibroblasts Stimulates Epithelial-Mesenchymal Transition and Cancer Stemness.* Cancer Research, 2010. **70**(17): p. 6945-6956.
60. Giannoni, E., et al., *Cancer associated fibroblasts exploit reactive oxygen species through a proinflammatory signature leading to epithelial mesenchymal transition and stemness.* Antioxidants & Redox Signaling, 2011. **14**(12): p. 2361-2371.
61. Farnsworth, W.E., *Prostate Stroma: Physiology.* The Prostate, 1999. **38**(1): p. 60-72.
62. Cunha, G.R., *The role of androgens in the epithelio-mesenchymal interactions involved in prostatic morphogenesis in embryonic mice.* The Anatomical Record, 1973. **175**(1): p. 87-96.
63. De Marzo, A.M., et al., *Proliferative Inflammatory Atrophy of the Prostate: Implications for Prostatic Carcinogenesis.* The American Journal of Pathology, 1999. **155**(6): p. 1985-1992.
64. De Marzo, A.M., et al., *Pathological and molecular mechanisms of prostate carcinogenesis: Implications for diagnosis, detection, prevention, and treatment.* Journal of Cellular Biochemistry, 2004. **91**(3): p. 459-477.
65. Ammirante, M., et al., *B-cell-derived lymphotoxin promotes castration-resistant prostate cancer.* Nature, 2010. **464**(7286): p. 302-305.
66. Luo, J.-L., et al., *Nuclear cytokine-activated IKK[agr] controls prostate cancer metastasis by repressing Maspin.* Nature, 2007. **446**(7136): p. 690-694.
67. Liotta, L.A. and E.C. Kohn, *The microenvironment of the tumour-host interface.* Nature, 2001. **411**(6835): p. 375-379.
68. Kalluri, R. and M. Zeisberg, *Fibroblasts in cancer.* Nat Rev Cancer, 2006. **6**(5): p. 392-401.
69. Joyce, J.A. and J.W. Pollard, *Microenvironmental regulation of metastasis.* Nat Rev Cancer, 2009. **9**(4): p. 239-252.
70. Silzle, T., et al., *The fibroblast: Sentinel cell and local immune modulator in tumor tissue.* International Journal of Cancer, 2004. **108**(2): p. 173-180.
71. Gabbiani, G., *The myofibroblast in wound healing and fibrocontractive diseases.* The Journal of Pathology, 2003. **200**(4): p. 500-503.
72. De Wever, O. and M. Mareel, *Role of tissue stroma in cancer cell invasion.* The Journal of Pathology, 2003. **200**(4): p. 429-447.
73. Tuxhorn, J.A., et al., *Reactive Stroma in Human Prostate Cancer: Induction of Myofibroblast Phenotype and Extracellular Matrix Remodeling.* Clinical Cancer Research, 2002. **8**(9): p. 2912-2923.
74. Olumi, A.F., et al., *Carcinoma-associated Fibroblasts Direct Tumor Progression of Initiated Human Prostatic Epithelium.* Cancer Research, 1999. **59**(19): p. 5002-5011.
75. Shappell, S.B., et al., *Prostate Pathology of Genetically Engineered Mice: Definitions and Classification. The Consensus Report from the Bar Harbor Meeting of the Mouse Models of Human Cancer Consortium Prostate Pathology Committee.* Cancer Research, 2004. **64**(6): p. 2270-2305.
76. Gingrich, J.R., et al., *Metastatic Prostate Cancer in a Transgenic Mouse.* Cancer Research, 1996. **56**(18): p. 4096-4102.
77. Kasper, S., et al., *Development, progression, and androgen-dependence of prostate tumors in probasin-large T antigen transgenic mice: a model for prostate cancer.* Laboratory investigation; a journal of technical methods and pathology, 1998. **78**(3): p. 319-333.
78. Kaplan-Lefko, P.J., et al., *Pathobiology of autochthonous prostate cancer in a pre-clinical transgenic mouse model.* The Prostate, 2003. **55**(3): p. 219-237.

79. Klezovitch, O., et al., *Hepsin promotes prostate cancer progression and metastasis.* Cancer Cell, 2004. **6**(2): p. 185-195.
80. Masumori, N., et al., *A Probasin-Large T Antigen Transgenic Mouse Line Develops Prostate Adenocarcinoma and Neuroendocrine Carcinoma with Metastatic Potential.* Cancer Research, 2001. **61**(5): p. 2239-2249.
81. Valkenburg, K.C. and B.O. Williams, *Mouse Models of Prostate Cancer.* Prostate Cancer, 2011. **2011**.
82. Ellwood-Yen, K., et al., *Myc-driven murine prostate cancer shares molecular features with human prostate tumors.* Cancer Cell, 2003. **4**(3): p. 223-238.
83. Acevedo, V.D., et al., *Inducible FGFR-1 Activation Leads to Irreversible Prostate Adenocarcinoma and an Epithelial-to-Mesenchymal Transition.* Cancer cell, 2007. **12**(6): p. 559-571.
84. Han, G., et al., *Mutation of the androgen receptor causes oncogenic transformation of the prostate.* Proceedings of the National Academy of Sciences of the United States of America, 2005. **102**(4): p. 1151-1156.
85. Podlasek, C.A., et al., *Prostate development requires Sonic hedgehog expressed by the urogenital sinus epithelium.* Developmental Biology, 1999. **209**(1): p. 28-39.
86. Chen, B.-Y., et al., *Hedgehog is involved in prostate basal cell hyperplasia formation and its progressing towards tumorigenesis.* Biochemical and Biophysical Research Communications, 2007. **357**(4): p. 1084-1089.
87. Chae, K.S., et al., *Opposite functions of HIF-α isoforms in VEGF induction by TGF-β1 under non-hypoxic conditions.* Oncogene, 2011. **30**(10): p. 1213-1228.
88. Goodyear, S.M., et al., *Role of the VEGFR3/VEGFD receptor axis in TGFβ1 activation of primary prostate cell lines.* The Prostate, 2009. **69**(9): p. 982-990.
89. Peraldo-Neia, C., et al., *Epidermal Growth Factor Receptor (EGFR) mutation analysis, gene expression profiling and EGFR protein expression in primary prostate cancer.* BMC Cancer, 2011. **11**(1): p. 31.
90. Mimeault, M., S.L. Johansson, and S.K. Batra, *Pathobiological Implications of the Expression of EGFR, pAkt, NF-κB and MIC-1 in Prostate Cancer Stem Cells and Their Progenies.* PLoS ONE, 2012. **7**(2): p. e31919.
91. Giannoni, E., et al., *Redox regulation of anoikis resistance of metastatic prostate cancer cells: key role for Src and EGFR-mediated pro-survival signals.* Oncogene, 2009. **28**(20): p. 2074-2086.
92. Antón Aparicio, L., et al., *Prostate carcinoma and stem cells.* Clinical and Translational Oncology, 2007. **9**(2): p. 66-76.
93. Wang, B.-E., et al., *Regulation of Epithelial Branching Morphogenesis and Cancer Cell Growth of the Prostate by Wnt Signaling.* PLoS ONE, 2008. **3**(5): p. e2186.
94. Bisson, I. and D.M. Prowse, *WNT signaling regulates self-renewal and differentiation of prostate cancer cells with stem cell characteristics.* Cell Research, 2009. **19**(6): p. 683-697.
95. Tobias Engl, B.R., Dana Marian, Christa Blumenberg, Iris Müller, Wolf-Dietrich Beecken, Jon Jones, Eva M Ringel, Jürgen Bereiter-Hahn, Dietger Jonas, and Roman A Blaheta, *CXCR4 Chemokine Receptor Mediates Prostate Tumor Cell Adhesion through α5 and β3 Integrins.* Neoplasia, 2006. **8**(4): p. 290 - 301.
96. Miki, J., et al., *Identification of Putative Stem Cell Markers, CD133 and CXCR4, in hTERT–Immortalized Primary Nonmalignant and Malignant Tumor-Derived Human Prostate*

Epithelial Cell Lines and in Prostate Cancer Specimens. Cancer Research, 2007. **67**(7): p. 3153-3161.
97. Sugahara, K. and H. Kitagawa, *Heparin and Heparan Sulfate Biosynthesis.* IUBMB Life, 2002. **54**(4): p. 163-175.
98. Silbert, J.E. and G. Sugumaran, *Biosynthesis of Chondroitin/Dermatan Sulfate.* IUBMB Life, 2002. **54**(4): p. 177-186.
99. Itano, N. and K. Kimata, *Mammalian Hyaluronan Synthases.* IUBMB Life, 2002. **54**(4): p. 195-199.
100. Bernfield, M., et al., *FUNCTIONS OF CELL SURFACE HEPARAN SULFATE PROTEOGLYCANS.* Annual Review of Biochemistry, 1999. **68**(1): p. 729-777.
101. Esko, J.D. and S.B. Selleck, *Order out of chaos: assembly of ligand binding sites in heparan sulfate.* Annu Rev Biochem, 2002. **71**: p. 435-71.
102. Bishop, J.R., M. Schuksz, and J.D. Esko, *Heparan sulphate proteoglycans fine-tune mammalian physiology.* Nature, 2007. **446**(7139): p. 1030-7.
103. Forsberg, E. and L. Kjellen, *Heparan sulfate: lessons from knockout mice.* J Clin Invest, 2001. **108**(2): p. 175-80.
104. Yoneda, A. and J.R. Couchman, *Regulation of cytoskeletal organization by syndecan transmembrane proteoglycans.* Matrix Biology, 2003. **22**(1): p. 25-33.
105. Carey, D.J., *Syndecans: multifunctional cell-surface co-receptors*.
106. Song, H.H. and J. Filmus, *The role of glypicans in mammalian development.* Biochimica et Biophysica Acta (BBA) - General Subjects, 2002. **1573**(3): p. 241-246.
107. Knox, S. and J. Whitelock, *Perlecan: how does one molecule do so many things?* Cellular and Molecular Life Sciences, 2006. **63**(21): p. 2435-2445.
108. Kjellen, L., *Glucosaminyl N-deacetylase/N-sulphotransferases in heparan sulphate biosynthesis and biology.* Biochem Soc Trans, 2003. **31**(2): p. 340-2.
109. Esko, J.D. and U. Lindahl, *Molecular diversity of heparan sulfate.* J Clin Invest, 2001. **108**(2): p. 169-73.
110. Stringer, S.E., *The role of heparan sulphate proteoglycans in angiogenesis.* Biochem Soc Trans, 2006. **34**(Pt 3): p. 451-3.
111. Presta, M., et al., *Fibroblast growth factor/fibroblast growth factor receptor system in angiogenesis.* Cytokine Growth Factor Rev, 2005. **16**(2): p. 159-78.
112. Iozzo, R.V. and J.D. San Antonio, *Heparan sulfate proteoglycans: heavy hitters in the angiogenesis arena.* J Clin Invest, 2001. **108**(3): p. 349-55.
113. Ledin, J., et al., *Heparan sulfate structure in mice with genetically modified heparan sulfate production.* J Biol Chem, 2004. **279**(41): p. 42732-41.
114. Allen, B.L., M.S. Filla, and A.C. Rapraeger, *Role of heparan sulfate as a tissue-specific regulator of FGF-4 and FGF receptor recognition.* J Cell Biol, 2001. **155**(5): p. 845-58.
115. Sasisekharan, R., et al., *Roles of heparan-sulphate glycosaminoglycans in cancer.* Nature Reviews. Cancer, 2002. **2**(7): p. 521-528.
116. Bishop, J.R., M. Schuksz, and J.D. Esko, *Heparan sulphate proteoglycans fine-tune mammalian physiology.* Nature, 2007. **446**(7139): p. 1030.
117. Kirkpatrick, C.A. and S.B. Selleck, *Heparan sulfate proteoglycans at a glance.* J Cell Sci, 2007. **120**(11): p. 1829-1832.
118. T ímár, J., et al., *Proteoglycans and tumor progression: Janus-faced molecules with contradictory functions in cancer.* Seminars in Cancer Biology, 2002. **12**(3): p. 173-186.

119. Liu, D., et al., *Dynamic Regulation of Tumor Growth and Metastasis by Heparan Sulfate Glycosaminoglycans.* Semin Thromb Hemost, 2002. **28**(01): p. 67-78.
120. Blackhall, F.H., et al., *Heparan sulfate proteoglycans and cancer.* British Journal of Cancer, 2001. **85**(8): p. 1094.
121. EM Selva, N.P., *Role of heparan sulfate proteoglycans in cell signaling and cancer* Advances in Cancer Research, 2001. **Vol. 83**: p. 67-80.
122. Lyon, M., et al., *Elucidation of the Structural Features of Heparan Sulfate Important for Interaction with the Hep-2 Domain of Fibronectin.* Journal of Biological Chemistry, 2000. **275**(7): p. 4599-4606.
123. Jayson, G.C., et al., *Heparan Sulfate Undergoes Specific Structural Changes during the Progression from Human Colon Adenoma to Carcinoma in Vitro.* Journal of Biological Chemistry, 1998. **273**(1): p. 51-57.
124. Nackaerts, K., et al., *Heparan sulfate proteoglycan expression in human lung-cancer cells.* International Journal of Cancer, 1997. **74**(3): p. 335-345.
125. Matsumoto, A., et al., *Reduced expression of syndecan-1 in human hepatocellular carcinoma with high metastatic potential.* International Journal of Cancer, 1997. **74**(5): p. 482-491.
126. Kiviniemi, J., et al., *Altered expression of syndecan-1 in prostate cancer.* APMIS: Acta Pathologica, Microbiologica, Et Immunologica Scandinavica, 2004. **112**(2): p. 89-97.
127. Sanderson, R.D., *Heparan sulfate proteoglycans in invasion and metastasis.* Seminars in Cell & Developmental Biology, 2001. **12**(2): p. 89-98.
128. Kleeff, J., et al., *The cell-surface heparan sulfate proteoglycan glypican-1 regulates growth factor action in pancreatic carcinoma cells and is overexpressed in human pancreatic cancer.* The Journal of Clinical Investigation, 1998. **102**(9): p. 1662-1673.
129. Lin, H., et al., *Frequent Silencing of the GPC3 Gene in Ovarian Cancer Cell Lines.* Cancer Res, 1999. **59**(4): p. 807-810.
130. Lin, A.E., et al., *Cardiac anomalies in the Simpson-Golabi-Behmel syndrome.* American Journal of Medical Genetics, 1999. **83**(5): p. 378-381.
131. Pilia G, H.-B.R., MacKenzie A, Baybayan P, Chen EY, Huber R, Neri G, Cao A, Forabosco A, Schlessinger D., *Mutations in GPC3, a glypican gene, cause the Simpson-Golabi-Behmel overgrowth syndrome.* Nat Genet., 1996. **12**(3): p. 241-247.
132. Hennekam, R., *Hereditary multiple exostoses.* J Med Genet., 1991. **28**(4): p. 262-266.
133. Hecht, J.T., et al., *Differentiation-induced loss of heparan sulfate in human exostosis derived chondrocytes.* Differentiation; Research In Biological Diversity, 2005. **73**(5): p. 212-221.
134. Hecht, J.T., Hogue, D., Strong, L.C., Hansen, M.F., Blanton, S.H., and Wagner, M., *Hereditary multiple exostosis and chondrosarcoma: linkage to chromosome II and loss of heterozygosity for EXT-linked markers on chromosomes II and 8.* Am J Hum Genet, 1995(56): p. 1125- 1131.
135. W H Raskind, E.U.C., H Chansky, and M Matsushita, *Loss of heterozygosity in chondrosarcomas for markers linked to hereditary multiple exostoses loci on chromosomes 8.* Am J Hum Genet., 1995. **56**(5): p. 1132-1139.
136. McCormick C, D.G., Tufaro F., *New perspectives on the molecular basis of hereditary bone tumours.* Mol Med Today, 1999. **5**(11): p. 481-486.
137. Ropero, S., et al., *Epigenetic loss of the familial tumor-suppressor gene exostosin-1 (EXT1) disrupts heparan sulfate synthesis in cancer cells.* Human Molecular Genetics, 2004. **13**(22): p. 2753-2765.

138. Murphy, P.M., *Chemokines and the Molecular Basis of Cancer Metastasis.* N Engl J Med, 2001. **345**(11): p. 833-835.
139. Iozzo, R.V. and J.D. San Antonio, *Heparan sulfate proteoglycans: heavy hitters in the angiogenesis arena.* The Journal of Clinical Investigation, 2001. **108**(3): p. 349-355.
140. Häcker, U., K. Nybakken, and N. Perrimon, *Heparan sulphate proteoglycans: the sweet side of development.* Nature Reviews. Molecular Cell Biology, 2005. **6**(7): p. 530-541.
141. Rapraeger, A.C., K. Alison, and B.B. Olwin, *Requirement of Heparan Sulfate for bFGF-Mediated Fibroblast Growth and Myoblast Differentiation.* Science, 1991. **252**(5013): p. 1705-1708.
142. Presta, M., et al., *Fibroblast growth factor/fibroblast growth factor receptor system in angiogenesis.* Cytokine & Growth Factor Reviews, 2005. **16**(2): p. 159-178.
143. Allen, B.L. and A.C. Rapraeger, *Spatial and Temporal Expression of Heparan Sulfate in Mouse Development Regulates FGF and FGF Receptor Assembly.* The Journal of Cell Biology, 2003. **163**(3): p. 637-648.
144. Esko, J.D. and U. Lindahl, *Molecular diversity of heparan sulfate.* The Journal of Clinical Investigation, 2001. **108**(2): p. 169-173.
145. Esko, J.D., K.S. Rostand, and J.L. Weinke, *Tumor Formation Dependent on Proteoglycan Biosynthesis.* Science, 1988. **241**(4869): p. 1092-1096.
146. Varki, N.M. and A. Varki, *Heparin Inhibition of Selectin-Mediated Interactions during the Hematogenous Phase of Carcinoma Metastasis: Rationale for Clinical Studies in Humans.* Semin Thromb Hemost, 2002. **28**(01): p. 53-66.
147. Tóvári, J., et al., *Role of sinusoidal heparan sulfate proteoglycan in liver metastasis formation.* International Journal of Cancer, 1997. **71**(5): p. 825-831.
148. Borsig, L., et al., *Heparin and Cancer Revisited: Mechanistic Connections Involving Platelets, P-Selectin, Carcinoma Mucins, and Tumor Metastasis.* Proceedings of the National Academy of Sciences of the United States of America, 2001. **98**(6): p. 3352-3357.
149. Borsig, L., et al., *Synergistic Effects of L- and P-Selectin in Facilitating Tumor Metastasis Can Involve Non-Mucin Ligands and Implicate Leukocytes as Enhancers of Metastasis.* Proceedings of the National Academy of Sciences of the United States of America, 2002. **99**(4): p. 2193-2198.
150. Wang, L., et al., *Heparin's anti-inflammatory effects require glucosamine 6-O-sulfation and are mediated by blockade of L- and P-selectins.* The Journal of Clinical Investigation, 2002. **110**(1): p. 127-136.
151. Vlodavsky, I. and Y. Friedmann, *Molecular properties and involvement of heparanase in cancer metastasis and angiogenesis.* The Journal of Clinical Investigation, 2001. **108**(3): p. 341-347.
152. Ferguson, B.W. and S. Datta, *Role of Heparan Sulfate 2-O-Sulfotransferase in Prostate Cancer Cell Proliferation, Invasion, and Growth Factor Signaling.* Prostate Cancer, 2011. **2011**.
153. Abate-Shen, C. and M.M. Shen, *Molecular genetics of prostate cancer.* Genes & Development, 2000. **14**(19): p. 2410-2434.
154. Witte, J.S., *Prostate cancer genomics: towards a new understanding.* Nat Rev Genet, 2009. **10**(2): p. 77-82.
155. Mimeault, M. and S.K. Batra, *Animal models relevant to human prostate carcinogenesis underlining the critical implication of prostatic stem/progenitor cells.* Biochimica et Biophysica Acta (BBA) - Reviews on Cancer, 2011. **1816**(1): p. 25-37.

156. Mimeault, M. and S.K. Batra, *Frequent Gene Products and Molecular Pathways Altered in Prostate Cancer– and Metastasis-Initiating Cells and Their Progenies and Novel Promising Multitargeted Therapies.* Mol Med., 2011. **17**(9-10): p. 949–964.
157. Lin, X., *Functions of heparan sulfate proteoglycans in cell signaling during development.* Development, 2004. **131**(24): p. 6009-6021.
158. Ai, X., et al., *QSulf1 remodels the 6-O sulfation states of cell surface heparan sulfate proteoglycans to promote Wnt signaling.* J. Cell Biol., 2003. **162**(2): p. 341-351.

FIGURES

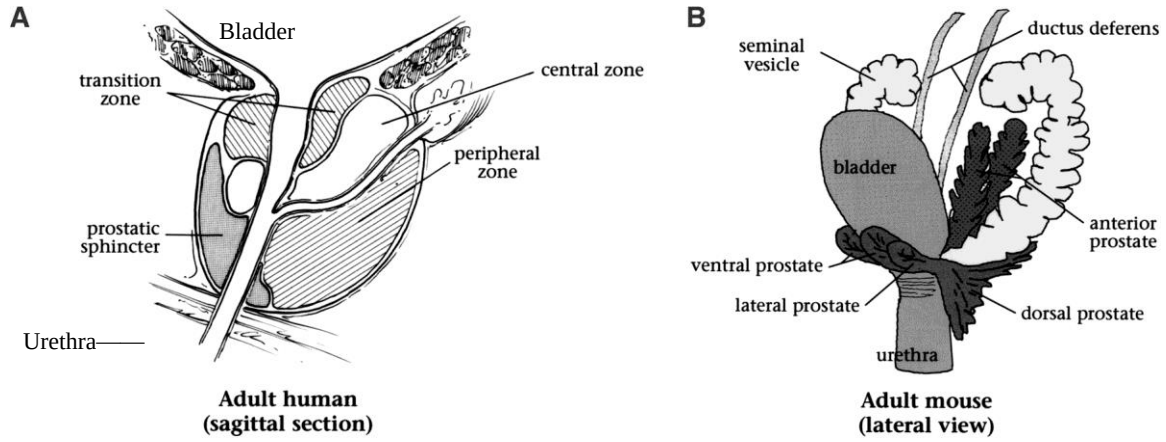

Figure 1.1 Schematic illustration of the anatomy of the human (A) and mouse (B) prostate. Human prostate is located under the bladder, connected to seminal vesicle and urethra. The mouse prostate location is similar to human with some morphology differences. It has several lobes; include coagulating gland (CG) or arterial prostate, ampullary glands, dorsal-lateral prostate and ventral prostate. Modified with permission from [153].

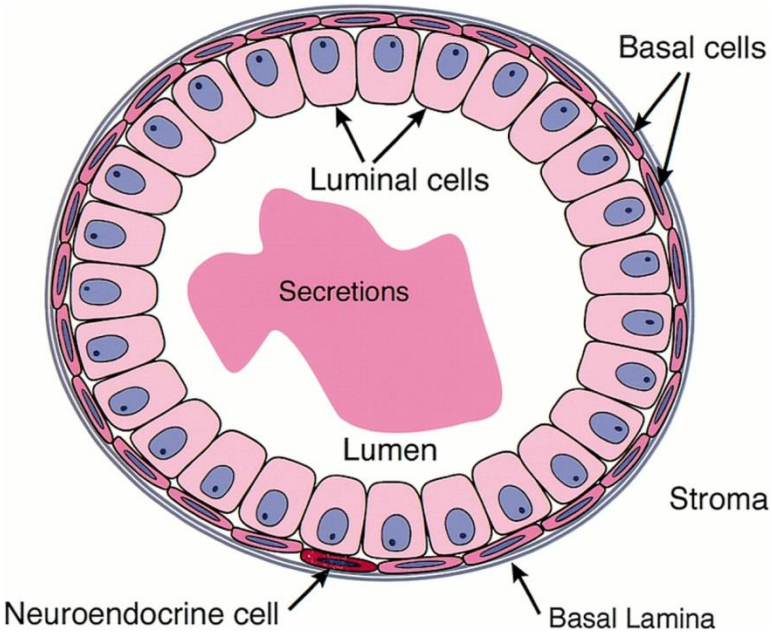

Figure 1.2 **Schematic depictions of the prostatic epithelial cell types.** Prostatic epithelium is mainly composed of basal and luminal cells along with a minor population of neuroendocrine cells. In normal prostate epithelium, a single layer of luminal cell and basal cells along with the basement membrane forms the wall of the prostate duct. Adapted with permission from [153].

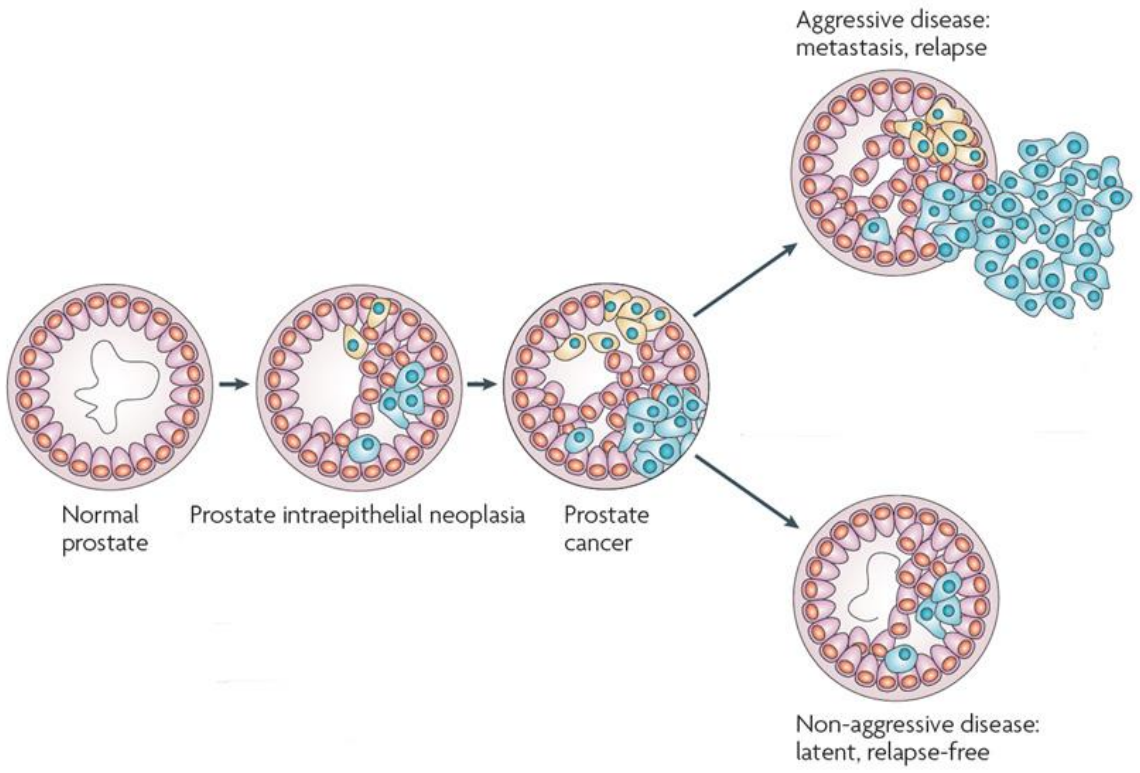

Figure 1.3. Prostate cancer progressions. The prostate cancer is developed from normal prostatic tissue, and the cancer development also goes through different stages, which includes: Normal prostate, PIN and then goes to invasive adenocarcinomas. PIN: Prostatic Intraepithelial Neoplasia. Adapted with permission from [154].

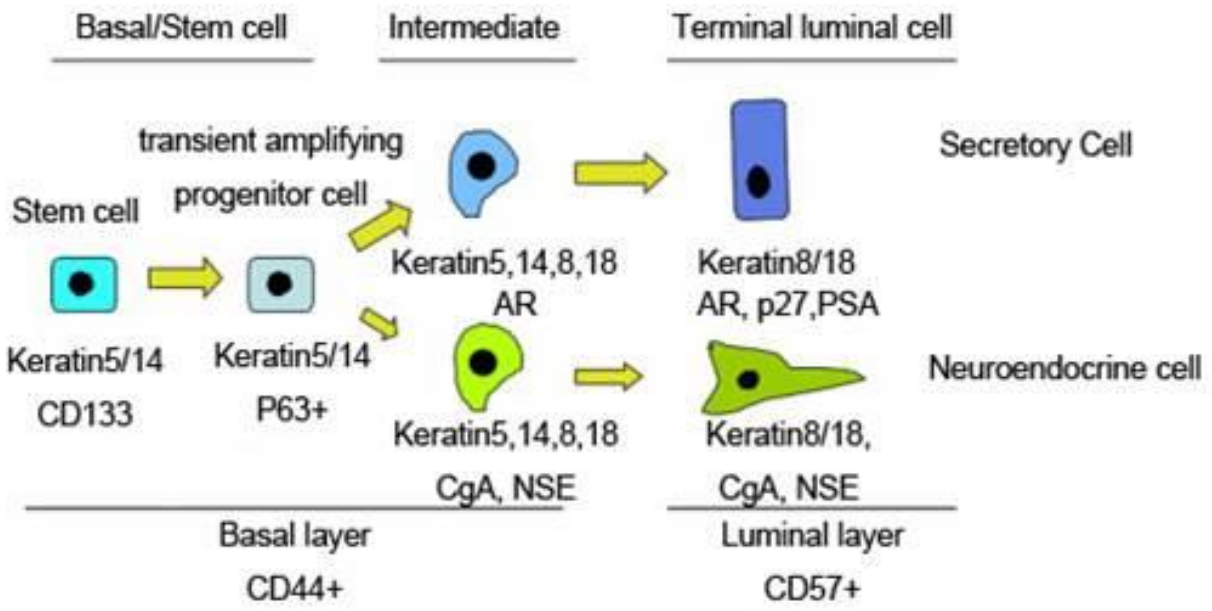

Figure 1.4 **Normal prostate epithelial cell differentiations.** Prostate epithelial stem/progenitor cells located within the proliferative basal cell compartment, which can differentiate into secretory luminal cells and neuroendocrine cells within the glandular epithelium. CgA: Chromogranin A; NSE: Neuron-specific enolase; AR: androgen receptor, PSA: prostate-specific antigen. Adapted with permission from [155].

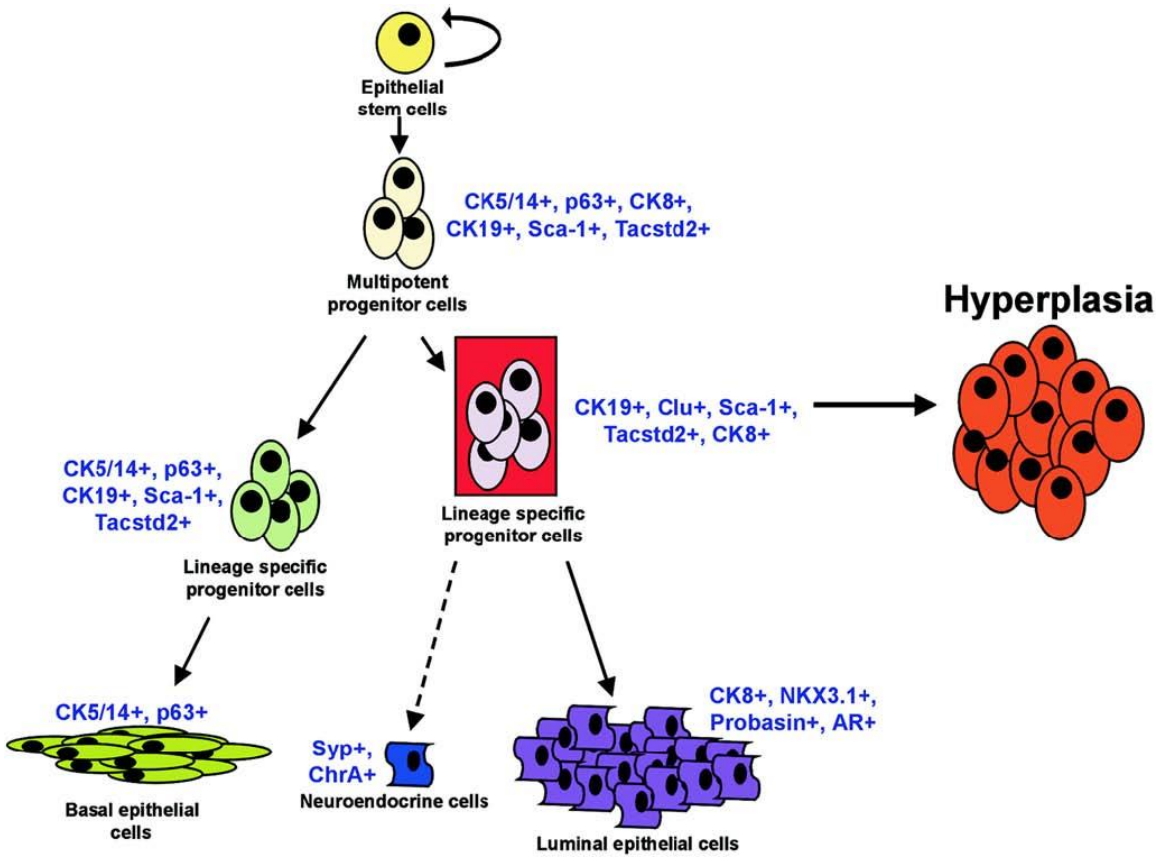

Figure 1.5 lineage-specific Clu^{+}Tacstd2^{+}Sca-1^{+} progenitor cells in the luminal epithelial cell layer as candidate tumor initiating cells in the PSA-Cre. Pten $^{loxP/loxP}$ mouse model share characteristics with previously postulated luminal intermediate/ TA(transit-amplifying)cells adapted with permission from [48]

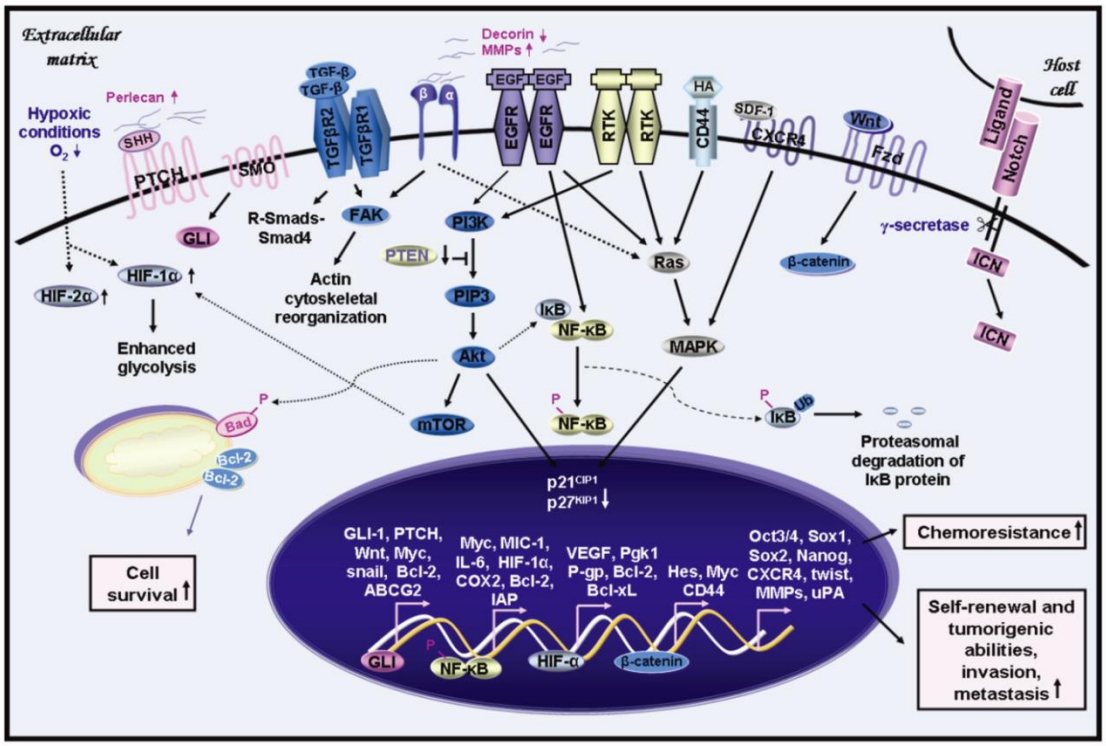

Figure 1.6 Signaling pathways involved in the malignant transformation of prostate stem/progenitor cells and their progenies during prostate cancer progression and metastasis. The activation of the SHH, TGF-β, EGFR, HA/CD44, SDF-1/CXCR4, and Wnt/ β-catenin signaling pathways may contribute to the sustained growth, survival and migration of Prostate cancer stem/progenitor cells and their progenies. Activation of the downstream signaling elements upregulated the expression of target genes involved in malignant transformation during the EMT process. The inhibition of $p21^{CIP1}$ and $p27^{KIP1}$ may promote the cell cycle progression and growth of cells. The enhanced expression of Bcl-2, Bcl-xl and IAP and phosphorylation of Bad may inhibit apoptosis and promote survival. The stimulation of HIFs under hypoxia condition may contribute to the enhanced glycolysis and prostate cancer cells become more malignant and chemoresistant. SHH: sonic hedgehog, HA: hyaluronan, IAP: inhibitor of apoptosis protein, EMT: epithelial-mesenchymal transition. Adapted with permission from [156].

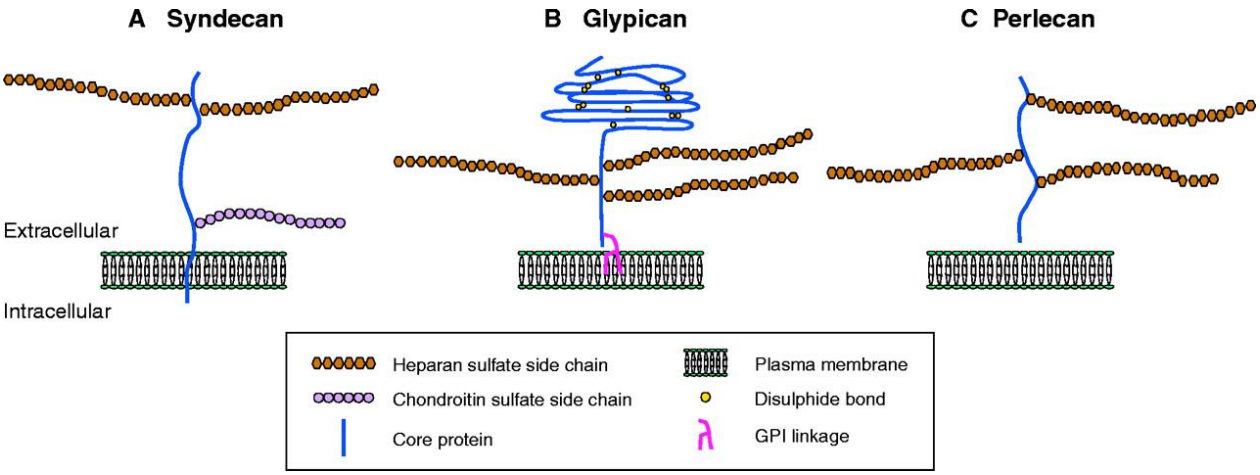

Figure 1.7 The three main classes of cell-surface heparan sulfate proteoglycans (HSPGs). (A) Syndecan core proteins are transmembrane proteins. Heparan sulfate (HS) chains attach to serine residues distal from the plasma membrane. Some syndecans also contain a chondroitin sulfate (CS) chain(s) that attaches to a serine residue(s) near the membrane. (B) The glypican core proteins are linked to the plasma membrane by a glycosylphosphatidylinositol (GPI) linkage. HS chains link to serine residues adjacent to the plasma membrane. (C) Perlecans are secreted HSPGs that carry HS chains. Adapted with permission from [157]

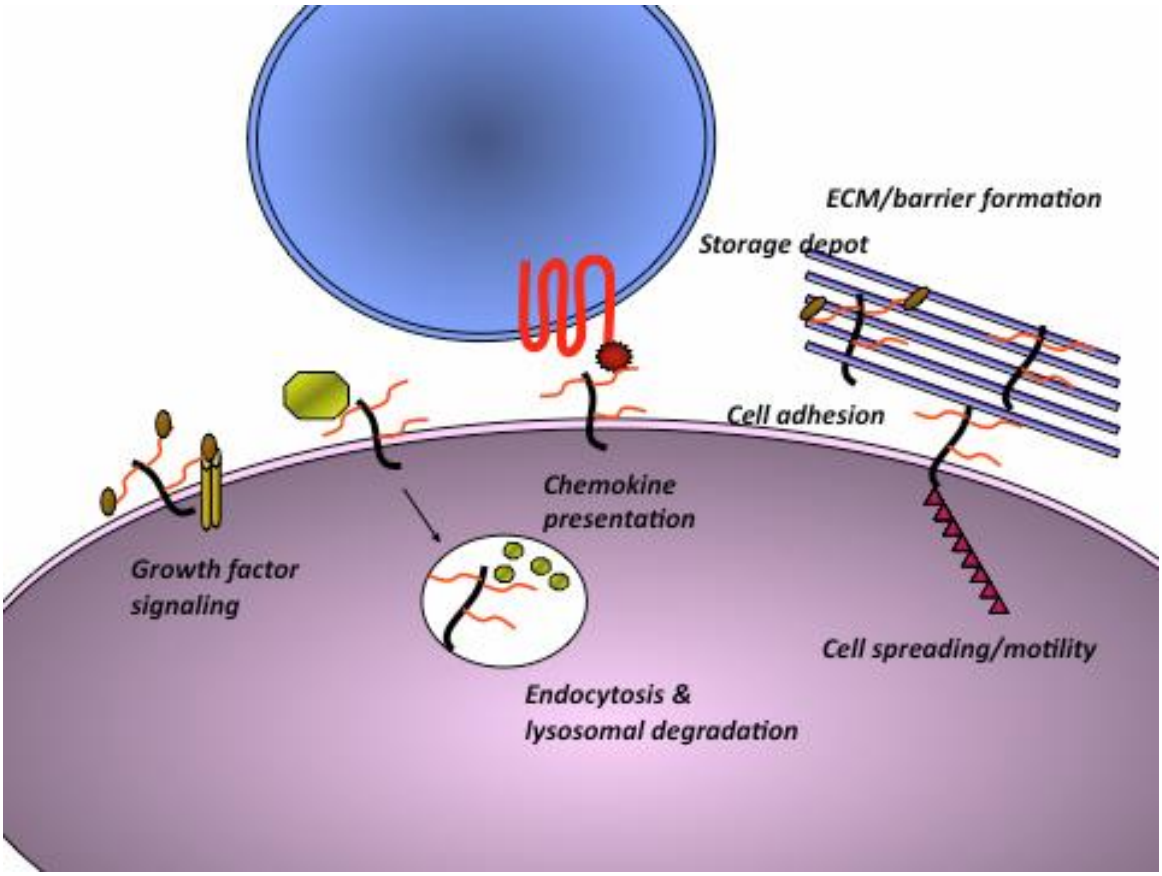

Figure 1.8 The roles of heparan sulfate in cell physiology. Heparan sulfate (HS) is required in most cell types for modulating cell signaling events. In hepatic cells, HS is involved the internalization of lipoproteins by acting as a bona fide receptor. At sites of injury, HS presents chemokines to adjacent leukocytes to trigger immune responses. HS binds to growth factors that may be stored in the extracellular matrix and that can be released through cleavage of the HS chain by heparanase. Acidic HS chains prevent crossing of solutes and act as physical barriers. HS, generally on syndecans, interact with components of the ECM to mediate functions that require remodeling of the cytoskeleton including cell adhesion, spreading and motility. Modified with permission from [116].

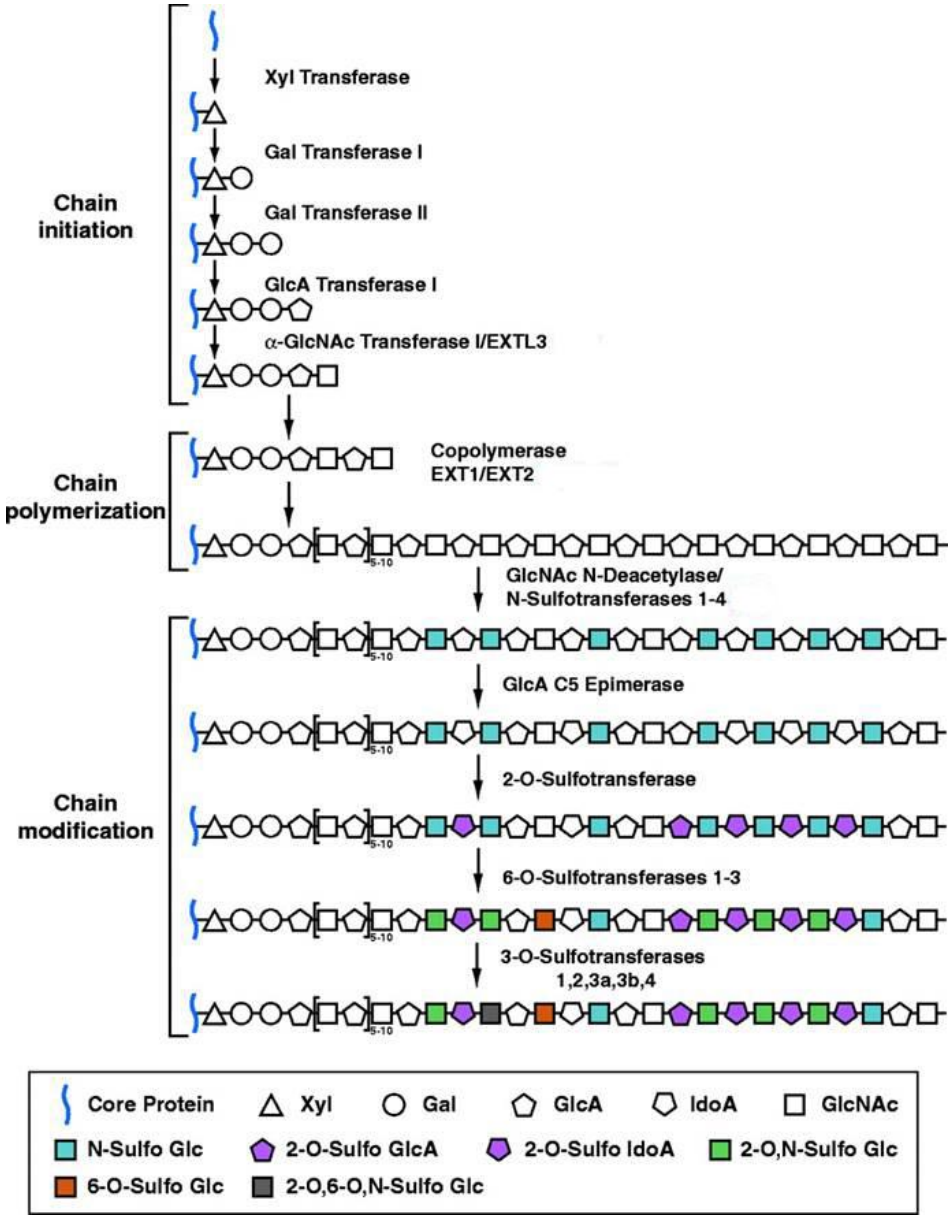

Figure 1.9 Heparan sulfate (HS) biosynthesis. Each sugar residue is depicted by a geometric symbol. In mammals, as many as 26 enzymes participate in the formation of HS chains. Central to HS formation is the co-polymerase complex composed of EXT1 and EXT2 that have both GlcA-transferase and GlcNAc-transferase activity and polymerize the HS chain in the Golgi apparatus. Adapted with permission from [157].

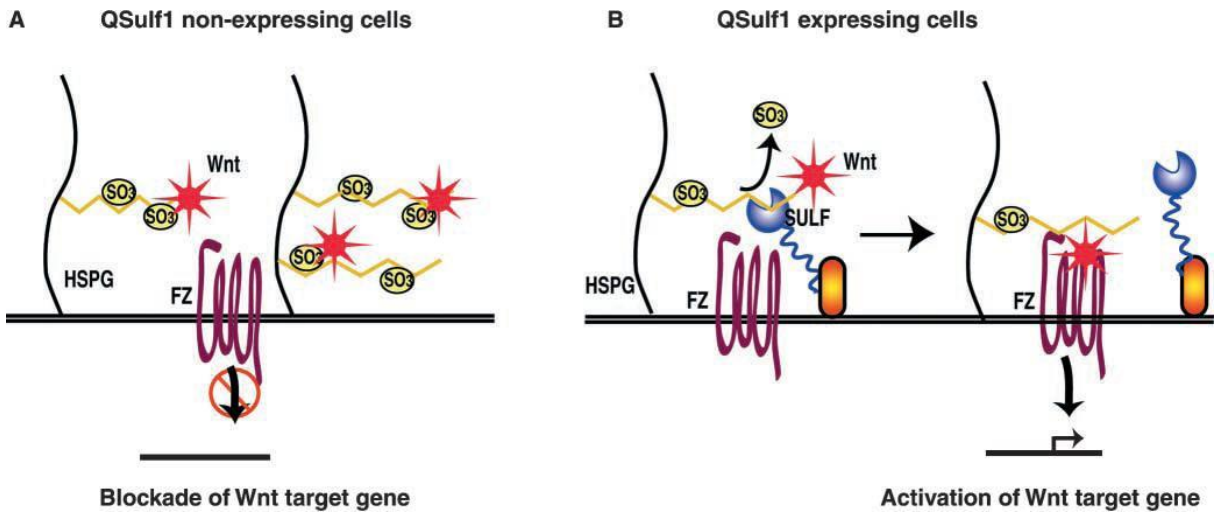

Figure1.10 A two-state catch or presentation model of QSulf1 regulation of Wnt signaling. (A) In QSulf1-nonexpressing embryonic cells, HS chains on cell surface HSPGs are in a 6-O–sulfated state, which binds with high affinities to catch Wnt ligands, preventing functional interactions of bound Wnts with their Frizzled receptors. (B) In QSulf1-expressing cells, selective 6-O desulfation activity of QSulf1 removes 6-O sulfates from HS chains on cell surface HSPGs to convert HS to a low affinity binding state for Wnts. 6-O–desulfated HS then can present Wnt ligands to Frizzled receptor and can form functionally active Wnt–HS–Frizzled receptor complexes for initiation of Wnt signal transduction. Adapted with permission from [158].

Tables

Table 1.1. Glycosaminoglycans. Glycosaminoglycans are composed of an N-acetyl-hexosamine and a hexose or hexuronic acid disaccharide repeat unit, and apart from hyaluronic acid are all sulfated.

Name	Uronic acid/ Hexose	Hexosamine	Linkage geometry
Heparan Sulfate	GlcA/IdoA	GlcNAc	**-4**GlcUA***β*1-4**GlcNAc***α*1-**
Chondroitin Sulfate	GalA	GalNAc	**-4**GlcUA***β*1-3**GalNAc***β*1-**
Dermatan Sulfate	GalA or IdoA	GalNAc	**-4**IdoUA***β*1-3**GalNAc***β*1-**
Keratan Sulfate	Gal	GlcNAc	**-3**Gal***β*1-4**GlcNAc***β*1-**
Hyaluronic Acid	GlcA	GlcNAc	**-4**GlcUA***β*1-3**GlcNAc***β*1-**

Table 1.2. Heparin/heparan sulfate-binding proteins (incomplete list)

Ligands	Heparan sulfate binding proteins
Growth factors	HB-EGFs (Heparin Binding Epidermal Growth Factors), FGFs (Fibroblast Growth Factors), VEGF (Vascular Endothelial Growth Factor), PDGF (Platelet-Derived Growth Factor), TGF-β (Transforming Growth Factor-β), HGF (Hepatocyte Growth Factor)
Extracellular matrix	Collagens, Fibronectin, Laminin, Tenascin, Thrombospondin I and II, Vitronectin
Morphogens	BMP 2, 4 and 7 (bone morphogenetic protein), Hh (Hedgehog) , Wnt (Wingless wg), Sprouty
Tissue remodeling factors	Tissue plasminogen activator; Plasminogen activator inhibitor; Protease nexin 1
Adhesion molecules and chemokines	L-selectin and P-selectin, N-CAM(Neural Cell Adhesion Molecule), PECAM-1(Platelet Endothelial Cell Adhesion Molecule) , MAC-1(Monocyte Adhesion Molecule) and chemokines, such as SDF-1

Adapted from [100].

Chapter 2: HEPARAN SULFATE IS REQUIRED FOR PROSTATE CANCER INITIATION AND PROGRESSION

Xuanyang Li, Tamas Nagy, Lianchun Wang. Manuscript to be submitted to *Cancer Research*.

Abstract

Prostate cancer (PCa) is one of the most prevalent forms of malignancy and the second most common cause of cancer-related death in men. The failure in treatment of this disease is our inability to prevent and control PCa growth and metastasis. A better understanding of the mechanisms underlying PCa pathogenesis will greatly enhance our effort to cure this life-threatening disease. Heparan sulfate (HS) is a linear, sulfated polysaccharide, and expresses abundantly in prostate and PCa tissues. Intriguingly, the HS content and sulfation modifications appear to increase when the prostate becomes malignance, suggesting that HS may critically modulate PCa pathogenesis. In current study, we specifically ablated Ext1, the enzyme that initiates HS biosynthesis, in mouse prostate at late development stage. The Ext1 ablation does not affect prostate development and function; instead, it protects the mice from tumorigenesis and invasion in a spontaneous PCa mouse model. Tissue staining showed that the Ext1 deficiency attenuated PCa cell proliferation, increased apoptosis, and blocked PCa stem/progenitor cell differentiation and epithelial-mesenchymal transition. The Ext1 deficiency PCa tissues also showed significant attenuation of fibrinosis, inflammation, MMP-9 activity and hypoxia. In summary, our studies demonstrate that HS functions via multiple mechanisms to promote PCa tumorigenesis and invasion, and also reveal that targeting HS may represent a novel and effective approach to cure PCa.

Introduction

Prostate cancer (PCa) continues to be a major health problem in the United States. This disease is estimated to account for 28.5% of all newly diagnosed malignancies among men in the United States in 2012. The American Cancer Society estimates that by the end of 2012, about 241, 740 men was expected to be diagnosed with PCa in the United States and 28, 170 men will die of it [1]. Make it the most commonly diagnosed cancer in men and the second second-leading cause of cancer death in men. For reasons that remain unclear, incidence rates are significantly higher in African Americans than in whites, 241 (per 100,000 men) versus 149, respectively, in 2008 [1]. Progressive prostate is commonly treated with androgen deprivation therapy; however, about 10% patients develop androgen-independent PCa, which is not actively proliferating and untreatable by using the current standard therapies. There has long been intensive interest in the basic mechanisms underlying PCa initiation and progression, and the potential to target these processes for therapeutic intervention of this life-threatening disease.

Heparan sulfate proteoglycans (HSPGs) are glycoconjugates composed of a core protein with one or more covalently attached HS chains [2-4]. HSPGs present abundantly on the cell surface (including syndecans and glypicans) and in the ECM (including perlecan, agrin and others) and because of their high negative charge, the HS chains widely bind to various of proteins under physiological conditions, including the members of the fibroblast growth factor (FGF) family and their receptor tyrosine kinases, transforming growth factors (TGFs), bone morphogenetic proteins (BMPs), Wnt proteins, chemokines and interleukins, as well as enzymes and enzyme inhibitors, lipases and apolipoproteins, and ECM and plasma proteins [5]. HSPGs are extraordinarily important in both development and cancer progression due to their regulation of cellular processes such as angiogenesis, tumor growth, proliferation, tumor invasion and

metastasis. HSPGs control various processes by modulating a variety of growth factor signaling pathways such as Sonic Hedgehog (SHH), FGF, VEGF, and TGFβ [2-4, 6, 7]. Most of the interactions of HSPGs with the ligands are mediated directly by the HS moieties [2-4, 8]. HS is a linear polysaccharide composed of glucosamine and uronic acid (glucuronic acid, GlcA, or iduronic acid, IdoA) disaccharide repeats with various sulfation modifications, and is typically 50-200 disaccharides in length.

HS is important for prostate branching morphogenesis. The development of prostate is a dynamic process and tightly controlled by androgen and HS-binding growth factors, such as FGF10[9-11]. HS abundantly presents in prostate tissue, especially at their attachment sites [12]. Interestingly, it was observed that HS content and degree of sulfation correlate with prostate development, suggesting that HS may regulate prostate development [13]. Recent studies demonstrated that Exogenous BMP4 and BMP7 in urogenital sinus (UGS) induced expression of Sulf1, a gene produces Sulfatase-1, inhibits bud development by reducing extracellular heparan sulfate (HS) 6-O sulfation and impairing FGF10 signaling by means of the ERK1/2 mitogen activated kinases [14]. FGF10 and FGF receptor 2 (FGFR2), which are facilitated by cell surface HS to form the FGF/FGFR2 signaling complex [15], are both essentially required for prostate development [9-11, 16, 17]. During prostatic organogenesis, messenger mRNA for FGF10 is localized in the mesenchyme, and the FGF10 receptor, FGFR2, is found in PECs of the urogenital sinus in embryos and in the distal signaling center of elongating and branching ducts in postnatal prostate. FGF10 can substitute for androgens in the organ culture of neonatal prostates, supporting extensive PEC growth and ductal-branching morphogenesis [10, 11]. Ablation of FGF10 alleles abrogates prostate development and diminishes androgen responsiveness of prostatic rudiments in organ-culture and tissue-recombination experiments [9].

Consistent with these observations, ablation of FGFR2, the high affinity receptor for FGF10 in PECs also disrupts prostate morphogenesis, which confirmed that FGF10-FGFR2 signaling is essential for prostate development [16, 17].

Various HS modulated growth factor signaling pathways are abnormally activated in many cancers including prostate cancer [18, 19]. Many heparan sulfate (HS)-binding molecules including growth factors, morphogens, adhesion molecules and chemokines, participate critically in these pathological processes. For example, upregulating transforming growth factor β (TGFβ), fibroblast growth factor (FGF) and morphogen Wnt promote PCa tumorigenesis [20-23]. The proteases matrix metalloproteinases (MMPs) facilitate PCa invasion, and chemokine SDF-1 promotes PCa metastasis [24-26]. With respect to cancer onset and progression, the structural diversity of tumor cell HS (both at the cell surface and ECM) enables them to modulate several aspects of tumor cell phenotype, including tumor cell growth, invasiveness and metastatic potential [27]. So, a given tumor-derived HS or HSPG can be tumor-promoting or anti-tumorigenic depending on whether it locates, anchored at the cell surface or present in the ECM, and depending on the HS sequence. The studies on HS or HSPGs have suggested that HS critically modulates multiple aspects of cancer biology [2, 5, 28-32]. Esko et al. found that subcutaneously injection of heparan sulfate-deficient Chinese hamster ovary cell mutants in nude mice did not produce tumors, suggesting that wild-type cell HSPGs enabled mutant cells to survive [33]. Reijmers et al. showed that RNAi mediated knockdown of syndecan-1 or EXT1 in human multiple myeloma cells leads to reduced growth rates and a strong increase of apoptosis, and dramatically suppresses the growth of metastatic myeloma in bone marrow after xenotransplantation of myeloma in Rag-$2^{-/-}\gamma c^{-/-}$ immunodeficient mice [34]. Ferguson and Datta recently demonstrated that knockdown of heparan sulfate 2-O-sulfotransferase (2OST) greatly

reduce proliferation and invasion of prostate cancer cells in the LNCaP-C4-2B model, while increase in actin and E-cadherin accumulation at the cell surface, a distinct sign of down-regulated epithelial-mesenchymal transition, thus reduced the metastatic potential [35]. These findings led to the hypothesis that that HS regulates prostate development and PCa tumorigenesis and metastasis *in vivo*.

Because HS structure is tempo-spatio regulated, and the xenograft tumor nude mice model missing the inflammation component, in order test these hypotheses we incorporated the conditional knockout Ext1 $^{loxP/loxP}$ allele to the Pten-null prostate cancer model to generate a mouse line that can simultaneously and prostate specifically knockout Ext1 and Pten. Our studies demonstrated that Ext1 ablation retards PCa tumorigenesis and invasion in *ΔPten* mice. We also observed reduced proliferation rate, increased apoptosis rate, and reduced proportion of malignant transit-amplifying (TA)/intermediate cells in *ΔExt1 ΔPten* mice compared with the Pten null prostate cancer model. Expression profiling analysis further indicates that changes in several growth factor signaling pathways may contribute to the inhibition of PCa initiation and progression in *ΔExt1 ΔPten* mouse prostates compared with *ΔPten* mice. The presence of cell surface HSPGs may provide a salvage pathway for uptake of circulating polyamines thereby sparing cells from the cytostatic effect of DFMO. It is believed that depletion of polyamines represents a strategy for the treatment of cancer [36]. All these evidence mentioned above suggesting HS is a promising therapeutic target for treating prostate cancer.

Experimental procedures

Animal Breeding

Pten $^{loxP/+}$ mice[C;129S4-Pten$^{tm1Hwu/J}$, #004597], carrying the loxp-modified Pten allele, were obtained from the Jackson Laboratory (Bar Harbor, Maine), Pb-Cre4^{+} mice [B6.Cg-Tg(Pbsn-cre)4Prb, #01XF5] were obtained from NCI Mouse Repository (Frederick, MD), Ext1 $^{loxP/+}$ mice, carrying the loxp-modified Ext1 allele were generated and maintained on a C57BL/6 background as described in reference[37]. Mice were housed at a specific pathogen-free facility, and the experimental protocol was approved by the Institutional Animal Care and Use Committee of the University of Georgia. Primers used to detect the transgenes for the purpose of genotyping and verification of deletions is listed in supplemental Table 2.S1.

Histology and immunochemistry analysis

Tissues were harvested and fixed with 4% paraformaldehyde overnight, rinsed well in PBS, and transferred to 70% ethanol. These paraffin-embedded tissues were sectioned (4 μm) and stained with hematoxylin & eosin solution (H&E, Sigma-Aldrich). All slides were analyzed blindly by veterinary pathologist in Department of Pathology, College of Veterinary Medicine, at University of Georgia.

All immunohistochemical staining was performed on 4 μm sections that were prepared from paraffin-embedded blocks and placed on charged glass slides. Antigen retrieval was performed by incubating the slides in 0.01 M citric acid buffer (pH 6.0) in pressure cooker for 20 min. Slides were then allowed to cool for 20 min in citric acid buffer. After washing in deionized water, the slides were then transferred to PBS (2 × 5 min each). The endogenous peroxidase activity was inactivated in a solution containing 0.3% hydrogen peroxide (H_2O_2). Blocking was performed in 10% normal serum with 1% BSA in TBS for 1 hour at RT. Primary antibody incubation was performed overnight at 4℃, followed by secondary antibody incubation at RT for

1 hour. The ABC staining system (Santa Cruz biotechnology Inc.) was used for signal amplification and chromagen visualization. Slides were counterstained in Mayer's hematoxylin, dehydrated, cleared, and coverslipped. Negative control slides were run without primary antibody. Control slides known to be positive for each antibody were incorporated. Anti-BrdU antibody was obtained from Developmental Studies Hybridoma Bank (catalog no.G3G4), and anti-ki67 antibody from Bethyl Laboratories, Inc. (catalog no. IHC - 00375).

Immunofluorescence

Double immunofluorescence (IF) was performed on cryosections of mouse prostate tissues. Blocking was performed in PBST with 10% normal serum for 1 hour at RT, and then incubated for 1 h at room temperature or 4℃ overnight with the following antibodies diluted according to manufacturers' instructions: anti-CK-5 and anti-CK-8 (Covance; catalog nos. AF 138 and HK-8), anti-AR (Millipore; catalog no. 06-680), anti-BCL-2 (BD Biosciences; catalog no. 610538), anti-P63 (Abcam; catalog no. ab124762). The slides were then incubated with secondary antibodies Alexa Fluor 488 conjugated goat anti-mouse IgG (Invitrogen; A11001) and Alexa fluor 594 conjugated goat anti-rabbit IgG (Invitrogen; A11037) in PBST with 1%BSA for 1 hour, and finally wash and mounted using VECTASHIELD® Mounting Medium with DAPI (Vector Laboratories; H-1200). Fluorescent images were captured using a Nikon Eclipse 90i microscope system.

Gelatin zymography

30 μg total protein of tissue extracts was electrophoresed under nonreducing conditions in a 10% acrylamide gel containing 0.1% gelatin (Life Technologies, Grand Island, NY), according to the method of Fisher and Werb [38]. After electrophoresis, the gels were washed at room

temperature for 1 h in 2.5% Triton X-100, 50 mm Tris-HCl, pH 7.5 and then incubated at 37 C overnight in buffer containing 150 mm NaCl, 5 mm CaCl2, 50 mm Tris-HCl, pH 7.6. Thereafter, gels were stained with 0.1%(wt/vol) Coomassie brilliant blue R-250 in 30% (vol/vol) isopropyl alcohol, 10% glacial acetic acid for 60 min and destained in 10% (vol/vol) methanol, 5% (vol/vol) glacial acetic acid. Semiquantification of the bands intensity corresponding to 92-kDa gelatinases was performed with imageJ software.

RNA preparation

For quantitative real-time qRT-PCR and microarray analyses, prostate tissues were removed from euthanized mice at 13 weeks or 5 weeks old. Dorsal, lateral, ventral and anterior prostate lobes were dissected and immersed immediately in RNALater (QIAGEN Inc.). All the lobes of an individual mouse were pooled and homogenized using a Kinematica PT 2100 homogenizer. RNA extraction was performed according to the standard protocol of RNeasy kit (QIAGEN Inc.).

Quantitative PCR

First-strand cDNA was synthesized from 200 ng of total RNA using the iScript cDNA Synthesis Kit (Bio-Rad). SYBR-Green RT-PCR was performed as described in reference[39]. The housekeeping gene GAPDH was included as loading control. Primers were designed to span introns to prevent detection of genomic DNA contaminants (Primers used are listed in supplemental Table 2.S2). P values were obtained using ANOVA analyses with 2 factors (genotype and run variation) in an additive model.

Expression profiling using DNA microarray

Nine samples of RNA derived from murine prostates were submitted to the DNA Array Core Facility at the Scripps Research Institute for microarray analyses, including three wild types (PBCre^{-}Pten$^{loxP/loxP}$ Ext1$^{loxP/loxP}$), three Pten knockouts (*ΔPten*) and three Pten and Ext1 knockout (*ΔExt1 ΔPten*). Affymetrix GeneChip Mouse Gene 1.0 ST Arrays were used to cover the whole-transcript; each array consisted of 28,853 unique mouse cDNAs.

Bioinformatics

All detected RNA transcripts in Gene Expression Microarray analysis were analyzed using Ingenuity Pathway Analysis (IPA, Ingenuity Systems, Redwood City, CA) by core analysis. The over represented biological processes, molecular functions and canonical pathways were generated based on information contained in the Ingenuity Pathways Knowledge Base. The significance of the association between the data set and the canonical pathway was measured in 2 ways: 1) A ratio of the number of molecules from the data set that map to the pathway divided by the total number of molecules that map to the canonical pathway is displayed. 2) Fisher's exact test was used to calculate a p-value determining the probability that the association between the genes in the data set and the canonical pathway is explained by chance alone.

Statistical analysis

Experimental data is presented as means ± SD from at least three independent experiments. Statistical analysis of the data was performed by Student's t-test. P values of ≤ 0.05 were considered statistically significant. Hierarchical cluster analysis was performed in R software environment (a GUN project) between *ΔPten* and *ΔExt1 ΔPten* mouse prostates to generate heat map using the hclust function.

Results

The expressions of HS biosynthetic genes are upregulated in prostate cancer

Although the etiopathogenesis of PCa is still largely unknown, clinical studies have mapped multiple gene mutations/deletions contributing to human PCa pathogenesis. Among these findings, *Pten* (*phosphatase and tensin homolog)* tumor suppressor gene deletions and/or mutations were found in 30% of the primary human PCas and 63% of the metastatic human PCa cases, placing *Pten* mutations among the most common genetic alterations in human PCa pathogenesis [40, 41]. Consistent with the clinical findings, prostate epithelial cells (PEC)-specific *Pten* knockout (*ΔPten*) mice develop spontaneous PCa which recapitulates the full pathological processes of PCa seen in humans with 100% penetrance and defined kinetics. This mutant mouse provides a suitable model system to examine the control mechanism of PCa pathogenesis.

HS was reported to express in prostate and in PCa tissues [42-46], however, whether HS expression correlates with PCa and its progression as well as whether HS functions to modulate PCa pathogenesis have not been known. To explore these possibilities, we initially generated *ΔPten* ($PBCre^{+}Pten^{loxP/loxP}$) mice by breeding transgenic *PBCre*$^{+}$ mice with $Pten^{loxP/loxP}$ mice. PBCre was reported to specifically ablate floxed gene in prostate epithelial cells (PEC). To confirm prostate-specific Pten deletion, the prostate lobes as well as other tissues from *ΔPten* mice at the age of 10 weeks were dissected and the status of Pten were examined by PCR and immunofluorescence (IF) analyses. PCR analysis showed that Pten deletion, which is indicated by excision of the exon 5 of Pten gene (Pten-), was specific to the prostate gland (Figure 2.1B). Immunofluorescence analysis demonstrated that Pten is highly expressed in wildtype prostatic epithelial cells, whereas absent in *ΔPten*-PECs (Figure 2.1A), which is consistent with previous report [47]. The AKT serine/threonine kinase is one of the primary targets of the PTEN

regulated signaling pathway. Elevated AKT phosphorylation and plasma membrane localization are indicative of Pten loss [47]. AKT phosphorylation is hardly detectable in the wild type prostate while highly expressed in *ΔPten* prostates (Figure 2.1A), further indicating that *Pten* was effectively ablated and activated downstream signaling that is required to initiate PCa tumorigenesis in our *ΔPten* mice.

The *ΔPten* PCa develops with a defined kinetics: hyperplasia at 4 weeks, prostatic intraepithelial neoplasia (PIN) at 5-7 weeks, invasive and metastatic cancer at 9 weeks and older [47, 48]. To determine whether HS expression correlate with PCa tumorigenesis, we compared the expression of HS biosynthetic enzymes in PCa and normal prostates collected from *ΔPten* and littermate wildtype mice, respectively, at 5 weeks of age. The expression of 21 HS biosynthetic genes in the collected prostates was determined by qRT-PCR analysis. Compared to wildtype prostates, the expression of 15 genes were upregulated and 2 genes were downregulated in *ΔPten* prostates (Figure 2.1C). The upregulated genes include Ext1 and Ext2, the HS chain elongation enzymes; the EXT-like genes Extl2 and Extl3, both involved in initiation of HS chain, Extl3 also involved in extension [49, 50]; Ndst1 and Ndst2, which are N-deacetylase/N-sulfotransferases act on discrete regions of the HS precursor, replacing N-acetyl groups with N-sulfates following the chain elongation [51]; 2-, 3-, and 6-O-sulphotransferase Hs2st, Hs3st1, Hs3st3a1, Hs3stb1, Hs3st6, Hs6st1 and Hs6st3. The two downregulated genes are Ndst3 and Hs6st2. Ndst3 is dispensable for development or adult homeostasis due to compensation by other Ndst isoforms [52]; Hs6st1 and Hs6st3 were highly expressed in Δ*Pten* prostates which may functionally compensate for the low expression of Hs6st2. In general, the expression of majority of HS biosynthesis genes, especially the dominantly functional genes such as Ext1, Ext2, Ndst1, Ndst2, Hs2st, Hs6st1 and Hs3st1, are upregulated in *ΔPten* prostates. To determine whether the

upregulated gene expression leads to HS structure alteration, we analyzed HS isolated from the collected prostates at 9-10 weeks of age.

In summary, these observations demonstrate that HS expression correlates with PCa and its progression, and suggest that HS may critically modulate PCa pathogenesis.

PB-Cre-mediated _Ext1_ ablation abolishes PEC-HS production, but does not affect prostate development and function.

HS has been shown to play essential role in organ development, such as brain. HS expresses abundantly in prostate, and especially several HS-dependent growth factors, such as FGF10 [9], are essentially required for prostate development, suggesting that HS might be required for prostate development. To address this issue, we specifically ablated *Ext1*, the gene that initiates HS biosynthesis, by breeding $Ext1^{loxP/loxP}$ mice with transgenic PB-Cre mice to generate *ΔExt1* ($PBCre^{+}Ext1^{loxP/loxP}$) mice. Mouse prostate development is initiated at embryonic day 17 (E17), completed approximately 80% by postnatal day 10 (P10), and the whole process is completed within 60-90 days [16, 53]. The *PB-Cre*-mediated gene inactivation occurs at P7 and progresses to the majority of PECs at P14 [54-56]. Therefore, *PB-Cre*-mediated gene ablation occurs after the major prostate developmental stage. To determine whether the *Ext1* allele was specifically ablated in *ΔExt1* prostate, genomic DNA from 6-week-old *ΔExt1* mouse prostates and other organs were analyzed by genomic PCR [37]. The *Ext1* deletion (***Ext1-***) was detected only in the *ΔExt1* prostate (all lobes), not in other organs (Fig. 2.3B), showing that the *PB-Cre*-mediated *Ext1* ablation is prostate-specific as reported [54-56]. As expected, anti-Ext1 and anti-HS antibody staining detected abolished Ext1 and HS expression in the *ΔExt1* prostates (Fig. 2.1D). To determine whether the *Ext1* deletion affects prostate development, 4- to 20-week-old mice

were examined. The *ΔExt1* prostates had normal numbered- and sized-prostatic lobes (Figure 2.1E, a-b). Macroscopic examination showed that the *ΔExt1* prostates have similar number of branches, diameter, and length of the ducts of wildtype controls (Figure 2.1E, c-d). H&E staining of the 10 weeks old prostate shows both wildtype and *ΔExt1* prostates have a single layer of epithelium surrounded by a prominent smooth muscle coat, similar numbers of the intraductal mucosal infolding, which are also consist of single layer of epithelium, and loosely arranged stroma around the gland (Figure 2.1E e-f). All these are characteristics of normal prostate. Our breeding records suggest that the male *ΔExt1* mice reproduced normally (data not shown), showing that PB-Cre-mediated *Ext1* ablation does not affect prostate development and function.

Prostate epithelial cell-specific ablation of Ext1 protects mice from PCa tumorigenesis

To assess the role of HS in PCa pathogenesis, we conditionally ablated Ext1 in the prostate epithelium of *ΔPten* mice. Prostates at different ages were collected and histologically examined after H&E staining. All 4- to 5-week-old *ΔPten* prostates developed severe neoplasia (Figure 2.2 B, E), and 13-week-old *ΔPten* prostates all developed high grade PIN (Figure 2.2 H,K,N) with some featuring of invasive prostatic carcinoma (IPC) (n=5 per group). Prostates from 4- to 5-week-old *ΔExt1 ΔPten* mice remained normal or only exhibited low grade hyperplasia (Figure 2.2 C, F), and the 13-week-old only showed low grade of PIN with some area remaining normal (Figure 2.2 I, L, O). Examination of older prostates, the difference became even visually distinguishable. Gross anatomy examination of prostates at 40 weeks of age shows that although *ΔExt1 ΔPten* prostates were larger than wild type, they were still significantly smaller than the *ΔPten* prostates (Figure 2.2P). Quantitation showed that the weight of the *ΔPten* prostates (1.312 gram, n=5) was about 20 times of wildtype control (0.066 gram, n=5), whereas the *ΔExt1 ΔPten*

prostates (0.266 gram, n=5) was only 4-times the size of the wildtype control (Figure 2.2Q). Collectively, our results demonstrate that Ext1 ablation blocks PCa tumorigenesis.

Ext1-deficient prostate cancer cells are less proliferative and more apoptotic

BrdU immunostaining and TUNEL assays were performed to examine whether the attenuated PCa tumorigenesis in *ΔExt1ΔPten* mice was associated with inhibition of proliferation and stimulation of apoptosis, respectively. BrdU immunostaining analysis was carried out with prostates collected from 13-weeks old mice two hours post BrdU injection, and observed that the number of BrdU-positive cells in prostates of *ΔExt1ΔPten* mice was significantly less as compared with the prostates of *ΔPten* mice (Figure 2.3A-C). This observation was also reflected by the calculated cell proliferation index rate. The proliferation index rate in *ΔExt1ΔPten* prostates was significantly lower than that of *ΔPten* prostates and was positively correlated with the decrease of prostate weight (Figure 2.3D). PCa cell apoptosis was assessed by TUNEL staining. TUNEL analysis of prostates at 13 weeks of age detects *ΔExt1ΔPten* prostate cells have significantly increased apoptosis on epithelial cells compare to *ΔPten* prostates. Quantification of TUNEL staining shows that *ΔExt1ΔPten* prostates have around 5-fold more cells undergoing apoptosis than the cells in *ΔPten* prostates (Figure 2.3E-H). Collectively, these observations demonstrate that attenuation of cell proliferation and increase in apoptosis both contribute to disrupted PCa tumorigenesis.

Ext1 deficiency disrupts prostate stem/progenitor cell differentiation

Recent studies proposed that the development of cancer may mainly derive from the clonal expansion of cancer stem cells and/or their early progenies. Cancer stem cells having a capacity of an aberrant differentiation potential may give rise to their daughter cells, the malignant transit

amplifying (TA)/ intermediate cells (IC) cells that exhibited various stages of differentiation, end up with terminally differentiated cancer cells [37]. The TA cells in PCa are immunophenotypically defined intermediate forms that express both cytokeratin (CK) 5 and 8 [37]. Co-immunofluorescence of 10-weeks old prostates showed that the CK5 and CK8 double positive cells were much less in *ΔExt1ΔPten* prostates compare with *ΔPten* prostates (Figure 2.3 I-K). As examples in higher magnification confocal pictures in Figure 2.3 I'-K', *ΔPten* prostates have a markedly enlarged area of CK5 and CK8 co-localized cells which indicate TA/IC cell populations, in contrast *ΔExt1ΔPten* prostates only have scattered TA/IC cells. The index "overlap coefficient" was applied to quantify the relative abundance of the CK5 and CK8 double positive cells, and determined that the overlap coefficient for *ΔExt1ΔPten* PECs was less than 2/3 of that in *ΔPten* prostates (Figure 2.3L). In summary, these observations demonstrate that Ext1 ablation also disturbs PCa stem cell differentiation into TA/IC cells, thereby contributing to the attenuation of PCa tumorigenesis.

Ext1 deficiency alters multiple signaling pathways associated with tumorigenesis

Our studies show that *ΔPten* prostates at the age of 4-5 weeks had developed higher grade of mPIN, in contrast *ΔExt1ΔPten* prostates showed normal structure or developed only hyperplasia at limited areas (Figure 2.2 A-F). Therefore, we assume that the tumorigenesis molecular events have already been triggered at the age of 5 weeks and are modulated by HS. In order to further investigate the molecular events associated with HS-promoted PCa tumorigenesis, we compared gene expression profiles of 5 weeks old *ΔExt1ΔPten* prostate with age-matched *ΔPten* prostates by Gene Expression microarray analysis. In total, 29,168 genes were examined and detected 24,034 genes that were expressed. Statistical analysis of the detected gene observed that

comparing to *ΔPten*, 1302 and 1446 genes were down- and up-regulated, respectively, in *ΔExt1ΔPten* prostates. The heatmap for the differential gene expression is shown in Figure 2.4 A.

To systematically decipher cellular functions regulated by HS, we performed pathway enrichment analysis of the detected transcripts with ingenuity pathway analysis software. In total, 25 functional networks were identified to be HS dependent. The top three identified functional networks include cell growth and proliferation, cellular survival and death, and cell cycle (Table 2.1), is in good agreement with the blockage of PCa tumorigenesis by Ext1 ablation as we have described. To systematically determine the molecular pathways modulated by HS in PCa tumorigenesis, Ingenuity knowledge-based signaling pathway analysis (IPA) was performed and determined that, compared to *ΔPten*, 19 signaling pathways were altered in the Δ*Ext1ΔPten* PCa cells (Figure 2.4B), including both intrinsic and extrinsic signaling.

The intrinsic hypoxia-inducible factor 1α (HIF1α) signaling was identified to the most significantly different pathway between *ΔPten* and Δ*Ext1ΔPten* prostates. To validate this finding, the mice were injected with pimonidazole, a chemical which probes cells residing in an environment with oxygen concentration less than 14 micromoles. Following, prostate tissue sections were stained for the hypoxia-probe with a specific antibody. As showing in Figure 2.4Ca-c, the *ΔPten* prostate had a very strong hypoxia staining, whereas the staining was barely seen in the *ΔExt1ΔPten* prostates. HIF1α signaling is known to be detectable as adaptive metabolic response to hypoxia, and is also activated to eliminate toxic metabolic waste products generated by the tumor-specific metabolism even under normoxic conditions. The high hypoxia exists in *ΔPten* prostate indicates that tumor-specific metabolism is active in the 5 weeks old *ΔPten* prostates, and the tumor-specific metabolism was attenuated by Ext1 deletion as manifested by low to no hypoxia in *ΔExt1ΔPten* prostates. The IPA-based signaling analysis also

identified alteration of intrinsic pathways of ERK/mitogen-activated protein kinases (MAPKs) and PI3K/AKT signaling, and these findings were further examined by anti-pERK and pAKT staining. As shown in Figure 2.3Cd-I, the both staining were significantly reduced in *ΔExt1ΔPten* prostates compared to *ΔPten* prostates, indicating that Ext1 ablation disrupts both signaling. Especially, the Pten mutant has been known to activate mainly PI3K/AKT pathway to lead to PCa, this observation also provided direct evidence showing that Ext1 deletion disrupts PI3K/AKT signaling to attenuate PCa tumorigenesis. In addition, the pERK staining appeared to be restricted in basal cells, suggesting that the blockage of PCa stem cell differentiation in *ΔExt1ΔPten* prostates may be due to the disruption of the HS-dependent pErk signaling.

The analysis of extrinsic signaling identified several signaling that were significantly different between *ΔPten* and *ΔExt1ΔPten* prostates, including Notch, epidermal growth factor (EGF), insulin-like growth factor I (IGF-I), hepatocyte growth factor (HGF), platelet-derived growth factor (PDGF), transforming growth factor β (TGF-β), fibroblast growth factor (FGF), vascular endothelial growth factor (VEGF) and sonic Hedgehog. The alteration of TGF-β and Hedgehog signaling were further confirmed by qRT-PCR analysis of their target gene expression. For the TGF-β signaling pathway, positive responsive genes *Id1* and *Col1a2* were downregulated, and the negative responsive gene *Myc* was upregulated of in *ΔExt1ΔPten compared to ΔPten* prostates; similarly, the positive responsive gene *Gli1 of* hedgedog signaling was downregulated, and the negative responsive gene *PAI-1* was upregulated of in *ΔExt1ΔPten compared to ΔPten* prostates. These observations demonstrate that Ext1 deletion disrupts both TGF-β and hedgedog signaling during PCa tumorigenesis. Our microarray-IPA analysis did not identify difference in Wnt signaling between *ΔExt1ΔPten* and *ΔPten* prostates. Considering that Wnt signaling critically promotes PCa tumorigenesis, we analyzed the expression of Wnt signaling related

genes, and found that the positive responsive gene *Axin1* was downregulated in the *ΔExt1ΔPten* prostates, suggesting that Ext1 deletion disrupts Wnt signaling as well. In summary, this gene expression microarray-IPA analysis and verification experiments demonstrate that Ext1 deficiency blocks PCa tumorigenesis via disruptions of multiple cellular functions and multiple molecular signaling.

Prostate epithelial cell-specific ablation of Ext1 protects mice from PCa invasion by inhibition of EMT and MMP-9

Histologically examinations of 13-week-old mouse prostates observed that invasive carcinoma occurred in all five *ΔPten* prostates examined, but not seen in any of the five similarly examined *ΔExt1ΔPten* (Figure 2.5 A-C), showing that Ext1 ablation disrupts local invasion of the PCa cells. For PCa becomes invasive, the PECs need to obtain motile ability via a process termed epithelial-to-mesenchymal transition (EMT), during this process the PECs loss their epithelial cell markers such as E-Cadherin and acquire mesenchyme cell features, such as expression of α-smooth muscle actin (αSMA), in normal prostate SMA is only expressed in the smooth muscle layer outside of the basal MPCs. To determine whether the Ext1 deletion blocks EMT thereby to disrupt PCa local invasion, the 13-weeks old prostate tissue sections were immunofluorescence stained for E-cadherin and αSMA respectively. As displayed in Fig. 2.5 D-I, the *ΔPten* PECs lost E-cadherin expression but strongly expressed αSMA, showing that the *ΔPten* PECs were undergoing EMT. *While, the ΔExt1ΔPten* MPCs remained strong E-cadherin expression with a low level expression of αSMA, indicating that Ext1 ablation inhibits EMT to disrupt PCa local invasion. To invade, PCa cells also frequently express and secrets various proteinases, most notably are the matrix metalloproteinases (MMP), to degrade surrounding tissues along their migration path. To test whether Ext1 ablation affects MMP activities, gelatin zymography

analysis was performed with 13-old prostates. As shown in Figure 2.5J, high MMP9 activity was detected high in *ΔPten* prostates and very low in *ΔExt1ΔPten* prostate. Quantitation showed that the MMP9 activity was 67% lower in *ΔExt1ΔPten than in ΔPten* prostates (Figure 2.5K). Collectively, these observations demonstrate that Ext1 ablation disturbs both EMT and MMP9 activity to block PCa local invasion.

Ext1 deficiency disrupts the protumorigenic prostate cancer cell-stroma fibroblast cross-talk and inflammation

Cancer progression is not solely regulated by the interruption of oncogene and tumor suppressor pathways, but also co-depends on the stromal compartment to create a more tumor promoting microenvironment. Recent studies support the notion that the growth and the invasive potential of carcinoma cells are influenced by host stromal cells, collectively called "reactive stroma" [57-59]. Fibroblasts and smooth muscle cells, the two main cell types in stroma, can flexibly regulate their proliferation rate and phenotype in response to the state of tissue homeostasis. Cancer cell proliferation and invasion through the basement membrane into the stromal compartment will disrupt the normal tissue homeostasis, and stimulate a potential stromal cells phenotypic switching, that is fibroblasts and smooth muscle cells switching into the myofibroblast phenotype. These morphologically transformed cells are also termed as tumor-associated fibroblasts (TAF) characterized by the expression of proteins such as fibroblast activation protein (FAP). The wound repair caused by cancer cell proliferation and invasion will activate TAFs synthesize the major extracellular matrix compartments of granulation tissue, like fibronectin, collagen type Ⅰ and Ⅲ, and many other glycoproteins and proteoglycans[60]. Normal mouse prostate epithelial acini are surrounded by a thin layer of smooth muscle cells, and rarely observable fibroblasts. When we histologically examined H&E staining *ΔPten* prostates, a high

thickness collagenous stroma was seen surrounding the PCa cells with the extra-prostatic compartment filled by dense collagen fibers, especially around the invasive carcinoma. In contrast, the *ΔExt1ΔPten* prostates showed a much thinner collagenous stroma surrounding PCa cells; even though they are still thicker than normal mouse prostate (Figure 2.6 A-C). Immunofluorescence staining of the prostate tissues observed that the expression of TAF was dramatically reduced in *ΔExt1ΔPten* prostates than in *ΔPten* prostates (Figure 2.6 D-F), showing that PCa cell-stimulated stromal cell switching to TAFs was disrupted in the *ΔExt1ΔPten* prostates. Collectively, these observations demonstrate that Ext1 ablation disrupts the protumorigenic cross-talk between PCa cell and the stromal cell, contributing to inhibition of PCa tumorigenesis and local invasion.

Ext1 deficiency attenuates inflammatory response in prostate cancer

Epidemiological data suggests a link between prostate inflammation and subsequent PCa development [61]. Recent genetic study in mice observed that a constitutive activation of IkB kinase 2 in prostate epithelium was insufficient for prostate transformation, but in combination with heterozygous loss of Pten led to an increase in tumor size, formation of cribriform structures, and increase in fiber in the fibroblastic stroma, proving the concept that inflammation promotes PCa progress [62]. Analog to clinical observations, chronic inflammation was reported to occur in *ΔPten* prostates in mice [62-65]. Consistent with these reports, examination of 13 weeks old prostates observed very a few leukocytes in wildtype stroma, indicating no inflammatory response in wildtype prostates (Figure 2.6G, G'); however, large foci of inflammatory cells (Figure 2.6H-1, H'-1) as well as high density of infiltrating leukocytes were seen in *ΔPten* stroma (Figure 2.6 H-2, H'-2), indicative of active chronic inflammation in *ΔPten* prostates. The inflammatory cell foci were not observed in *ΔExt1ΔPten* stroma, meanwhile, the

density of infiltrating leukocytes was much lower compared to the *ΔPten* prostates (Figure 2.6 I, I'). In together, these observations demonstrate that Ext1 deletion disrupts leukocyte infiltration, thereby inhibiting inflammation-promoting effect on PCa tumorigenesis and progression.

Discussion

HS has long been thought to critically modulate cancer pathogenesis. However, due to difficulty in analyzing HS structure and expression, to date only a few studies have directly examine the role of HS in tumorigenesis. These studies observed that HS-deficient Chinese hamster ovary cells failed to form tumor in nude mice; similarly, knockdown of Ext1 leads to reduced growth rate and a strong increase of apoptosis in a myeloma xenotransplantation model in Rag-$2^{-/-}\gamma(c)^{-/-}$ mice, and silencing HS2st expression attenuates human PCa cell growth and survival in vitro. These studies demonstrated an essential role of HS in tumorigenesis; however, many critical issues have not been resolved, including the roles and underlying mechanisms of HS in cancer invasion and metastasis. Furthermore, the microenvironments of naturally occurring cancers and the tissue/cell type specific regulatory roles of HS need to be critically considered in order to understand the actual roles of HS in cancer pathogenesis. In present studies we used a conditional gene targeting approach to abolish HS expression of PCa initiating cells in mice by simultaneous ablation of *Ext1* and *Pten*, allowing determining the roles and the underlying mechanisms of HS in PCa pathogenesis ranging from onset to local invasion under naturally occurring conditions. We observed that Ext1 blocks PCa tumorigenesis and the following local invasion. These observations demonstrate that HS functions to promote both tumorigenesis and progression, and reveal HS as a novel candidate to develop anti-cancer therapeutics that targets multiple protumorigenic pathways.

The Pten deletion was identified to lead to the expansion of a prostatic stem/progenitor cell subpopulation that is the tumor-initiating cells in the *ΔPten* PCa model. The tumor-initiating cells are drug-resistant and are responsible for tumor relapse, representing a challenging issue in the treatment of cancer. In this study, Ext1 deletion reduces the portion of TA/IC cell population as well as P63+ or CK5+ cell population, showing that HS is required the self-renewal and/or differentiation of PCa stem/progenitor cell. Although, the molecular mechanisms that control PCa stem cell self-renewal and differentiation are largely unknown, recent studies have suggested that the activation of the SHH pathway may induce a transitory differentiation of prostatic stem/ progenitor cells into $CD44^{+}/P63^{-/+}$ hyperplasia basal cells with an intermediate phenotype ($CK8^{+}/14^{+}$), and this early transforming event may culminate in tumorigenesis by giving rise to $CD44^{+}$ PCa cells expressing PTCH1 and GLI [66]. Meanwhile, we previously reported that Ext1 deletion disrupts FGF-signaling mediated commitment of lineage differentiation of mouse embryonic stem cells, suggesting that a similar molecular mechanism may exist to control the cell fate of proliferating prostatic stem cells. In this study, our gene expression microarray-IPA, examination of target gene expression by qRT-PCR and p-ERK staining observed that both FGF and SHH signaling were attenuated, suggesting that Ext1 deletion may disrupt FGF and SHH signaling to lead to the reduced numbers of stem cells and the TA/IC subpopulation in the *ΔExt1ΔPten* prostates compared to *ΔPten* prostates.

EMT is an essential feature for epithelial tumor to become invasive. In this study, we found that Ext1 deletion inhibits EMT, observing the first in vivo evidence showing that HS essentially modulate EMT in PCa progression. Several signaling pathways have been known to critically promote the EMT process, including TGF-β, FGF and Notch. Actually all these pathways were observed to be altered in our Gene Expression Microarray-IPA and target expression analysis,

suggesting that HS may functions through facilitation of the TGF-β, FGF and Notch signaling to promote the EMT in PCa progression.

Except EMT, the invasive cancer cells also need to degrade the extracellular matrix to clear the path for invasion. For these purposes, cancer cells generate secrets extracellular matrix proteinases, including endopeptidases such as MMPs, and post-proline dipeptidyl aminopeptidease such as FAP. FAP is not only a marker of reactive fibroblasts in tumor, and also has both dipeptidyl peptidase and endopeptidase activity capable to degrade gelation and type I collagen. In our study, we observed that MMP-9 activity and FAP staining both were dramatically reduced in *ΔExt1ΔPten* prostates, indicating that HS functions to sustain MMP-9 activity and FAP expression to promote tumor invasion. This observation also reveals another molecular mechanism for HS to participate in PCa progression.

Inflammation and tumorigenesis are intimately linked. Chronic inflammation can drive tumorigenesis, and tumors are inherently proinflammatory, with infiltrating leukocytes thought to be critical for tumor maintenance and progression. This has been demonstrated in PCa pathogenesis too. For example, chronic bacterial inflammation was observed to induced PIN in mouse prostate [67] and constitutive activation of IKK2, a key mediator of inflammatory response, in epithelium compartment increases the PCa size and fibrinosis in heterozygous Pten knockout mice [62]. Chronic inflammatory response was reported to occur in ΔPten mice too with myeloid cells as the main infiltrating leukocytes [63, 65]. Consistent with these reports, we observed sever chronic inflammation, such inflammatory cell foci, in *ΔPten* prostates too, however, only very minor infiltrating leukocytes were seen in the *ΔExt1ΔPten* prostates, unveiling that HS also functions to promote inflammatory response, by which to promote tumorigenesis.

In summary, our current study observed that HS functions to promote both tumorigenesis and local invasion, revealing HS a key promoting molecule in PCa pathogenesis. Our mechanism studies delineated that HS functions to promote cell proliferation, survival, and self-renewal and /or differentiation of stem/progenitors as well as inflammation to enhance PCa tumorigenesis. This mechanism study also deciphered that HS promotes EMT and sustains the MMP9 activity and FAP expression to promote PCa invasion. Therefore, our study demonstrates that HS promotes multiple major protumorigenic pathways to enhance PCa tumorigenesis and local invasion, and this study also reveal targeting HS may represent a novel direction to develop multi-effect anti-cancer drug.

References

1. American-Cancer-Society., *Cancer Facts and Figures 2012,* 2012, American Cancer Society: Atlanta.
2. Bernfield, M., et al., *FUNCTIONS OF CELL SURFACE HEPARAN SULFATE PROTEOGLYCANS.* Annual Review of Biochemistry, 1999. **68**(1): p. 729-777.
3. Esko, J.D. and S.B. Selleck, *Order out of chaos: assembly of ligand binding sites in heparan sulfate.* Annu Rev Biochem, 2002. **71**: p. 435-71.
4. Bishop, J.R., M. Schuksz, and J.D. Esko, *Heparan sulphate proteoglycans fine-tune mammalian physiology.* Nature, 2007. **446**(7139): p. 1030-7.
5. Bishop, J.R., M. Schuksz, and J.D. Esko, *Heparan sulphate proteoglycans fine-tune mammalian physiology.* Nature, 2007. **446**(7139): p. 1030.
6. Forsberg, E. and L. Kjellen, *Heparan sulfate: lessons from knockout mice.* J Clin Invest, 2001. **108**(2): p. 175-80.
7. Lin, X., *Functions of heparan sulfate proteoglycans in cell signaling during development.* Development, 2004. **131**(24): p. 6009-6021.
8. Rapraeger, A.C., *Heparan sulfate-growth factor interactions.* Methods Cell Biol, 2002. **69**: p. 83-109.
9. Donjacour, A.A., A.A. Thomson, and G.R. Cunha, *FGF-10 plays an essential role in the growth of the fetal prostate.* Dev Biol, 2003. **261**(1): p. 39-54.
10. Huang, L., et al., *The role of Fgf10 signaling in branching morphogenesis and gene expression of the rat prostate gland: lobe-specific suppression by neonatal estrogens.* Dev Biol, 2005. **278**(2): p. 396-414.
11. Thomson, A.A. and G.R. Cunha, *Prostatic growth and development are regulated by FGF10.* Development, 1999. **126**(16): p. 3693-701.
12. Dhom, G., *Epidemiologic aspects of latent and clinically manifest carcinoma of the prostate.* Journal of Cancer Research and Clinical Oncology, 1983. **106**(3): p. 210-218.
13. Carter, B.S., H.B. Carter, and J.T. Isaacs, *EPIDEMIOLOGIC EVIDENCE REGARDING PREDISPOSING FACTORS TO PROSTATE-CANCER.* Prostate, 1990. **16**(3): p. 187-197.
14. Miller, G.J., *Prostate cancer among the chinese: Pathologic, epidemiologic and nutritional considerations*, in *Advanced therapy of prostate disease*, I.M.T. By Martin I. Resnick, Editor. 2000, B.C. Decker: London. p. 18-27.
15. Allen, B.L., M.S. Filla, and A.C. Rapraeger, *Role of heparan sulfate as a tissue-specific regulator of FGF-4 and FGF receptor recognition.* J Cell Biol, 2001. **155**(5): p. 845-58.
16. Mawhinney, M.G. and B.L. Neubauer, *ACTIONS OF ESTROGEN IN THE MALE.* Investigative Urology, 1979. **16**(6): p. 409-420.
17. Prehn, R.T., *On the Prevention and Therapy of Prostate Cancer by Androgen Administration.* Cancer Research, 1999. **59**(17): p. 4161-4164.
18. American-Cancer-Society., *Cancer Facts and Figures 2009,* 2009, American Cancer Society: Atlanta.
19. Zhu, M.-L. and N. Kyprianou, *Androgen receptor and growth factor signaling cross-talk in prostate cancer cells.* Endocrine-Related Cancer, 2008. **15**(4): p. 841-849.
20. Reynolds, A.R. and N. Kyprianou, *Growth factor signalling in prostatic growth: significance in tumour development and therapeutic targeting.* British Journal of Pharmacology, 2006. **147**(S2): p. S144-S152.

21. Jones, E., H. Pu, and N. Kyprianou, *Targeting TGF-β in prostate cancer: therapeutic possibilities during tumor progression.* Expert Opinion on Therapeutic Targets, 2009. **13**(2): p. 227-234.
22. Lin, Y. and F. Wang, *FGF signalling in prostate development, tissue homoeostasis and tumorigenesis.* Bioscience Reports, 2010. **30**(5): p. 285-291.
23. Yardy, G.W. and S.F. Brewster, *Wnt signalling and prostate cancer.* Prostate Cancer Prostatic Dis, 2005. **8**(2): p. 119-126.
24. Lynch, C.C., et al., *MMP-7 promotes prostate cancer-induced osteolysis via the solubilization of RANKL.* Cancer Cell, 2005. **7**(5): p. 485-496.
25. Wilson, S.R., et al., *Amplification of MMP-2 and MMP-9 production by prostate cancer cell lines via activation of protease-activated receptors.* The Prostate, 2004. **60**(2): p. 168-174.
26. Sun, Y.-X., et al., *Expression of CXCR4 and CXCL12 (SDF-1) in human prostate cancers (PCa) in vivo.* Journal of Cellular Biochemistry, 2003. **89**(3): p. 462-473.
27. Sasisekharan, R., et al., *Roles of heparan-sulphate glycosaminoglycans in cancer.* Nature Reviews. Cancer, 2002. **2**(7): p. 521-528.
28. Kirkpatrick, C.A. and S.B. Selleck, *Heparan sulfate proteoglycans at a glance.* J Cell Sci, 2007. **120**(11): p. 1829-1832.
29. T ím á r, J., et al., *Proteoglycans and tumor progression: Janus-faced molecules with contradictory functions in cancer.* Seminars in Cancer Biology, 2002. **12**(3): p. 173-186.
30. Liu, D., et al., *Dynamic Regulation of Tumor Growth and Metastasis by Heparan Sulfate Glycosaminoglycans.* Semin Thromb Hemost, 2002. **28**(01): p. 67-78.
31. Blackhall, F.H., et al., *Heparan sulfate proteoglycans and cancer.* British Journal of Cancer, 2001. **85**(8): p. 1094.
32. EM Selva, N.P., *Role of heparan sulfate proteoglycans in cell signaling and cancer* Advances in Cancer Research, 2001. **Vol. 83**: p. 67-80.
33. Esko, J.D., K.S. Rostand, and J.L. Weinke, *Tumor Formation Dependent on Proteoglycan Biosynthesis.* Science, 1988. **241**(4869): p. 1092-1096.
34. Reijmers, R.M., et al., *Targeting EXT1 reveals a crucial role for heparan sulfate in the growth of multiple myeloma.* Blood, 2010. **115**(3): p. 601-604.
35. De Marzo, A.M., et al., *Human prostate cancer precursors and pathobiology.* Urology, 2003. **62**(5, Supplement 1): p. 55-62.
36. Danforth, K.N., et al., *Polymorphic variants in PTGS2 and prostate cancer risk: results from two large nested case–control studies.* Carcinogenesis, 2008. **29**(3): p. 568-572.
37. Inatani, M., et al., *Mammalian Brain Morphogenesis and Midline Axon Guidance Require Heparan Sulfate.* Science, 2003. **302**(5647): p. 1044-1046.
38. Fisher, S.J. and Z. Werb, *The catabolism of extracellular matrix components.* Extracellular Matrix: A Practical Approach, 1995: p. 261-287.
39. Nairn, A.V., et al., *Glycomics of Proteoglycan Biosynthesis in Murine Embryonic Stem Cell Differentiation.* Journal of Proteome Research, 2007. **6**(11): p. 4374-4387.
40. Suzuki, H., et al., *Interfocal heterogeneity of PTEN/MMAC1 gene alterations in multiple metastatic prostate cancer tissues.* Cancer Res, 1998. **58**(2): p. 204-9.
41. Dahia, P.L., *PTEN, a unique tumor suppressor gene.* Endocr Relat Cancer, 2000. **7**(2): p. 115-29.
42. Klerk, D.P.D. and H.J. Human, *Fluctuations in prostatic glycosaminoglycans during fetal and pubertal growth.* The Prostate, 1985. **6**(2): p. 169-175.

43. Terry DE, C.A., *Glycosaminoglycans in the three lobes of the rat prostate following castration and testosterone treatment.* Biochemistry and cell biology, 1996. **74**(5): p. 653-658.
44. IIDA, S., et al., *Analysis of glycosaminoglycans in human prostate by high-performance liquid chromatography.* British Journal of Urology, 1997. **79**(5): p. 763-769.
45. Schamhart, D.H.J. and K.H. Kurth, *Role of proteoglycans in cell adhesion of prostate cancer cells: From review to experiment.* Urological Research, 1997. **25**(0): p. S89-S96.
46. Mitropoulos, D., et al., *Terazosin Modifies the Content of Glycosaminoglycans and the Activity of Matrix Metalloproteinase 2 in the Rat Ventral Prostate.* European Urology, 2007. **51**(2): p. 447-456.
47. Wang, S., et al., *Prostate-specific deletion of the murine Pten tumor suppressor gene leads to metastatic prostate cancer.* Cancer Cell, 2003. **4**(3): p. 209-221.
48. Wang, S., et al., *Pten deletion leads to the expansion of a prostatic stem/progenitor cell subpopulation and tumor initiation.* Proceedings of the National Academy of Sciences of the United States of America, 2006. **103**(5): p. 1480-1485.
49. Fernandez, P., et al., *COX-2 promoter polymorphisms and the association with prostate cancer risk in South African men.* Carcinogenesis, 2008. **29**(12): p. 2347-2350.
50. Zabaleta, J., et al., *Cytokine genetic polymorphisms and prostate cancer aggressiveness.* Carcinogenesis, 2009. **30**(8): p. 1358-1362.
51. Kjellen, L., *Glucosaminyl N-deacetylase/N-sulphotransferases in heparan sulphate biosynthesis and biology.* Biochem Soc Trans, 2003. **31**(2): p. 340-2.
52. Wang, M.-H., et al., *Association of IL10 and Other immune response- and obesity-related genes with prostate cancer in CLUE II.* The Prostate, 2009. **69**(8): p. 874-885.
53. Cunha, G.R., et al., *Hormonal, cellular, and molecular regulation of normal and neoplastic prostatic development.* J Steroid Biochem Mol Biol, 2004. **92**(4): p. 221-36.
54. Wu, X., et al., *Generation of a prostate epithelial cell-specific Cre transgenic mouse model for tissue-specific gene ablation.* Mech Dev, 2001. **101**(1-2): p. 61-9.
55. Pierce, B., et al., *C-reactive protein, interleukin-6, and prostate cancer risk in men aged 65 years and older.* Cancer Causes and Control, 2009. **20**(7): p. 1193-1203.
56. Wang, S., et al., *Prostate-specific deletion of the murine Pten tumor suppressor gene leads to metastatic prostate cancer.* Cancer Cell, 2003. **4**(3): p. 209-21.
57. Liotta, L.A. and E.C. Kohn, *The microenvironment of the tumour-host interface.* Nature, 2001. **411**(6835): p. 375-379.
58. Kalluri, R. and M. Zeisberg, *Fibroblasts in cancer.* Nat Rev Cancer, 2006. **6**(5): p. 392-401.
59. Joyce, J.A. and J.W. Pollard, *Microenvironmental regulation of metastasis.* Nat Rev Cancer, 2009. **9**(4): p. 239-252.
60. Tuxhorn, J.A., G.E. Ayala, and D.R. Rowley, *REACTIVE STROMA IN PROSTATE CANCER PROGRESSION.* The Journal of Urology, 2001. **166**(6): p. 2472-2483.
61. De Marzo, A.M., et al., *Inflammation in prostate carcinogenesis.* Nat Rev Cancer, 2007. **7**(4): p. 256-269.
62. JA, B.A.E.D.K.N.L.E.S.-S.M.S., *Persistent inflammation leads to proliferative neoplasia and loss of smooth muscle cells in a prostate tumor model.* Neoplasia, 2011. **13**(8): p. 692-703.

63. Svensson, R.U., et al., *Slow Disease Progression in a C57BL/6 Pten-Deficient Mouse Model of Prostate Cancer.* The American Journal of Pathology, 2011. **179**(1): p. 502-512.
64. Maxwell, P.J., et al., *Potentiation of Inflammatory CXCL8 Signalling Sustains Cell Survival in PTEN-deficient Prostate Carcinoma.* European Urology, (0).
65. Zhang, Q., et al., *Interleukin-17 Promotes Formation and Growth of Prostate Adenocarcinoma in Mouse Models.* Cancer Research, 2012. **72**(10): p. 2589-2599.
66. Chen, B.-Y., et al., *Hedgehog is involved in prostate basal cell hyperplasia formation and its progressing towards tumorigenesis.* Biochemical and Biophysical Research Communications, 2007. **357**(4): p. 1084-1089.
67. Elkahwaji, J.E., R.J. Hauke, and C.M. Brawner, *Chronic bacterial inflammation induces prostatic intraepithelial neoplasia in mouse prostate.* Br J Cancer, 2009. **101**(10): p. 1740-1748.
68. Bolte, S. and F.P. CordeliÈRes, *A guided tour into subcellular colocalization analysis in light microscopy.* Journal of Microscopy, 2006. **224**(3): p. 213-232.
69. Lesche, R., et al., *Cre/loxP-mediated inactivation of the murine Pten tumor suppressor gene.* genesis, 2002. **32**(2): p. 148-149.

Figures

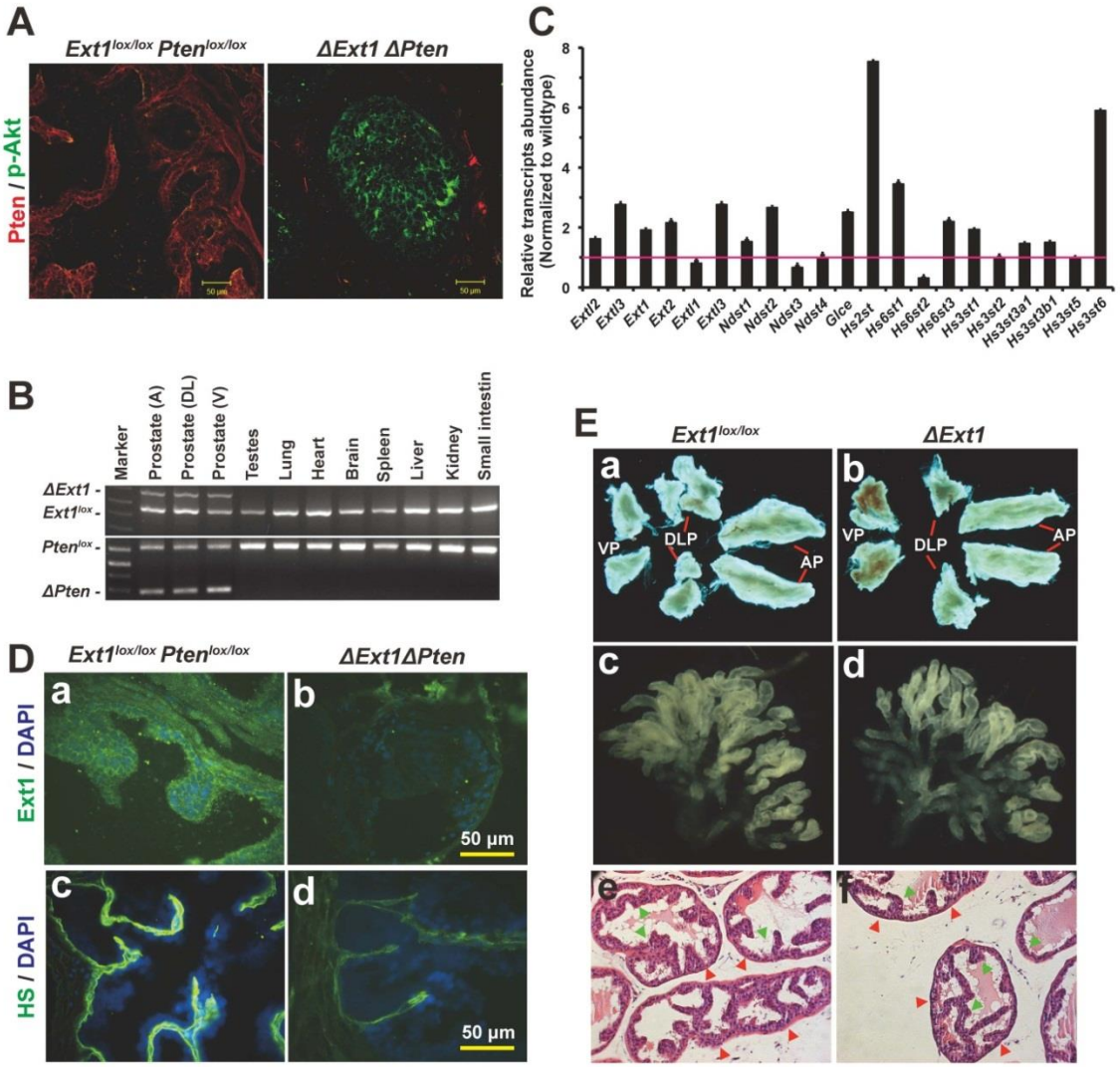

Figure 2.1. HS expression in PCa tissue, and conditional deletions of *Pten* and *Ext1* in the prostate epithelium.

A. Immunofluorescent staining of Pten and p-AKT. Cryosections of 10-week-old wildtype ($Pten^{lox/lox}$) and *ΔPten-/-* prostates (PCa tissues) were co-stained with anti-Pten antibody (Red) and anti-p-AKT antibody (green). In *ΔPten* prostates, the expression of Pten was diminished accompanied with p-AKT activation. The figures are representative of examination of 3 mice per genotype.

B. Prostate-specific *Pten* and *Ext1* deletion. Genomic DNAs were prepared from individual prostate lobe and indicated tissues of 10-week-old male mice. PCR analysis of genomic DNA showed that the deletion of *Ext1* and *Pten* both were prostate-specific and occurred in all prostate lobes. A, anterior prostate; DL, dorsal-lateral prostate; V, ventral prostate.

C. Expression of HS biosynthetic genes in 12-weeks old *ΔPten-/-* prostates and littermate wildtype were determined by qRT-PCR analysis. The transcript abundance in *ΔPten-/-* prostates was normalized to the wildtype control and presents as mean + SE. N = 3 mice per group.

D. Immunofluorescent staining of Ext1 and HS. Cryosections of 10-week-old prostates were stained with anti-Ext1 antibody (green in a & b) or anti-HS antibody (green in c & d). Cell nuclei were stained by DAPI (blue). In *ΔExt1* prostates, the expression of Ext1 and HS were diminished in prostate epithelium. The figures are representative of examination of 3-4 mice per genotype.

E. Morphology of *ΔExt1* prostate. Anatomical (a, b; 5 weeks old), macroscopic (c, d; prostate branching morphogenesis, 5 weeks old) and histological (e, f; H&E staining, 10 weeks old) analysis of prostates.

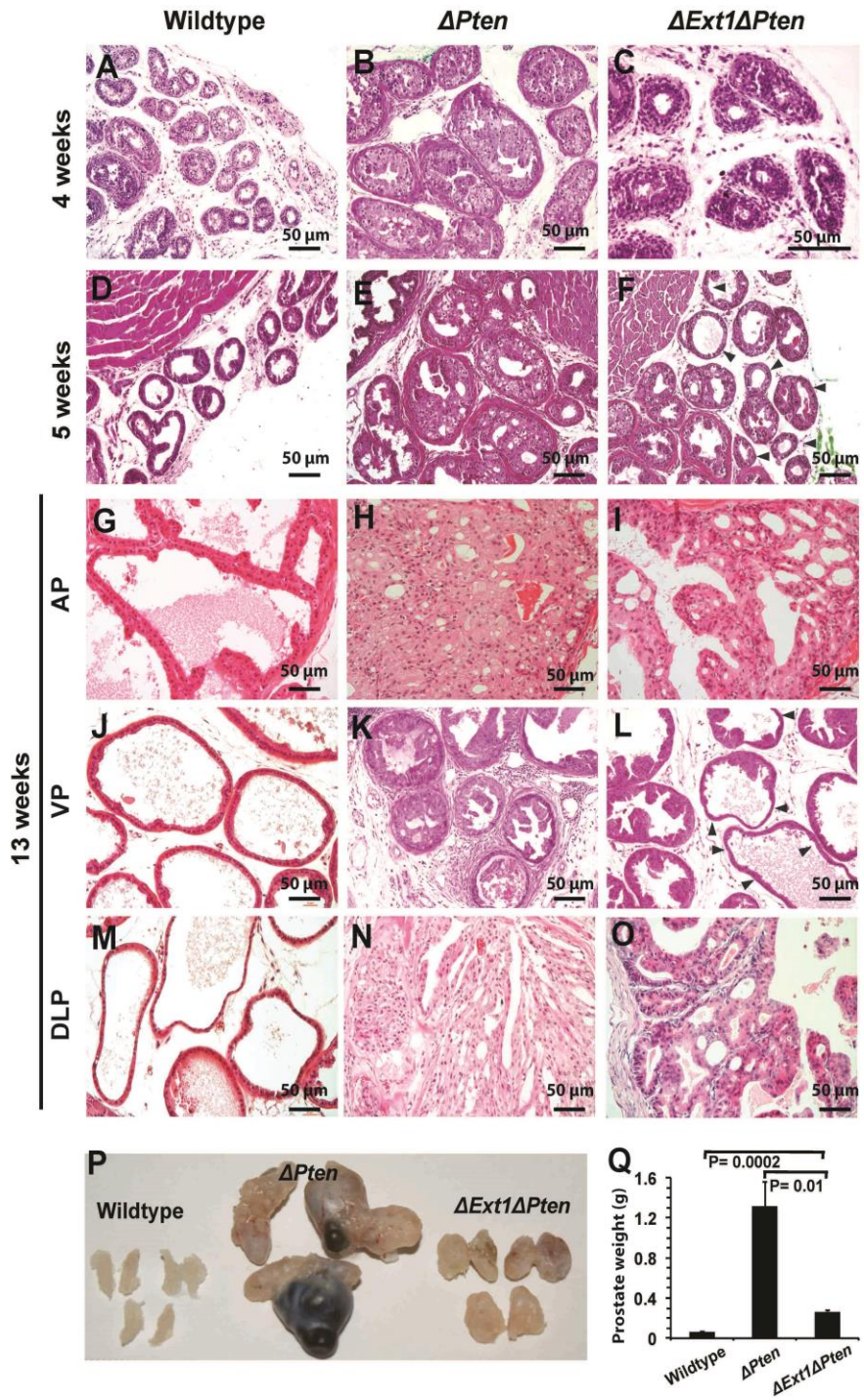

Figure 2.2. *Ext1* ablation retards prostate cancer tumorigenesis and progression

A-O. H&E staining. Cryosections of 4-, 5- and 13-weeks old prostates were H&E stained. At 4-weeks of age, most of the *ΔPten* prostate ducts developed PIN versus normal histology exhibited

by the littermate *ΔExt1ΔPten* prostates s (A-C). At 5-weeks, all the *ΔPten* prostates progressed to high grade PIN, whereas the littermate *ΔExt1ΔPten* prostates showed only early stage PIN with many epithelial cell layers remaining normal (pointed by black arrowheads). At 13 weeks, all the *ΔPten* prostates progressed to cancer, whereas the littermate *ΔExt1ΔPten* prostates progressed to middle PIN stage with some regions remaining normal (pointed by black arrowheads) (G-O). Five mice per group were examined.

P, Q. Size and weight of prostates. Gross anatomy of representative anterior prostates at 40 weeks of age were shown (P) and their weights were quantified (Q). Five-six mice per group were examined. Statistical analysis was carried out by Student's t-test.

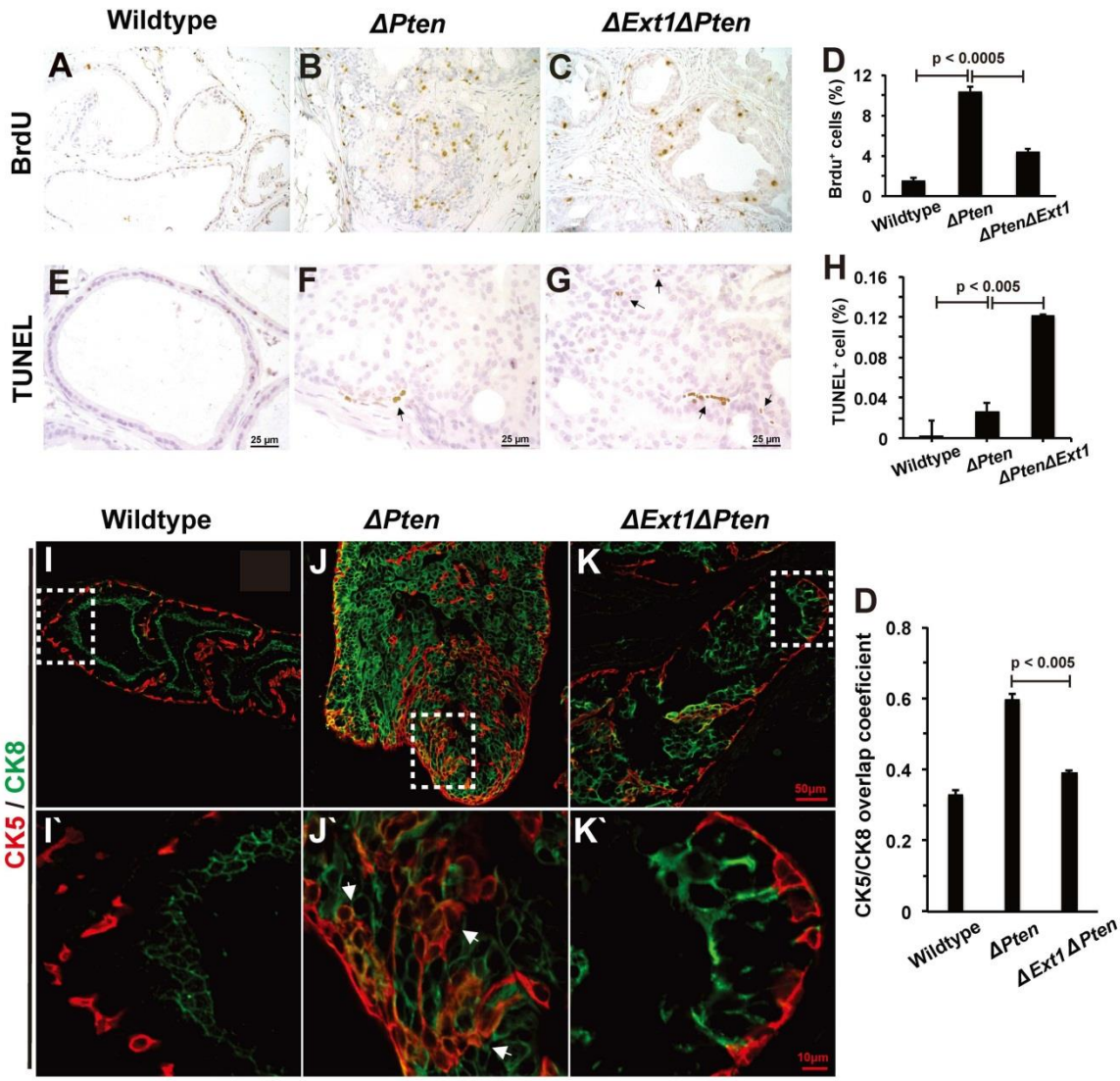

Figure 2.3. *Ext1* ablation attenuates PCa cell proliferation, induces apoptosis and disrupts prostate cancer stem/progenitor cell differentiation

A-D. BrdU staining. Prostates were harvested from BrdU injected 13 weeks old mice. Paraffin sections were prepared and stained for $BrdU^+$ cells (brown dots)(A-C). Quantitation determined that the number of $BrdU^+$ cells in *ΔExt1ΔPten* prostates was significantly reduced compared to littermate *ΔPten* prostates (D).

E-H. Apoptotic cells (pointed by arrows) in paraffin section of 13-weeks old prostates were stained with a TUNEL kit (E-G). Quantitation determined that apoptotic cells were significantly more in *ΔExt1 ΔPten* prostates than in littermate *ΔPten* prostates (H).

I-L. Staining of prostate stem/progenitor cells. Cryosections of 10-weeks old prostates were co-immunostained for CK5 (red) and CK8 (green)(I-K). Framed regions in I-K were shown at higher magnification in I'-K', correspondingly. Compared to *ΔPten* prostates, the double positive transient amplifying/intermediate prostate progenitor ($CK5^+/CK8^+$) cells in *ΔExt1ΔPten* prostates was reduced (L). Five sections per prostate and 4-5 mice per genotype were examined for each measurement, and the $CK5^+/CK8^+$ cells was quantified using "overlap coefficient" index [68]. The statistical analysis was carried out by student's t-test.

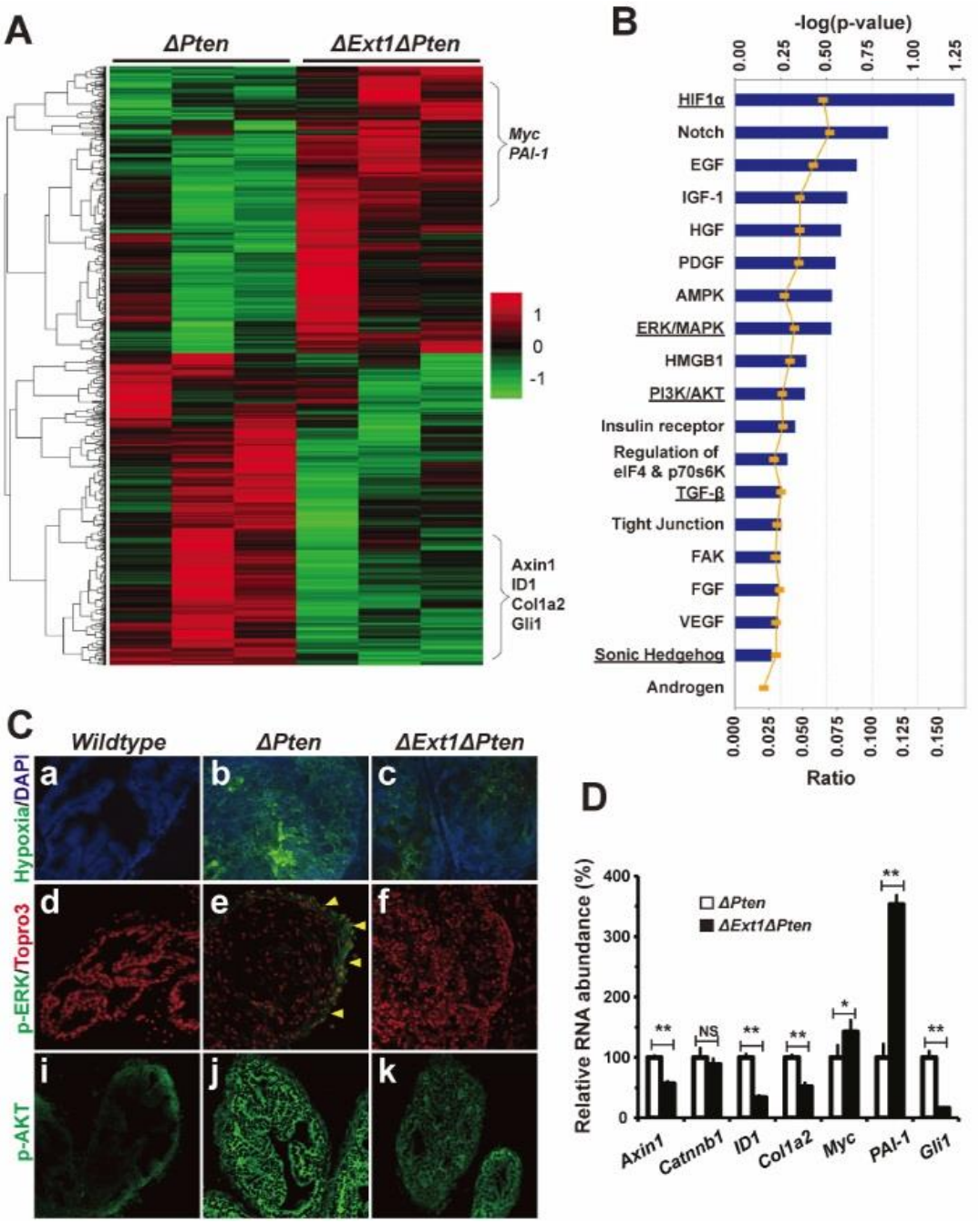

Figure 2.4. Transcript analysis revealed multiple molecular pathways modulated by HS at PCa tumorigenesis.

A: Heatmap of the differentially expressed genes between *ΔPten* and *ΔExt1ΔPten* prostates at 5 weeks of age in Gene Expression microarray analysis. N=3 per group.

B. Ingenuity knowledge-based signaling pathway analysis (IPA) compared the transcriptome between the 5-weeks old *ΔPten and ΔExt1ΔPten* prostates and determined the molecular pathways modulated by HS in PCa tumorigenesis. The underlying signaling was alternatively confirmed to be different between *ΔExt1ΔPten* and *1ΔPten* prostates as shown in C & D.

C. Hypoxia, p-ERK and p-AKT staining. a-c: Prostate cryosections were prepared from hypoxia indicator injected 6-weeks old mice, and the formed protein adduct in tissue under low oxygen concentration was stained with a specific antibody (green). The *ΔPten* prostates showed a very strong hypoxia staining, whereas the *ΔExt1ΔPten* prostates showed a very weak staining, barely above the normal prostate control. d-k: Cryosections of 6-weeks old prostates were co-immunostained for p-ERK (green) and nuclei (Tropro3, red)(d-f) or only for p-AKT (green)(i-k). Positive p-ERK staining was only seen in the basal epithelial cell regions (pointed by arrowheads). Representatives are shown from examinations of 4-5 mice per genotype.

D. qRT-PCR analysis of target gene expression of microarray-bioinformatics analysis-identified signaling pathways, including Wnt, TGFβ and Hedgedog signaling. The data was normalized to wildtype littermate control. N= 4-5 mice per group. The statistical analysis was carried out by student's t-test.

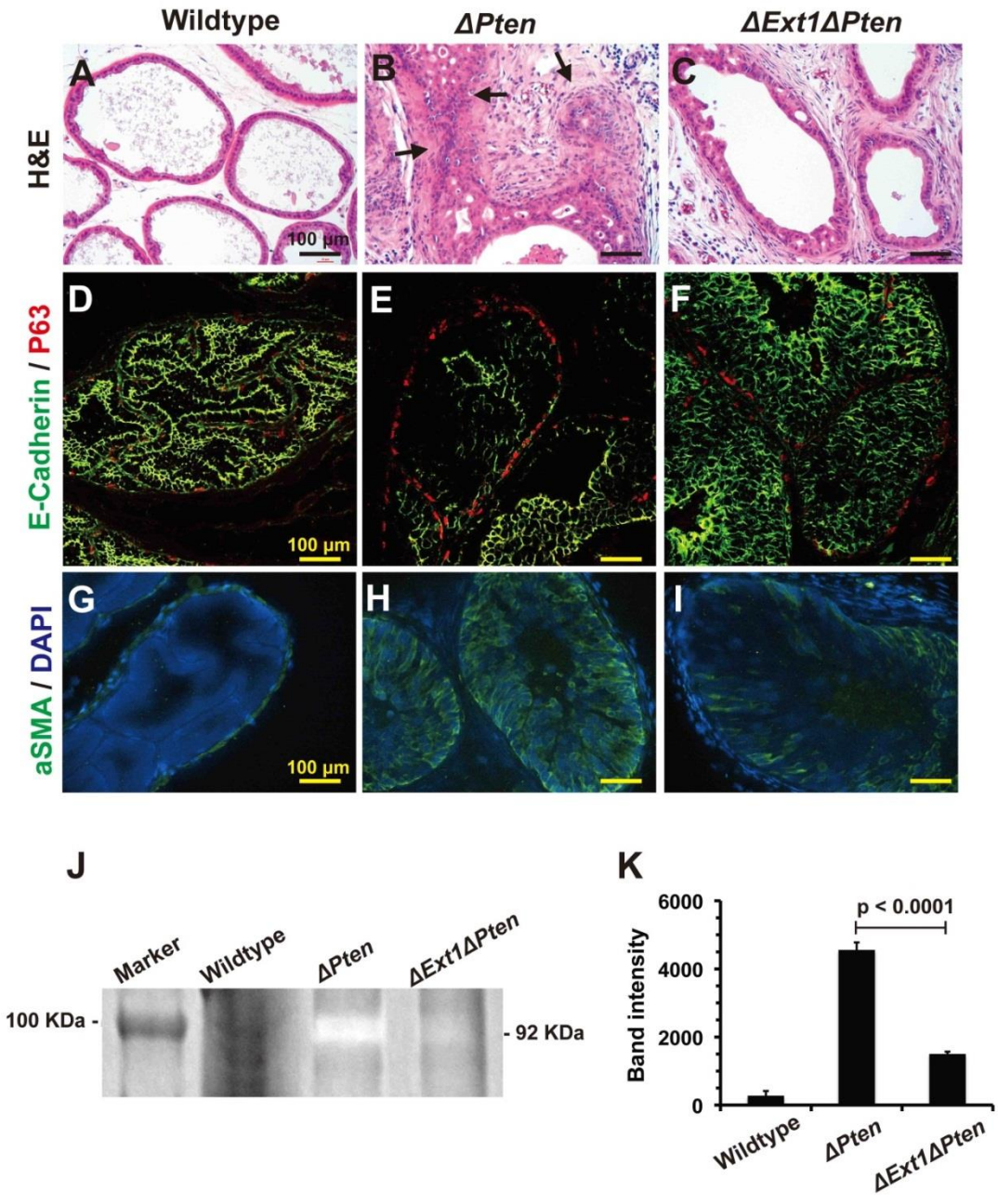

Figure 2.5. Ext1 ablation attenuates PCa invasion accompanying with disruption of both EMT and MMP-9 activity.

A. H&E staining of paraffin sections of 13-weeks old prostates. Tumor invasions were pointed by arrows. Representative from examination of 5-6 mice per genotype.

B. Immunofluorescent staining for E-cadherin (Green), P63 (red) and αSMA (green) expression. Compared to ΔPten prostates that were undergoing EMT by losing E-Cadherin while acquiring αSMA expression, the *ΔExt1ΔPten* PCa cells retained high expression of E-Cadherin with low expression of αSMA expression, showing that *Ext1* ablation disrupted PCa EMT.

C. Zymography analysis. The supernatant of prostate tissue lysates were analyzed by gelatin zymography assay. The *ΔPten* prostates showed a very strong gelatin degradation band at 92 KDa corresponding to MMP-9, whereas the same-sized band was barely seen in the *ΔExt1ΔPten* prostate samples. Three mice per genotype were examined. The statistical analysis was carried out by student's t-test.

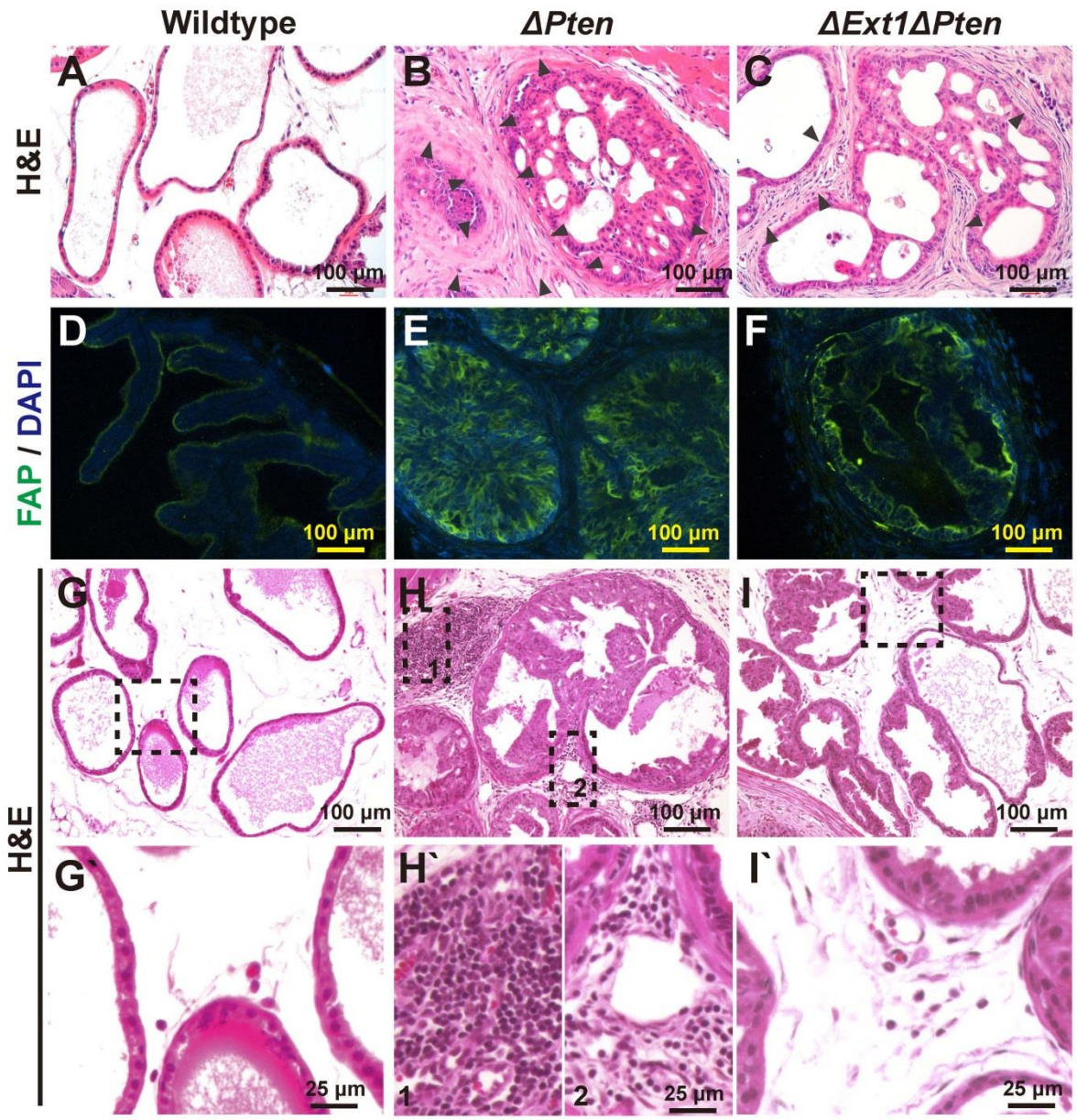

Figure 2.6. ***Ext1*** **ablation attenuates fibrinosis and inflammation, and ameliorates hypoxia in PCa tissue.**

A-C. Fibrinosis. Paraffin sections of 13 weeks old prostates were H&E stained, and fibrotic tissues were pointed by arrows.

D-F. Staining for tumor-associated fibroblasts. The cryosections of 13-weeks of prostates were stained with anti-activated fibroblast protein (AFP), a marker of tumor-associated fibroblasts.

Significantly reduced AFP staining was observed in *ΔExt1ΔPten* prostates compared to *ΔPten* prostates. The pictures are representative in examination of 4-5 mice per genotype.

G-I. Inflammatory cells. H&E staining of 13-weeks old mice prostates showed that inflammatory cells, including myeloid cells and lymphocytes, were abundant in *ΔPten* prostates, but dramatically reduced in *ΔExt1ΔPten* prostates. The framed regions were shown in high magnification in G'-I', correspondingly.

Table 2.1: Top molecular and cellular functions modulated by HS in PCa pathogenesis. Ingenuity knowledge-based molecular and cellular functions analysis of the *ΔPten* and *ΔExt1ΔPten* prostate transcriptome shows significant enrichment of cellular growth and proliferation and cell death and survival molecular events.

Name	Number of Molecules
Cellular Growth and Proliferation	202
Cell Death and Survival	189
Cell Cycle	93
Lipid Metabolism	61
Small Molecule Biochemistry	75

Table 2.2. Genes examined and corresponding primer sets used for the qRT-PCR analysis. Primer sequences are shown 5' to 3'.

Gene	Forward Primer	Reverse Primer
Id1	AGAACCGCAAAGTGAGCAAG	GCTGCAGGTCCCTGATGTAG
Axin1	CTCCAAGCAGAGGACAAAATCA	GGATGGGTTCCCCACAGAAATA
Ctnnb1	GCAGCAGCAGTTTGTGGA	TGTGGAGAGCTCCAGTACACC
Col1a2	GCAGGTTCACCTACTCTGTCCT	CTTGCCCCATTCATTTGTCT
Myc	CCTAGTGCTGCATGAGGAGA	TCTTCCTCATCTTCTTGCTCTTC
PAI-1	TTCAGCCCTTGCTTGCCTC	ACACTTTTACTCCGAAGTCGGT
Gli1	CCAAGCCAACTTTATGTCAGGG	AGCCCGCTTCTTTGTTAATTTGA
GAPDH	ATGACATCAAGAAGGTGGTG	CATACCAGGAAATGAGCTTG

Table 2.3. Primers for genotyping. PB-Cre genotyping following the B6.Cg-Tg(Pbsn-cre)4Prb PCR Protocol from NCI Mouse Repository. Pten primers are adapted from [69], and Ext1 primers are adopted from [37]. Primer sequences are shown 5' to 3' with primer name.

Gene genotyped	Forward Primer	Reverse Primer
PB-Cre	P021:CTGAAGAATGGGACAGGCATTG	C031:CATCACTCGTTGCATCGACC
Pten	6637:TCCCAGAGTTCATACCAGGA	6925:GCAATGGCCAGTACTAGTGAAC 7319:AATCTGTGCATGAAGGGAAC
Ext1	BURN51:GGAGTGTGGATGAGTTGAAG	BURN52: CAACACTTTCAGCTCCAGTC BURN29: AGAACAGGTACCCATGTTC

Table 2.4. Primers for evaluating expression of HS biosynthetic genes. Primer sequences are shown 5' to 3'.

Gene Name	Forward Primer	Reverse Primer
Extl2	GCCACATCTGCAAACTTCCGG	ACACAAGGATGACCACCAGGG
Extl3	CCACCCTATGCCTCACCTAA	GTTCCAGCCACGGTAACAGT
Ext1	TGGAGTCCTGCTTCGATTTC	CTTTCTGCTGCGGGTACAC
Ext2	ACGTCACCCTGTTCTCCATC	CAATGGAGTGAGGCCAGAAC
Extl1	ACCCAGAAGATGTCGCACA	CACTTGGAGGTGTCAAAGCA
Ndst1	GGAATCCAGTCGCTTCAAAT	GTCTGTGAGTGTGGGCATGT
Ndst2	GGGATTCCTACGGATCTGG	TAGAGCTGCGAGTGGATGG
Ndst3	GGTGTTTGTGGAGAGCCAGT	GAACCGGATGGATTCTAGCA
Ndst4	TCAGGTCACCAGCACTGAAG	GAATGAAGCCCTTCCTGTACC
Glce	TCTCAACCACAGCCCACATGG	GGCCAGCCACCTTTCTCATCC
Hs2st1	GACTTCATCATGCTGCTCGA	TGTACGGTAGAGGTCGGTAGC
Hs6st1	GTGTGGAGGTGGATGAGGAC	TACAGCTGCATGTCCAGGTC
Hs6st2	AGAGTTCGGCCAGGTTTGTA	GAAGTCTACCTTGCGCAGGA
Hs6st3	GTTCGTGCCTCGATTCAACT	GCCCTTTGATGTTGAAGTCC
Hs3st1	GCTCAAACAGCAGGAGCTTC	ATTGGATGCTGTGCCTTCTC
Hs3st2	GGAATTGGTGTGCCTACAGC	TTGTTGGACTTGATGGCTGA
Hs3st3a1	CGCAGCATCTTCAGGAAGT	GCCAGGCAGTAGAAGACGTAG
Hs3st3b1	GAGCCAGGAGGAGCAGAGT	CGCTGAAGAAGCTGGAGATG
Hs3st5	GTGGTCAAAGCTTCCCAAGA	TGTACCACTCAATGCCCTTG
Hs3st6	GCATTGGCCTCTATGCTCAG	CAGGAAGTGGGACAGAGGAA

CHAPTER 3: CHARACTERIZATION OF GLYCOSAMINOGLYCANS BY ^{15}N-NMR SPECTROSCOPY AND *IN VIVO* ISOTOPIC LABELING

Vitor H. Pomin, Joshua S. Sharp, Xuanyang Li, Lianchun Wang, and James H. Prestegard., Analytical Chemistry, 2010. **83**(3): p. 1162-1162. Reprinted with permission from ppublisher.

Abstract

Characterization of glycosaminoglycans (GAGs), including chondroitin sulfate (CS), dermatan sulfate (DS) and heparan sulfate (HS), is important in developing an understanding of cellular function and in assuring quality of preparations destined for biomedical applications. While use of ^{1}H and ^{13}C NMR spectroscopy has become common in characterization of these materials, spectra are complex and difficult to interpret when a more heterogeneous GAG type or a mixture of several types is present. Herein a method based on ^{1}H-^{15}N two dimensional NMR experiments is described. The ^{15}N- and ^{1}H-chemical shifts of amide signals from ^{15}N-containing acetylgalactosamines in CSs are shown to be quite sensitive to the sites of sulfation (4-, 6- or 4,6-), and easily distinguishable from those of DS. The amide signals from residual ^{15}N-containing acetylglucosamines in HS are shown to be diagnostic of the presence of these GAG components as well. Most data were collected at natural abundance of ^{15}N despite its low percentage. However enrichment of the ^{15}N-content in GAGs using metabolic incorporation from ^{15}N-glutamine added to cell culture media is also demonstrated, and used to distinguish metabolic states in different cell types.

Keywords: glycosaminoglycan sulfation, metabolic labeling, heparin, heparan sulfate, chondroitin sulfate, dermatan sulfate

Introduction

Glycosaminoglycans (GAGs) are important components of the extracellular matrix (ECM).[1-3] These glycans are commonly attached to a membrane protein core to form the cell surface proteoglycans found virtually in all mammalian cells.[4] As a part of the ECM they influence numerous physiological processes, including organogenesis/growth control,[5, 6] cell adhesion,[7] angiogenesis,[8] wound healing,[9, 10] tumorigenesis,[10, 11] morphogenesis,[12, 13] inflammation,[14-16] haemostasis,[17, 18] and neural development/regeneration.[19-22] GAGs also participate as receptors of various pathogens during the process of infection,[23] and they have found applications in the treatment of diseases,[24-26] for example, in the use of heparins for the treatment of acute coronary conditions.[27-30] In many cases it is clear that biological function is dependent on specific structures (motifs) along the backbone of these complex polymeric carbohydrates.[3, 31] Therefore, improvements in methods of characterization have become a high priority. The importance of this characterization was brought home in early 2008 when contamination of the medical supply of low-molecular-weight heparin, with what proved to be oversulfated chondroitin sulfate (OSCS),[32-34] resulted in a worldwide withdrawal of the product. While characterization methods have improved, there is still a need for facile methods for rapid recognition of GAG types, particularly when mixtures of types are involved. These may occur in crude preparations or in isolates from cell surface proteoglycans where changes in sulfation or distribution among GAG types within stages of cell development may be of interest. Here we describe methodology, based on the use of ^{1}H-^{15}N heteronuclear NMR methods, that we believe to be useful in the characterization of various GAG types. We also show that supplementation with ^{15}N-enriched metabolic precursor during cell

growth can be used to monitor differences in GAG composition among various cell types and/or on changes in growth conditions.

GAGs are linear carbohydrate polymers built on alternating hexosamine and uronic acid units.[3] For example, chondroitin sulfates (CSs), the most abundant GAG in the human body,[3] are composed of alternating β1-4-linked glucuronic acids (GlcA) and β1-3-linked N-acetylgalactosamines (GalNAc).[31] Their major structural heterogeneity arises mostly from different sulfation patterns, which correlate with changes in biological actions.[31, 35] The GalNAc residues can be mostly 4-sulfated (CS-A), almost entirely 6-sulfated (CS-C), highly 4,6-di-sulfated (CS-E, or OSCS), and sometimes also sulfated at the 2-position of the GlcA units (CS-D).[31]

Restricting our attention to the most abundant GAGs of mammalian cell surface proteoglycans, two other species are of primary interest, dermatan sulfate (DS), and heparan sulfate (HS). Dermatan sulfate (DS), which also contains GalNAc as its amino sugar, is a close relative of CS, but the GlcA of CS is largely replaced by its 5' epimer, iduronic acid (IdoA).[31] Heparan sulfate (HS) is more complex, being characterized by mixtures of GlcA and IdoA as its uronic acid component respectively β1-4 and α1-4 linked to an N-substituted glucosamine derivative (GlcNX). The GlcNX is α1-4 linked to the next uronic acid. Sulfation occurs at the nitrogen of the amino sugar in addition to various *O*-sulfated sites (mostly at 6- and rarely at 3-positions) on the GlcNX residues. Sulfated regions tend to cluster in segments interspersed with stretches of non-sulfated N-acetylglucosamine residues.[36] Representative structures of these GAGs are shown in Figure 3.1.

Given that the primary variations in ECM GAGs, are in the types of hexosamine (glucose or galactose based), and the different patterns of sulfation, mainly also on the hexosamines, it

should not be surprising that a chemical group on these amino sugars would make a good probe of structural variations. ^{1}H-^{15}N Heteronuclear Single Quantum Coherence (HSQC) experiments are widely used as two dimensional (2D) NMR methods for structural characterization in proteins and carbohydrates. For example, in proteins, chemical shifts of both the nitrogen and the proton of the amide groups respond to the torsional angles of bonds connecting the amide group to the polypeptide chain, as well as substituents on the α-carbon bonded to the nitrogen.[37, 38] Similar effects should exist for the amide ^{1}H-^{15}N pair in acetylated sugars, and influences from sites of glycosylation, anomeric configurations, neighboring residue types, and so forth, should also occur. In addition, charged groups, such as sulfates, that characterize HS, DS, and CS polymers, can have long-range effects on chemical shifts that might increase chemical shift sensitivity to sulfation patterns. A few recent reports on ^{15}N-HSs and ^{15}N-hyaluronic acids confirm sensitivity to some of these structural features,[39-43] however, the latter studies have not explored sensitivity related to sulfation patterns.

One of the primary limitations of GAG analysis by ^{15}N-NMR spectroscopy is that of sensitivity. This can be improved through ^{15}N isotopic enrichment of amide sites, something that has been accomplished for GAGs that can be synthesized beginning with bacterial products.[40, 42] This is not an option for analysis of commercial products, but availability of adequate amounts of material is not usually a problem in these instances. For mammalian cell investigations, where large amounts of material is usually not available, there is however an alternative. Recently the incorporation of ^{15}N from the side chain nitrogen of glutamine (Gln) has been demonstrated and used effectively in making Mass Spectroscopy (MS) analysis more quantitative.[44] Basically the side chain nitrogen makes its way into hexosamines through the pathway illustrated at Figure 3.2. As will be further described, there are a few other destinations for these nitrogens, including

bases of nucleic acids. However, widespread incorporation in protenacious materials seems relatively low. We will take advantage of metabolic labeling from Gln for ^{15}N enrichment of cellular GAGs in the applications that follow.

Based on the above considerations we here undertake a systematic investigation of the effect of sulfation at different sites in one class of GAGs, namely CS polymers and oligomers, tracking positions of ^{1}H-^{15}N cross-peaks in HSQC spectra. Results show that the chemical shifts of ^{15}N-resonances of amide protons of GalNAc residues in CS types are quite sensitive to different sulfation patterns, and that the positions of these resonances can be used to assess sulfate distributions in polymeric as well as oligomeric materials. The distinct positions of ^{1}H-^{15}N cross-peaks of other types of GAGs such as DS, and HS are also diagnostic, allowing identification of each type of these ECM GAGs in complex mixtures. Applications to the characterization of GAGs isolated from two types of cultured mammalian cells, mouse lung endothelium cells, and the Chinese hamster ovary (CHO) cells, are also presented. Sensitivity in these experiments was enhanced by taking advantage of the transfer of the side chain nitrogens of ^{15}N-Gln to N-acetylhexosaminyl units (GalNAc and GlcNAc) of GAGs during their biosynthesis, resulting in 20-25 fold improvement in NMR detectability.

Materials and Methods

Materials. The sodium salt of chondroitin sulfate A from bovine trachea (~65% of the residues have A type 4-*O*-sulfation, and the balance have C type 6-*O*-sulfation), the sodium salt of chondroitin sulfate C from shark cartilage (>95% of the residues have C type sulfation, and the balance have A type sulfation), the sodium salt of chondroitin sulfate B (dermatan sulfate) from porcine intestinal mucosa, hyaluronidase from sheep testes (type V), chondroitinase ABC lyase from *Proteus vulgaris*, Amberlite CG-120 resin, pyridine 99.8% anhydrous, N-acetyl-D-

glucosamine (minimum 99%), N-acetyl-D-galactosamine (approx. 98%), and Sephadex G-15 resin (Fractionation Range of dextrans <1.5 kDa) were purchased from Sigma-Aldrich Co (St. Louis MO). A pre-packed Zorbax strong anion exchange (SAX) semi-preparative column (9.4 x 250 mm, 5 Micron) was purchased from Agilent Technologies (St. Louis MO). Bio-Gel P-10 Gel resin (Fractionation range of dextrans from ~1.5 to ~20 kDa) in fine polyacrylamide beads, and the polypropylene chromatographic columns (120 x 1.5 cm for size exclusion chromatography, and 1.0 x 50 cm for desalting) were purchased from Bio-Rad Life Science (Hercules, CA). 3 mm glass NMR tubes were purchased from VWR Scientific (Rochester, NY). Oversulfated chondroitin sulfate and mammalian heparan sulfate were provided by Dr. Roberto J.C. Fonseca, and Angélica M. Gomes, respectively, both from the Institute of Medical Biochemistry, Federal University of Rio de Janeiro, RJ, Brazil. L-Glutamine (AMIDE-15N, 98%+), and deuterium oxide "100%" (D 99,96%) were purchased from Cambridge Isotope Laboratories, Inc. (Andover, MA). The endothelial cell line was derived from C57BL/6J mouse lung as reported previously.[45] The CHO K1 cells were generously provided by Dr. Jeffrey D. Esko (University of California San Diego School of Medicine). The cell culture medium DMEM and L-glutamine-free DMEM, and related cell culture supplements including penicillin-streptomycin and non-essential amino acids were obtained from Invitrogen (Carlsbad, CA). Fetal bovine serum (FBS) was purchased from Atlanta Biologicals (Lawrenceville, GA). ACS-grade 88% formic acid was purchased from J.T. Baker (Phillipsburg, NJ). HPLC-grade methanol and dimethyl sulfoxide (DMSO) were purchased from Fisher Scientific (Fair Lawn, NJ).

^{15}N-Isotopic Labeling of Cellular GAGs. The mouse lung endothelial cells and CHO cells were cultured until confluent at established conditions as reported previously.[45, 46] After initial

washing with L-Gln-free DMEM (2 x 3 min), the confluent cells were further washed by incubating with L-Gln-free DMEM at 37 ^{o}C under 5% CO_2 for 15 min. Following this the cells were cultured with L-Gln-free DMEM supplemented with 2 mM ^{15}N-Gln at 37 ^{o}C under 5% CO_2 for 24 hours. The culture media were collected and supernatants were pooled after centrifugation (2.000 rpm for 5 min). The cell pellets and the monolayer cells in culture plates were lysed with 0.1 N NaOH. The cell lysates were adjusted to pH 7.0 with 1 N HAc and then pooled with the supernatant. The pooled solution was added with 0.166 volume protease solution [1mg/ml pronase in 0.24M NaAc (pH6.5) + 1.92M NaCl] and digested overnight at 40 ^{o}C. For GAG isolation, the digested solution was loaded to a DEAE-Sephadex column (3 ml bed volume, Pharmacia) that was pre-treated with equilibration buffer [20 mM NaAc (pH 6.0) + 0.25 M NaCl]. The column was initially washed with 30 ml of the equilibration buffer, the GAGs were then eluted from the column with 20 mM sodium acetate + 1M NaCl and collected. The GAGs (plus other high negative charge non-GAG molecules) were desalted through a PD-10 column (Sephadex^{TM} G-25 TM, GE Healthcare) following the manufacturer's instructions.

Preparation of Unlabeled Samples and Cellular ^{15}N-Labeled GAG Oligosaccharides. CS-A from bovine trachea (150 mg) was digested with 1 mg of chondroitinase ABC (0.33UI) in 5 mL digesting buffer (50 mM Tris-HCl, pH 8.0, 150 mM sodium acetate, 100 μg/mL of bovine serum albumin) at 37 ^{o}C for 150 min. The digested sample was heated (boiled) at 100 ^{o}C for 15 min to stop digestion. CS-C from shark cartilage (150 mg) was digested with 10 mg of hyaluronidase in 3 mL 50 mM sodium phosphate, 150 mM NaCl (pH 6.0) at 37 ^{o}C for 24 hours. The digested sample was heated (boiled) at 100 ^{o}C for 15 min. A 3 mL sample from each digestion (heterogeneous CS oligosaccharide mixtures) was subjected to size-exclusion chromatography

on a Bio-Gel P-10 column (120 x 1.5 cm) using an elution solution of 10% ethanol, 1 M NaCl at a flow-rate of 1 mL/15 min. Peaks corresponding to fractionated oligosaccharides were pooled and desalted on a Sephadex G-15 column (1.0 x 50 cm) using an elution solution of 1% butanol in distilled water. The respective masses of the oligosaccharides were determined by analysis on a ThermoFinnigan LCQ Advantage MS instrument. The lyase- or hydrolase-digested dimers and hexamers were selected for further separation and analysis. These samples were freeze-dried after desalting and ~5 mg of the powered material was dissolved in ~100 μL H_2O with the pH previously adjusted to 5.0 with 0.1 M HCl. Then about ~ 50 μL of four different lyase- and hydrolase-treated samples (three CS hexamers, and one CS dimers) were subjected to SAX-High Pressure Liquid Chromatography (HPLC) using a linear NaCl gradient from 0 to 2 M in H_2O with pH previously adjusted to 5.0 with HCl, over a 50 min period at a flow rate of 3.0 mL/min. The separations were monitored by absorption at 214 nm and 232 nm for the hydrolase- and lyase-products respectively. The peaks were collected separately, desalted on a Sephadex G-15 column, lyophilized, and weighed. To provide samples having terminal sugars reduced to their corresponding galactitol forms (-ol), powered samples from commercial sources were treated with an equivalent weight of $NaBH_4$ in 1 mL water for 3 hours. The reactions were then stopped by adding a molar equivalent of acetic acid and incubating for 1 hour in an ice-bath, followed by desalting on a Sephadex G-15 column.

The respective structures of dimers and hexamers (ΔC4S, ΔC6S, ΔC444S-ol, C644S-ol, ΔC664S-ol, and C666S-ol) were determined by one and two dimensional NMR experiments (1D ^1H, $^1H/^1H$ Double quantum filtered correlation spectroscopy (DQF-COSY), $^1H/^1H$ Total correlation spectroscopy (TOCSY), $^1H/^{13}C$ Heteronuclear Multiple Quantum Coherence (HMQC), and $^1H/^{15}N$ Heteronuclear Single Quantum Coherence (HSQC)). The structural

nomenclature used above is exemplified with the ΔC4S, and C644S-ol. These respectively correspond to [ΔGlcA-β(1→3)GalNAc-4(SO_3^-)], and [GlcA-β(1→3)GalNAc-6(SO_3^-)-β(1→4)GlcA-β(1→3)GalNAc-6(SO_3^-)-β(1→4) GlcA-β(1→3)GalNAc-4(SO_3^-)-ol], where the symbol Δ indicates 4,5-unsaturation on the GlcA produced by ABC chondroitinase cleavage.

The GAG samples from endothelial and CHO cells were treated similarly. However, because of a suspicion that samples may carry contamination from released nucleic acids (another abundant negatively charged polymeric cellular component), half of the sample from the endothelial cellular preparation was treated with 200 μL of nucleases (1.32 mg/mL DNAse/RNAse) in Lysis buffer (75 mM tris, 300 mM NaCl, 200 mM EDTA, pH 7.7) plus 10 μL 1M $MgSO_4$ and 10 μL 0.1 M phenylmethanesulphonylfluoride (PMSF) at room temperature for 19 hours. The other half was not treated. Both halves were dissolved in 200 μL of the ABC lyase buffer and treated with 0.33UI of the chondroitinase ABC at 37 ^oC for 19 hours. Both samples were then separately applied to a Sephadex G-15 column and the peaks eluted with 1% butanol in water were individually pooled, lyophilized and analyzed by ^{15}N-gHSQC (digested material, Figure 3.S2A) and TOCSY (for both digested and undigested materials, Figure 3.S2B and S2C respectively). Curiously, the nuclease-untreated endothelial sample (pool of negatively charged molecules) was resistant to the chondroitinase ABC lyase. This lack of enzymatic activity is likely due to inhibition of the enzymes by nucleic acids which are competing with the natural substrate (Figure 3.S2B *vs*. S2C). After some NMR analysis (Figure 3.S3A-C), the nuclease/ABC-treated sample was applied to the SAX-HPLC, and the 4-sulfated dimers were separated from 6-sulfated dimers and from minor amounts (10%) of other oligosaccharides, mainly monomers and tetramers. The 4-sulfated chondroitin sulfate dimer was desalted on a Sephadex G-15 column and then analyzed by both NMR (Figure 3.S3D) and MS (Figure 3.7).

NMR Experiments. For 1D ^{1}H, $^{1}H/^{1}H$ DQF-COSY, $^{1}H/^{1}H$ TOCSY, and $^{1}H/^{13}C$ gHSQC spectra, the samples were dissolved in 130 μL 100% D_2O and transferred into 3 mm NMR tubes. For $^{1}H/^{15}N$ gHSQC spectra, the samples were dissolved in 130 μL 50 mM acetate buffer 12.5% D_2O (pH 4.5) 0.1 % sodium azide and transferred into a 3 mm NMR tube.

All NMR experiments were recorded at 25 ^{o}C on a Varian Inova spectrometer (with a triple resonance cold probe) operating at 800 MHz for ^{1}H, 200 MHz for ^{13}C, and 80 MHz for ^{15}N. The 1D ^{1}H spectra were recorded with 128 scans with a spectral width of 7 kHz, carrier position at the HOD peak (4.773 ppm), acquisition time set to 2 sec, and water presaturation pulse set to the position of the carrier for a period equal to the recovery delay, 1.5 sec.

The DQF-COSY spectra were run with spectral widths of 6 kHz, and acquisition time of 0.175s using 32 scans per t1 increment (128 points) to achieve a time domain matrix of 2048 x 256 complex points (real and imaginary parts). The TOCSY spectra were run with spectral widths of 6 kHz, and acquisition time of 0.175s using 96 scans per t1 increment (64 points) to achieve a time domain matrix of 2110 x 128 complex points, using a spin-lock field of 9 kHz, and a mixing time of 60 ms. ^{1}H-^{13}C HMQC spectra were run with acquisition time of 0.128s using 144 scans per t1 increment (128 points) to achieve a time domain matrix of 1366 × 256 complex points. ^{1}H-^{15}N HSQC spectra were recorded with acquisition time of 0.095s and with192 scans per t1 increment (128 points) to achieve a time domain matrix of 1366 × 256 complex points. The all processing was done with NMRPipe software.[47] All spectra were apodized in both dimensions with the automatic function cosine-bells, together with automatic zero-filling to double the sizes followed by rounding to the nearest power of 2. Reported chemical shifts for ^{1}H and ^{13}C are relative to the trimethylsilylpropionic acid, and liquid ammonia for ^{15}N.

MS analysis. Mass spectrometric analysis of GAG disaccharides derived from endothelial cells was performed by nanospray ionization in the negative ion mode, and analyzed with an LTQ-FT hybrid mass spectrometer (Thermo Scientific, Waltham, MA) operating in the linear ion trap only mode. One volume of GAG sample in 50 mM sodium acetate buffer was diluted with two volumes of methanol, to a final concentration estimated to be ~10 μM. The sample was infused through a hand-pulled silica capillary at a flow rate of ~0.6 μL/min, with an electrospray voltage of 2.6 kV. Spectra were accumulated for one minute and averaged to increase the signal-to-noise ratio. Isotopic distribution modeling was performed using IsoPro 3.0.

Results

^{15}N-NMR analysis of galactosaminoglycans. In order to establish the viability of ^{1}H-^{15}N HSQC spectra as a tool for recognition and characterization of GAGs, in particular their sulfation patterns or the linked uronic acid types, a series of GAG polymers were examined (Figure 3.3). These are available in substantial quantities and observation through HSQC spectra at natural abundance of ^{15}N (0.3%) is possible. First,

^{15}N-gHSQC spectra were run on the high-molecular weight CS standards at approximately 15 mg/ml, including CS-A (Figure 3.3A) which is primarily 4-sulfated (65%) and less 6-sulfation (35%), CS-C (Figure 3.3B) which is nearly completely 6-sulfated, and OSCS (Figure 3.3C) which is more than 75% sulfated at both 4- and 6-positions. Comparison of CS-A and CS-C spectra (Figure 3.3A *vs* 3B) shows that the ^{15}N-chemical shifts of amide groups from 4-sulfated GalNAc units are significantly more upfield than ^{15}N-resonances from 6-sulfated GalNAc residues; the ^{15}N-resonance of the GalNAc residues of the OSCS, which have both types of sulfation shows a resonance at an ^{15}N shift midway between that of the 4- and 6-sulfated species

(Figure 3.3C). More specifically, these resonances occur at 120.9 ppm, 121.6 ppm and 121.2 ppm, respectively (Table 3.1). The ^{1}H-resonances of the GalNAc units, in this series of GAGs, show a minimal dependence on sulfation position.

Dermatan sulfate (DS), which also belongs to the class of galactosaminoglycans like the CSs, still contains a GalNAc with β(1-4) linkage to an uronic acid. However, the uronic acid of DS is primarily iduronic acid (IdoA) with its linkage to GalNAc denoted α(1-3) rather than β(1-3) as in the GlcA of CSs. Note, as shown in Figure 3.1B *vs.*1A, that the change from β to α is the result of the dependence of nomenclature on the chirality of the C5 carbon rather than an actual change in linkage geometry. DS is predominantly 4-*O*-sulfated (Figure 3.1B). So, in comparison to the 4-*O*-sulfated CS, the structural difference is actually mainly epimerization at the C5 carbon (Figure 3.1A *vs*. 1B). Comparison of cross-peak positions should, therefore reflect simply the effect of moving the uronic acid carboxyl group from an equitorial to an axial position. Figure 3.3D shows a down field shift in the proton chemical shift of about 0.13 ppm compared to that of CS-A (Figure 3.3A), and a minimal change in the ^{15}N chemical shift (Table 3.1).

^{15}N-NMR analysis of HS polymers. Heparan sulfate (HS) is built on a different backbone than CS and DS polymers, having a β1-4 substituted (if glucuronic acid) and α1-4 linked GlcNAc instead of a β1-3 substituted and β1-4 linked GalNAc unit. It can also contain IdoA residues where its linkage nomenclature changes to α (Figure 3.1C). Many of the GlcNAc residues of HS are normally converted to N-sulfated forms, for which an N-H signal in the HSQC spectrum is hard to observe. This cross-peak has been observed by Zhang and coworkers,[48] but it is very weak in this report as well. It is possible that observation is difficult because of enhanced proton exchange among protonated sites resulting in peak broadening or transfer of magnetization from a saturated water resonance. This N-sulfation is followed by epimerization of the linked GlcAs to

IdoAs along with additional *O*-sulfation. However, stretches of the original GlcNAc residues linked to unepimerized GlcAs usually persist, and N-H signals from these residues are easier to observe by NMR. Figure 3.3E shows the spectrum of a HS preparation with a resonance for the amide protons of the ^{15}*N*-acetylated glucosamine residues that is more downfield than those of ^{15}*N*-acetylated galactosamine residues. The ^{15}N chemical shift is also about 2 ppm further downfield than GalNAc compounds (Table 4.1). Comparison with the cross-peak from the α-anomer in a ^{1}H-^{15}N HSQC spectrum of the monomeric GlcNAc shows reasonable agreement (Figure 3.S1A). Small differences (~ 0.22 and ~ 0.66 ppm in H and N, respectively, Table 3.1) are assumed to arise from the linkage to an uronic acid and substitution at the 4-position. Hence, comparison of HSQC spectra of different GAGs suggests that ^{1}H-^{15}N resonances can be exploited for diagnostic studies of GAG composition, clearly delineating GlcNAc and GalNAc composition (similarly to commercial standard acetylhexosamines as shown in Table 4.1), and clearly reporting on the extent of 4- and/or 6-sulfation of these same amino sugars (Figure 3.3A-D).

^{15}N-NMR analysis of 4- and/or 6-sulfated CS oligomers. If short oligomers, rather than long polymers, are to be assayed, additional effects due to the absence of substitutions, or anomeric mutarotation at the reducing end enters. This can be seen in ^{15}N-gHSQC spectra of CS oligosaccharides with different sulfation patterns (disaccharides in Figure 3.4, and hexasaccharides in Figure 3.5). CS dimers were obtained by digestion of standard CS-A with chondroitinase ABC. Extensive digestion produces two disaccharides differing in sulfation position (4- or 6-) with an additional 4-5 double bond in the non-reducing end GlcA units. Both purified disaccharides revealed two ^{1}H-^{15}N cross-peaks which are related to the α- and β-anomeric equilibrium in aqueous solution (Figure 3.4). The ΔC4S disaccharide (Figure 3.4A) has

its amide protons for α- and β- anomers at δ_H/δ_N = 8.353/120.60 ppm and δ_H/δ_N = 8.136/121.34 ppm respectively (Table 3.1). The ΔC6S disaccharide (Figure 3.4B) has its α- and β-amide protons at δ_H/δ_N = 8.241/121.80 ppm and δ_H/δ_N = 8.092/122.75 ppm respectively (Table 3.1). Both 4- and 6-sulfated CS dimers show higher populations of β-anomers in comparison to those of α-anomers in a ratio of 6.5/3.5. The β-anomer amide ^{1}H-resonance in the disaccharide with GalNAc at the reducing end is 0.15 to 0.20 ppm downfield of the amide proton resonance in the polymeric CS (Table 3.1). The ^{15}N-chemical shifts are downfield by about 1 ppm relative to the polymeric material (Table 3.1), but the difference between amide ^{1}H-chemical shifts of 4- and 6-*O*-sulfated disaccharides remains somewhat more than 0.1 ppm (Table 3.1), suggesting that this difference remains diagnostically useful.

The ^{15}N-HSQC spectra of the CS hexamers with different sulfation patterns obtained from ABC lyase or hyaluronidase digestion are very illustrative of the efficacy of the ^{15}N-^{1}H HSQC analysis for fast NMR assignment of sulfation types of CS derivatives (Figure 3.5). Before recording the ^{15}N-gHSQC spectra, these hexamers were reduced to eliminate superposition of peaks from α- and β-anomers, and their structures were independently determined by a combination of 2D NMR experiments, including DQF-COSY, TOCSY and ^{13}C-gHSQC (data not shown). The ^{15}N-HSQC spectra of these hexamers showed the same upfield and downfield relationship of ^{15}N-resonances for the amide protons of 4- and 6-sulfated GalNAc units, supporting the fact that this pattern can be widely used for recognition and assignment of sulfate sites. All the ^{1}H-^{15}N cross-peaks of the 4-sulfated units have ^{15}N-chemical shifts between 120.3-120.6 ppm, whereas the ^{15}N-chemical shifts from 6-sulfated GalNAc units are between 121.2-121.6 ppm (Figure 3.5).

^{15}N labeled GAGs from cell culture. One of the potential applications of a ^{1}H-^{15}N HSQC analysis of GAGs would be the determination of their composition as a function of cell type and

growth conditions. However, the amount of material isolated from cell culture is apt to be small, and sensitivity is low at the 0.3% abundance of ^{15}N. This limitation makes the development of an *in vivo* ^{15}N-labeling technique worthwhile. After supplementation of media with ^{15}N-Gln in mouse lung endothelium or CHO cell culture for 24h, GAG polymers were isolated as described in the methods section. Each preparation yielded approximately 600 μg of total ^{15}N-labeled material allowing ^{15}N-gHSQC spectra to be rapidly recorded (Figure 3.6). The endothelial labeled material (Figure 3.6A) clearly shows peaks characteristic of 4- and 6-sulfated CSs (compare to Figure 3.3A). However, other downfield ^{15}N-resonances also are present. Treatment with DNase and RNAse, followed by separation from low-molecular-weight materials on a Sephadex-G15 column eliminated these additional peaks suggesting they arise from nucleic acid contaminants from the initial step of GAG isolation. Curiously, there is no significant peak characteristic of HS in this cell type even though clear evidence for the existence of HS in endothelial cells has been previously demonstrated.[49] This could be due either to the absence of large amounts of HS under our specific labeling conditions, or a very high level of N-sulfation, since the observation of N-sulfated amides in standard HS samples proved to be difficult.

Conversely, material isolated from CHO cells (Figure 3.6B) revealed significant resonances characteristic of N-acetyls in HS molecules together with measurable resonances characteristic of C4S (compare Figure 3.6B with 3A). There are some more dispersed peaks near the primary HS resonance. These multiple peaks (dashed ellipse at Figure 3.6B) may belong to GlcNAc residues from a more heterogeneous region in HS, characterized by a mixture of both 6-*O*-sulfated and non-*O*-sulfated GlcNAc units together with adjacent uronic acid residues modified

or not by epimerization and/or 2-sulfation (see Figure 3.1C). Neither cell type showed evidence for expression of ^{15}N-DS-proteoglycans.

The level of ^{15}N-incorporation in the cellular GAG samples is clearly significant given the ease of observation. Using intensities of cross-peaks in comparison to the standard samples, labeling at a level of 5-10% was estimated. This represents enhancement over natural abundance by a factor of 15-30. To confirm this level of enrichment, the sample of endothelial CS was degraded to ΔC4S and ΔC6S disaccharides using nuclease treatment followed by chondroitinase ABC digestion, and subsequently analyzed by MS. These dimer products were purified by size exclusion and strong anion exchange chromatography, and then they were fully characterized by high resolution NMR spectroscopy (Figure 3.S2 and S3 at supplementary material).

An MS spectrum of the pure ΔC4S dimers obtained from the last purification on the HPLC-SAX chromatography is presented in Figure 3.7. In Figure 3.7A the experimental spectrum is compared to a simulated isotopomer profile assuming natural abundances of ^{15}N, ^{13}C, and ^{2}H. Note that the simulation of the M+1 peak in particular does not have sufficient intensity. Raising the ^{15}N abundance to 8% produces a very good fit (Figure 3.7B), while assuming the ^{15}N abundance of 10% produces a small overestimation. The ^{15}N abundance of 8% calculated with MS agrees quite well with the previous NMR-based estimates.

Discussion

In this work we have demonstrated that GAGs commonly found at the cell surface proteoglycans of mammalian cells can easily be analyzed based on ^{1}H-^{15}N^{-} HSQC NMR experiments. CS, DS, and HS all give cross peaks in distinct regions of the NMR spectrum. In addition, the 4- and/or 6-sulfation patterns of CS polymers or oligomers can be identified. As long as resonances are reasonably sharp and adequate relaxation delays are achieved, relative amounts of various

components of these ECM GAGs can be quantified. Analysis can also be carried out on crude isolates released from cell surfaces by lysis, pronase digestion, and retention on anion exchange chromatographic media. GAG composition analysis by conventional means usually requires additional separation and digestion steps, after which identification of sulfation sites is normally done by additional HPLC-analysis and/or a combination of NMR and MS analysis.[50] These procedures represent significantly more effort and often lead to uncertainties in quantitation because of incomplete digestion and molecule dependent MS and HPLC response.

The NMR methods presented here do have their own limitations. HS detection described here is currently through their residual N-acetyl groups, making characterization dependent on the extent of N-sulfation. However, detection of sulfated amides is possible under some conditions,[48] and conditions might be adjusted to achieve this more routinely. NMR is also not a highly sensitive method and this is a potential problem here because of the low magnetogyric ratio and low natural abundance of the ^{15}N isotope (0.37%). Although the natural abundance of the ^{15}N-isotope remains a problem, observation by indirect detection through protons avoids problems with a low magnetogyric ratio and provides sufficient improvement in sensitivity to characterize materials even at natural abundance (~5 mg samples with about 120 min acquisition). The methods can therefore be of use in the characterization of commercial products where amounts of material are seldom a concern, including the low molecular weight heparins recently under scrutiny for OSCS contamination.[51] For analysis of cell culture products enrichment in ^{15}N to levels approaching 10% has been demonstrated. This opens the possibility of studying metabolic variations in the production of GAGs throughout the cell cycle and under the influence of various environmental factors.

It is not surprising that ^{15}N and ^{1}H chemical shifts would be sensitive to structural differences in hexosamine rings such as exist between GalNAc and GlcNAc. However, the sensitivity of amide ^{15}N and ^{1}H chemical shifts relative to changes in more remote groups is perhaps surprising. The 4-sulfate, 6-sulfate, and epimeric carboxylate of the substituted uronic acid are 5, 7, and 6 bonds removed respectively. However, in each case, we are dealing with a charged or partially charged group. Electric field effects on chemical shifts indeed can be quite long range.[52, 53] Interpretation as the sum of field projections on bonds and field squared effects also makes them non-additive as observed in comparing 4-, 6-, and 4- plus 6-sulfations. Effects of titration of carboxylate groups in fatty acids on polarizable C-C double bonds can produce shifts of as much as a ppm even when olefinic carbons are 6 bonds removed from the carboxyl.[54, 55] Similar effects exist for N-H bonds of amides in peptides.[53] The positions of sulfates and carboxyls depend on conformation, but they are approximately 5.7 and 4.3 Å away from the amide nitrogen of the 4-*O*-sulfated GalNAc of CS in an acceptable low energy model of the fragments. At this distance, assuming a charge of -1, an effective dielectric of 5, an optimum projection, and using the formulas given at the work of Hass *et al*.,[53] a contribution to the ^{15}N chemical shift of 1.4 ppm would be observed. Hence, it is possible to rationalize the sensitivity to sulfate placement. The effects are, nevertheless, useful indicators of GAG composition regardless of their origin (Table 3.1 presents offsets due to addition of charged groups at various sites, or pairs of sites, that can be used as empirical guide). If the origin is electrostatic, an additional issue is raised, namely the importance of controlling factors which might modulate these effects, such as the types and concentration of counter-ions in assay solutions (50 mM Na^{+} and pH 4.5 in the data presented here).

The potential applications of the assay methods suggested herein are broad. The ^{15}N-NMR spectra of GAGs might, for example, be used for auxiliary quality control procedures in checking for the presence of OSCS-contaminations in clinical samples of heparin,[32, 51] since the ^{15}N and ^{1}H chemical shifts of glucosamine and galactosamine residues are quite distinct (Figure 3.3A-D *vs*. 3E, Table 3.1). In this case, the speed of the method could be considerably improved by replacing the 2D ^{1}H-^{15}N HSQC acquisitions with a 1D ^{15}N-filtered ^{1}H-observe acquisition that resolves primarily based on proton chemical shifts. Interpretation in terms of molecular characteristics of different species in mixed samples may also be more straightforward than methods currently suggested like the diffusion ordered NMR spectroscopy,[56] or the combination of 1D ^{1}H-NMR spectra with polyacrylamide gel electrophoresis (PAGE).[57]

Applications to metabolic monitoring of GAG production in various cell types should also be possible. We provided a preliminary demonstration with applications to endothelial, and CHO cells. These applications were not pursued in a well-controlled and systematic way that would allow biologically relevant conclusions, but the dramatic differences observed between cell types suggest the potential of these applications. The ECM GAGs are known to turn over in response to various environmental effects,[58-60] and composition is known to vary with differentiation during development.[61] In the work presented, the endothelium and CHO cells showed different patterns of ^{15}N-labeled GAGs in their cell surface proteoglycans (Figure 3.6). The endothelial cells synthesized significant amounts of ^{15}N-CS (Figure 3.6A) with the same 4-/6-sulfation ratio 6.5/3.5 as the standard CS-A extracted from bovine trachea (Figure 3.3A), but the complete absence of cross-peaks characteristic of HS. CHO cells, on the other hand, showed mostly cross-peaks characteristic of ^{15}N-HSs. A peak characteristic of 4-sulfated CS is also observed, but a 6-sulfated peak is not. In addition, the labeled cellular GAG analysis showed

clearly total absence of ^{15}N-DS proteoglycans in both cell types. The absence of these GAG types might be due to lack of sensitivity related to their low occurrence in these cells. The additional absence of an HS cross-peak in isolates from endothelial cells is intriguing since these cells have previously been reported to have significant levels of HS.[49] It is possible that the unlabeled material is primarily from initial cell growth, or that there was a substantial pool of unlabeled, Golgi resident, GlcNAc that went directly into HS, whereas the GalNAc that went into CS was produced more directly from newly synthesized, and labeled GlcNAc units. It is also possible that the HS synthesized in endothelial cells is highly N-sulfated and just a few of the GlcNAc groups that we use for HS detection remain. CHO cells and endothelial cells under the growth conditions used here are clearly metabolically different. Further studies of the time course of ^{15}N-labeled GAG production in these cells, beginning with the labeling procedure at the initial stages of the cell growth, would certainly be of interest. The methods described here could easily be adapted to this kind of future analysis.

Acknowledgments. This work was supported by grant from the National Center for Research Resources of the National Institute of Health (NIH), RR005351. VHP was supported by a post-doctoral fellowship (PDE #201019/2008-6) from Conselho Nacional de Desenvolvimento Científico e Tecnológico (CNPq), Brazil. We are also grateful to Lidia Nieto for the NMR assignments of the standard unsaturated CS dimers, to John Glushka for his technical assistance on the NMR experiments, to Christian Heiss for the MS analysis of the CS dimers and hexamers, and to Laura Morris for the computational assistance.

SUPPORTING INFORMATION AVAILABLE

Figures presenting NMR analysis of additional standards and characterization of the endothelial CS lyase digested products are available free of charge via the Internet at http://pubs.acs.org.

Reference

1. Heino, J. and J. Kapyla, *Cellular Receptors of Extracellular Matrix Molecules.* Current Pharmaceutical Design, 2009. **15**(12): p. 1309-1317.
2. Yu, F., et al., *Conformational preferences of chondroitin sulfate oligomers using partially oriented NMR spectroscopy of C-13-labeled acetyl groups.* Journal of the American Chemical Society, 2007. **129**(43): p. 13288-13297.
3. Gandhi, N.S. and R.L. Mancera, *The Structure of Glycosaminoglycans and their Interactions with Proteins.* Chemical Biology & Drug Design, 2008. **72**(6): p. 455-482.
4. Iozzo, R.V., *Matrix proteoglycans: From molecular design to cellular function.* Annual Review of Biochemistry, 1998. **67**: p. 609-652.
5. Beaulieu, J.F., P.H. Vachon, and S. Chartrand, *IMMUNOLOCALIZATION OF EXTRACELLULAR-MATRIX COMPONENTS DURING ORGANOGENESIS IN THE HUMAN SMALL-INTESTINE.* Anatomy and Embryology, 1991. **183**(4): p. 363-369.
6. Cohn, R.H., J.J. Cassiman, and M.R. Bernfield, *RELATIONSHIP OF TRANSFORMATION, CELL DENSITY, AND GROWTH-CONTROL TO CELLULAR DISTRIBUTION OF NEWLY SYNTHESIZED GLYCOSAMINOGLYCAN.* Journal of Cell Biology, 1976. **71**(1): p. 280-294.
7. Bruns, R.R. and J. Gross, *COLLAGEN AND GLYCOSAMINOGLYCANS IN CELL-ADHESION.* Experimental Cell Research, 1980. **128**(1): p. 1-7.
8. Aviezer, D., et al., *PERLECAN, BASAL LAMINA PROTEOGLYCAN, PROMOTES BASIC FIBROBLAST GROWTH FACTOR-RECEPTOR BINDING, MITOGENESIS, AND ANGIOGENESIS.* Cell, 1994. **79**(6): p. 1005-1013.

9. Gorio, A., et al., *Glycosaminoglycan supplementation promotes nerve regeneration and muscle reinnervation.* European Journal of Neuroscience, 1997. **9**(8): p. 1748-1753.

10. Cattaruzza, S. and R. Perris, *Proteoglycan control of cell movement during wound healing and cancer spreading.* Matrix Biology, 2005. **24**(6): p. 400-417.

11. Muramatsu, T. and H. Muramatsu, *Glycosaminoglycan-binding cytokines as tumor markers.* Proteomics, 2008. **8**(16): p. 3350-3359.

12. Domowicz, M., D. Mangoura, and N.B. Schwartz, *Cell specific-chondroitin sulfate proteoglycan expression during CNS morphogenesis in the chick embryo.* International Journal of Developmental Neuroscience, 2000. **18**(7): p. 629-641.

13. Thesleff, I., et al., *CELL-SURFACE PROTEOGLYCAN EXPRESSION CORRELATES WITH EPITHELIAL MESENCHYMAL INTERACTION DURING TOOTH MORPHOGENESIS.* Developmental Biology, 1988. **129**(2): p. 565-572.

14. Kaplan, C.D., et al., *Development of inflammation in proteoglycan-induced arthritis is dependent on Fc gamma R regulation of the cytokine/chemokine environment.* Journal of Immunology, 2002. **169**(10): p. 5851-5859.

15. Koninger, J., et al., *The ECM proteoglycan decorin links desmoplasia and inflammation in chronic pancreatitis.* Journal of Clinical Pathology, 2006. **59**(1): p. 21-27.

16. Doodes, P.D., et al., *CCR5 Is Involved in Resolution of Inflammation in Proteoglycan-Induced Arthritis.* Arthritis and Rheumatism, 2009. **60**(10): p. 2945-2953.

17. De Mattos, D.A., et al., *Heparan sulfates from arteries and veins differ in their antithrombin-mediated anticoagulant activity.* Journal of Thrombosis and Haemostasis, 2008. **6**(11): p. 1987-1990.

18. He, L., et al., *Vascular dermatan sulfate regulates the antithrombotic activity of heparin cofactor II.* Blood, 2008. **111**(8): p. 4118-4125.

19. Inatani, M., et al., *Upregulated expression of N-syndecan, a transmembrane heparan sulfate proteoglycan, in differentiated neural stem cells.* Brain Research, 2001. **920**(1-2): p. 217-221.

20. Pettway, Z., et al., *Age-dependent inhibition of neural crest migration by the notochord correlates with alterations in the S103L chondroitin sulfate proteoglycan.* Experimental Cell Research, 1996. **225**(1): p. 195-206.

21. Perris, R., et al., *Inhibitory effects of PG-H/aggrecan and PG-M/versican on avian neural crest cell migration.* Faseb Journal, 1996. **10**(2): p. 293-301.

22. Tully, S.E., et al., *A chondroitin sulfate small molecule that stimulates neuronal growth.* Journal of the American Chemical Society, 2004. **126**(25): p. 7736-7737.

23. vanPutten, J.P.M., S.F. Hayes, and T.D. Duensing, *Natural proteoglycan receptor analogs determine the dynamics of Opa adhesin-mediated gonococcal infection of Chang epithelial cells.* Infection and Immunity, 1997. **65**(12): p. 5028-5034.

24. Dean, D.D., et al., *AMELIORATION OF LAPINE OSTEOARTHRITIS BY TREATMENT WITH GLYCOSAMINOGLYCAN PEPTIDE ASSOCIATION COMPLEX (RUMALON).* Arthritis and Rheumatism, 1991. **34**(3): p. 304-313.

25. Todhunter, R.J. and G. Lust, *POLYSULFATED GLYCOSAMINOGLYCAN IN THE TREATMENT OF OSTEOARTHRITIS.* Journal of the American Veterinary Medical Association, 1994. **204**(8): p. 1245-1251.

26. Fellstrom, B., et al., *TREATMENT OF RENAL CALCIUM STONE DISEASE WITH THE SYNTHETIC GLYCOSAMINOGLYCAN PENTOSAN POLYSULFATE.* World Journal of Urology, 1994. **12**(1): p. 52-54.

27. Siragusa, S., et al., *Low-molecular-weight heparins and unfractionated heparin in the treatment of patients with acute venous thromboembolism: Results of a meta-analysis.* American Journal of Medicine, 1996. **100**(3): p. 269-277.

28. Hull, R.D., et al., *The treatment of proximal vein thrombosis with subcutaneous low-molecular-weight heparin compared with continuous intravenous heparin.* Clinical and Applied Thrombosis-Hemostasis, 1995. **1**(2): p. 151-159.

29. Koopman, M.M.W., et al., *Treatment of venous thrombosis with intravenous unfractionated heparin administered in the hospital as compared with subcutaneous low-molecular-weight heparin administered at home.* New England Journal of Medicine, 1996. **334**(11): p. 682-687.

30. Fareed, J., D.A. Hoppensteadt, and R.L. Bick, *Management of thrombotic and cardiovascular disorders in the new millenium.* Clinical and Applied Thrombosis-Hemostasis, 2003. **9**(2): p. 101-108.

31. Sugahara, K., et al., *Recent advances in the structural biology of chondroitin sulfate and dermatan sulfate.* Current Opinion in Structural Biology, 2003. **13**(5): p. 612-620.

32. Guerrini, M., et al., *Oversulfated chondroitin sulfate is a contaminant in heparin associated with adverse clinical events.* Nature Biotechnology, 2008. **26**(6): p. 669-675.

33. Kishimoto, T.K., et al., *Contaminated heparin associated with adverse clinical events and activation of the contact system.* New England Journal of Medicine, 2008. **358**(23): p. 2457-2467.

34. Blossom, D.B., et al., *Outbreak of Adverse Reactions Associated with Contaminated Heparin.* New England Journal of Medicine, 2008. **359**(25): p. 2674-2684.

35. Gama, C.I., et al., *Sulfation patterns of glycosaminoglycans encode molecular recognition and activity.* Nature Chemical Biology, 2006. **2**(9): p. 467-473.

36. Esko, J.D. and U. Lindahl, *Molecular diversity of heparan sulfate.* Journal of Clinical Investigation, 2001. **108**(2): p. 169-173.

37. Wang, Y.J. and O. Jardetzky, *Probability-based protein secondary structure identification using combined NMR chemical-shift data.* Protein Science, 2002. **11**(4): p. 852-861.

38. Wishart, D.S., et al., *H-1, C-13 AND N-15 CHEMICAL-SHIFT REFERENCING IN BIOMOLECULAR NMR.* Journal of Biomolecular Nmr, 1995. **6**(2): p. 135-140.

39. Blundell, C.D., et al., *Use of N-15-NMR to resolve molecular details in isotopically-enriched carbohydrates: sequence-specific observations in hyaluronan oligomers up to decasaccharides.* Glycobiology, 2004. **14**(11): p. 999-1009.

40. Mobli, M., M. Nilsson, and A. Almond, *The structural plasticity of heparan sulfate NA-domains and hence their role in mediating multivalent interactions is confirmed by high-accuracy N-15-NMR relaxation studies.* Glycoconjugate Journal, 2008. **25**(5): p. 401-414.

41. Almond, A., P.L. DeAngelis, and C.D. Blundell, *Dynamics of hyaluronan oligosaccharides revealed by N-15 relaxation.* Journal of the American Chemical Society, 2005. **127**(4): p. 1086-1087.

42. Blundell, C.D. and A. Almond, *Temperature dependencies of amide H-1- and N-15-chemical shifts in hyaluronan oligosaccharides.* Magnetic Resonance in Chemistry, 2007. **45**(5): p. 430-433.

43. Sattelle, B.M., et al., *A #D-structural model of unsulfated chondroitin from high-field NMR: 4-sulfation has littel effect n backbone conformation.* Carbohydrate Research, 2010. **345**: p. 291-302.

44. Orlando, R., et al., *IDAWG: Metabolic Incorporation of Stable Isotope Labels for Quantitative Glycomics of Cultured Cells.* Journal of Proteome Research, 2009. **8**(8): p. 3816-3823.

45. Fuster, M.M., et al., *Genetic alteration of endothelial heparan sulfate selectively inhibits tumor angiogenesis.* Journal of Cell Biology, 2007. **177**(3): p. 539-549.

46. Wei, G., et al., *Location of the glucuronosyltransferase domain in the heparan sulfate copolymerase EXT1 by analysis of Chinese hamster ovary cell mutants.* Journal of Biological Chemistry, 2000. **275**(36): p. 27733-27740.

47. Delaglio, F., et al., *NMRPIPE - A MULTIDIMENSIONAL SPECTRAL PROCESSING SYSTEM BASED ON UNIX PIPES.* Journal of Biomolecular Nmr, 1995. **6**(3): p. 277-293.

48. Zhang, Z.Q., et al., *Solution structures of chemoenzymatically synthesized heparin and its precursors.* Journal of the American Chemical Society, 2008. **130**(39): p. 12998-13007.

49. Wang, L.C., et al., *Endothelial heparan sulfate deficiency impairs L-selectin- and chemokine-mediated neutrophil trafficking during inflammatory responses.* Nature Immunology, 2005. **6**(9): p. 902-910.

50. Sasisekharan, R., R. Raman, and V. Prabhakar, *Glycomics approach to structure-function relationships of glycosaminoglycans.* Annual Review of Biomedical Engineering, 2006. **8**: p. 181-231.

51. Zhang, Z.Q., et al., *Oversulfated chondroitin sulfate: Impact of a heparin impurity, associated with adverse clinical events, on low-molecular-weight heparin preparation.* Journal of Medicinal Chemistry, 2008. **51**(18): p. 5498-5501.

52. Bader, R., *Utilizing the Charge Field Effect on Amide N-15 Chemical Shifts for Protein Structure Validation.* Journal of Physical Chemistry B, 2009. **113**(1): p. 347-358.

53. Hass, M.A.S., M.R. Jensen, and J.J. Led, *Probing electric fields in proteins in solution by NMR spectroscopy.* Proteins-Structure Function and Bioinformatics, 2008. **72**(1): p. 333-343.

54. Batchelo.Jg, R.J. Cushley, and Prestega.Jh, *C-13 FOURIER-TRANSFORM NUCLEAR MAGNETIC-RESONANCE .8. ROLE OF STERIC AND ELECTRIC-FIELD EFFECTS IN FATTY-ACID SPECTRA.* Journal of Organic Chemistry, 1974. **39**(12): p. 1698-1705.

55. Batchelo.Jg, et al., *ELECTRIC-FIELD EFFECTS IN C-13 NUCLEAR MAGNETIC-RESONANCE SPECTRA OF UNSATURATED FATTY-ACIDS - POTENTIAL TOOL FOR CONFORMATIONAL-ANALYSIS.* Journal of the American Chemical Society, 1973. **95**(19): p. 6358-6364.

56. Sitkowski, J., et al., *Assessment of Oversulfated Chondroitin Sulfate in Low Molecular Weight and Unfractioned Heparins Diffusion Ordered Nuclear Magnetic Resonance Spectroscopy Method.* Journal of Medicinal Chemistry, 2008. **51**(24): p. 7663-7665.

57. Zhang, Z.Q., et al., *Analysis of Pharmaceutical Heparins and Potential Contaminants Using H-1-NMR and PAGE.* Journal of Pharmaceutical Sciences, 2009. **98**(11): p. 4017-4026.

58. Gressner, A.M., *EFFECTS OF CONDITIONED MEDIA FROM NORMAL AND REGENERATING HEPATOCYTES ON PROLIFERATION AND PROTEOGLYCAN SYNTHESIS OF RAT-LIVER FAT STORING CELLS IN CULTURE.* Biological Chemistry Hoppe-Seyler, 1989. **370**(9): p. 902-903.

59. Gressner, A.M. and S. Schafer, *COMPARISON OF SULFATED GLYCOSAMINOGLYCAN AND HYALURONATE SYNTHESIS AND SECRETION IN CULTURED-HEPATOCYTES, FAT STORING CELLS, AND KUPFFER CELLS.* Journal of Clinical Chemistry and Clinical Biochemistry, 1989. **27**(3): p. 141-149.

60. Gressner, A.M., H. Pazen, and H. Greiling, *BIOSYNTHESIS OF GLYCOSAMINOGLYCANS IN NORMAL RAT-LIVER AND IN RESPONSE TO EXPERIMENTAL HEPATIC INJURY.* Hoppe-Seylers Zeitschrift fur Physiologische Chemie, 1977. **358**(7): p. 825-833.

61. Oohira, A., et al., *DEVELOPMENTAL-CHANGE IN THE GLYCOSAMINOGLYCAN COMPOSITION OF THE RAT-BRAIN.* Journal of Neurochemistry, 1986. **47**(2): p. 588-593.

Figure and tables

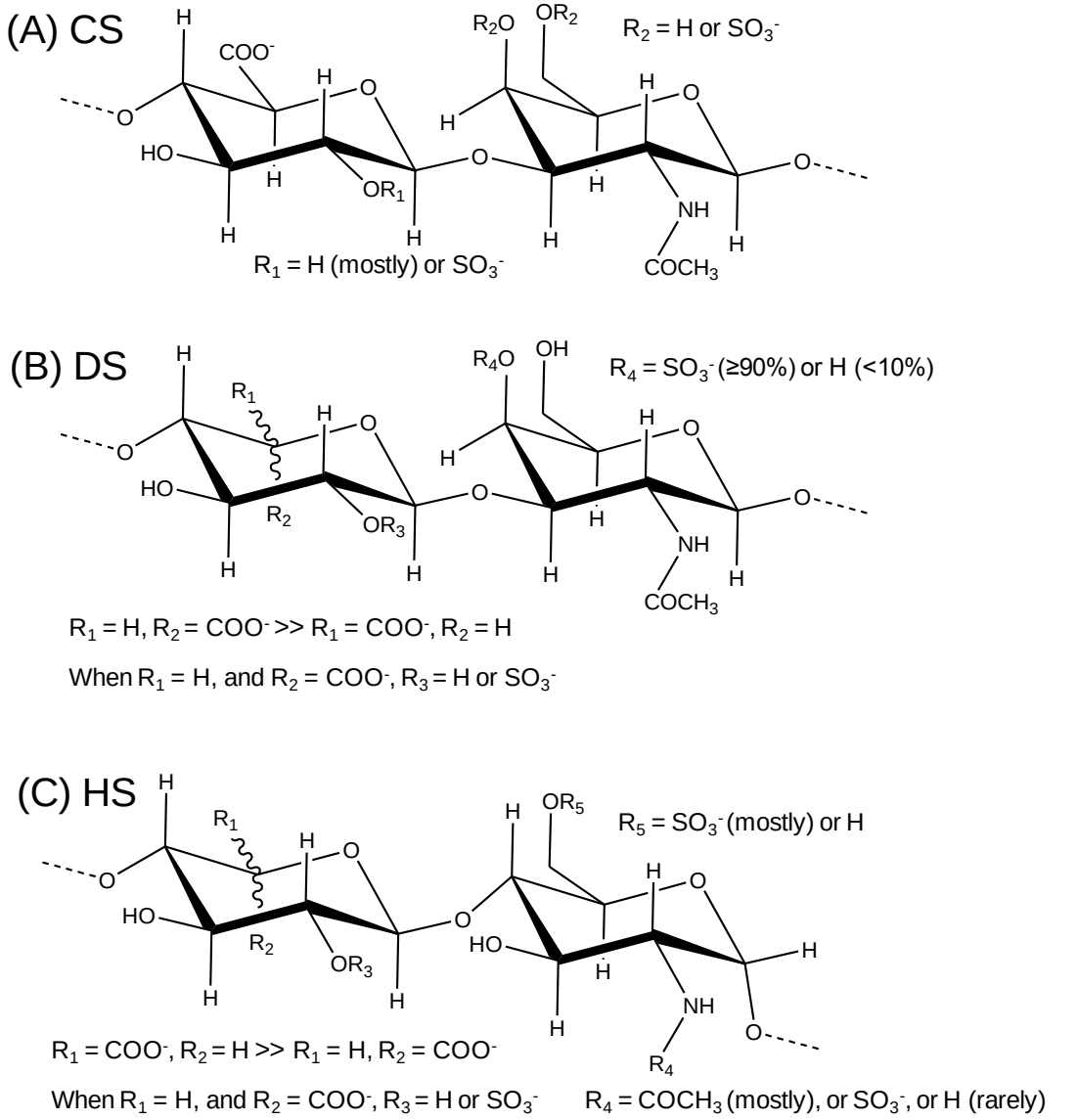

Figure 3.1. Major repeating disaccharide units of the most abundant ECM GAGs found in mammalian cell surface proteoglycans. (A) The backbone of CS is homogeneously composed of [-4)-GlcA-β(1-3)-GalNAc-β(1-]$_n$. (B) The backbone of DS (also known as CS-B) is mostly composed of [-4)-IdoA-α(1-3)-GalNAc-β(1-]$_n$, but it also contains minor amounts of [-4)-GlcA-β(1-3)-GalNAc-β(1-]$_n$. (C) The HS backbone is mostly composed of [-4)-GlcA-β(1-4)-GlcNAc-α(1-]$_n$, but it also contains regions of [-4)-IdoA-α(1-4)-GlcNAc-α(1-]$_n$.

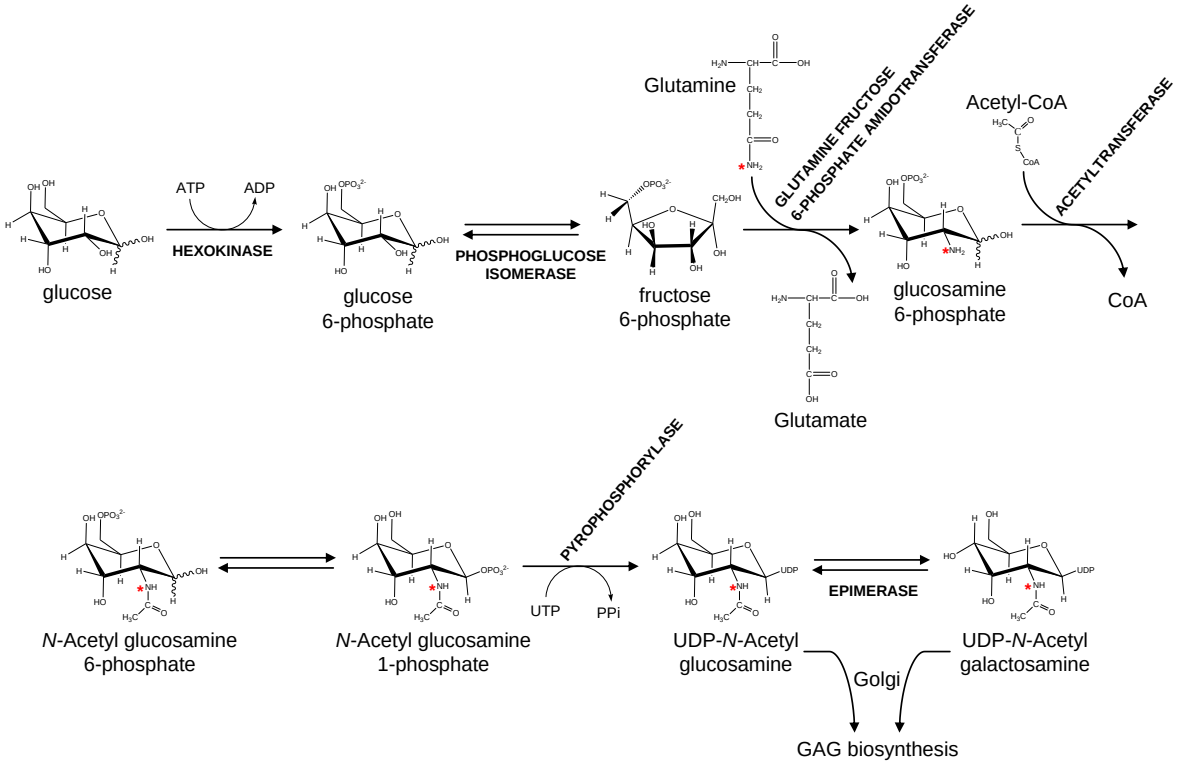

Figure 3.2. Schematic representation of the cytosolic biosynthesis of ^{15}N-labeled N-acetyl hexosamines that will be further used inside the Golgi apparatus for building up the GAG backbones in proteoglycans. The names of the enzymes are fully written in upper cases while the substrates and products are mostly written in lower cases. The ^{15}N-labeled sites are indicated with red asterisks. For more details about GAG biosynthesis see also Sugahara *et al.*,2003[31], or Esko and Lindahl, 2001[36].

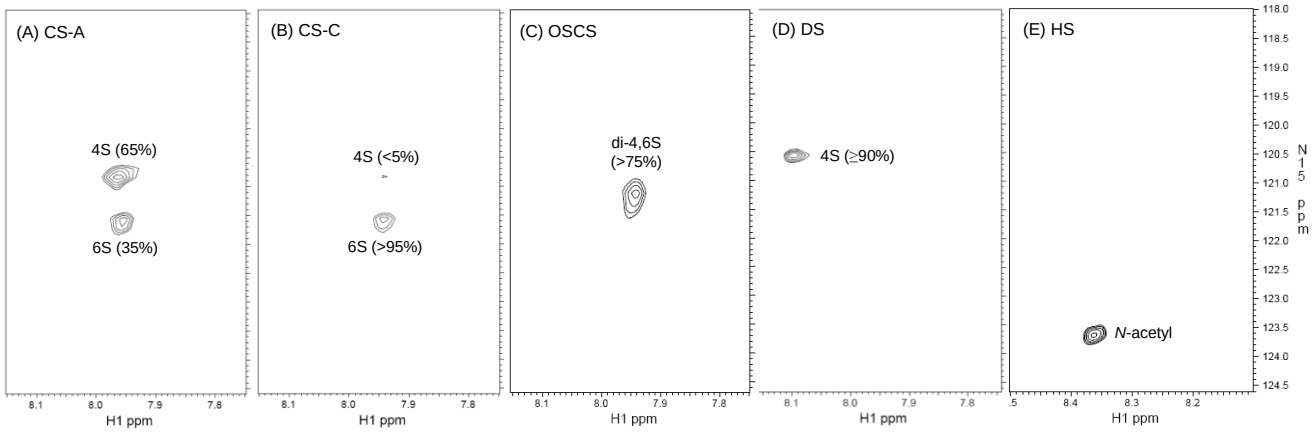

Figure 3.3. Comparative NMR analysis of ^{1}H- and ^{15}N-chemical shifts of amide protons from CS types (A-D), and mammalian HS (E) using ^{1}H-^{15}N-gHSQC spectra. (A) The CS-A from bovine trachea possesses ~ 65% of 4-sulfation, and ~ 35% of 6-sulfation GalNAc residues, whereas (B) the CS-C from shark cartilage has over 95% 6-sulfation GalNAc units. (C) The OSCS possesses over 75% of 4,6-di-sulfation GalNAc units. (D) The DS, also known as CS-B, from porcine intestinal mucosa is composed of ≥ 90% 4-sulfated GalNAc units. (E) The mammalian HS reveals only one peak that necessarily belongs to its ^{15}N-acetylated glucosaminyl unit. Note the different ^{1}H chemical shift scale in (E).

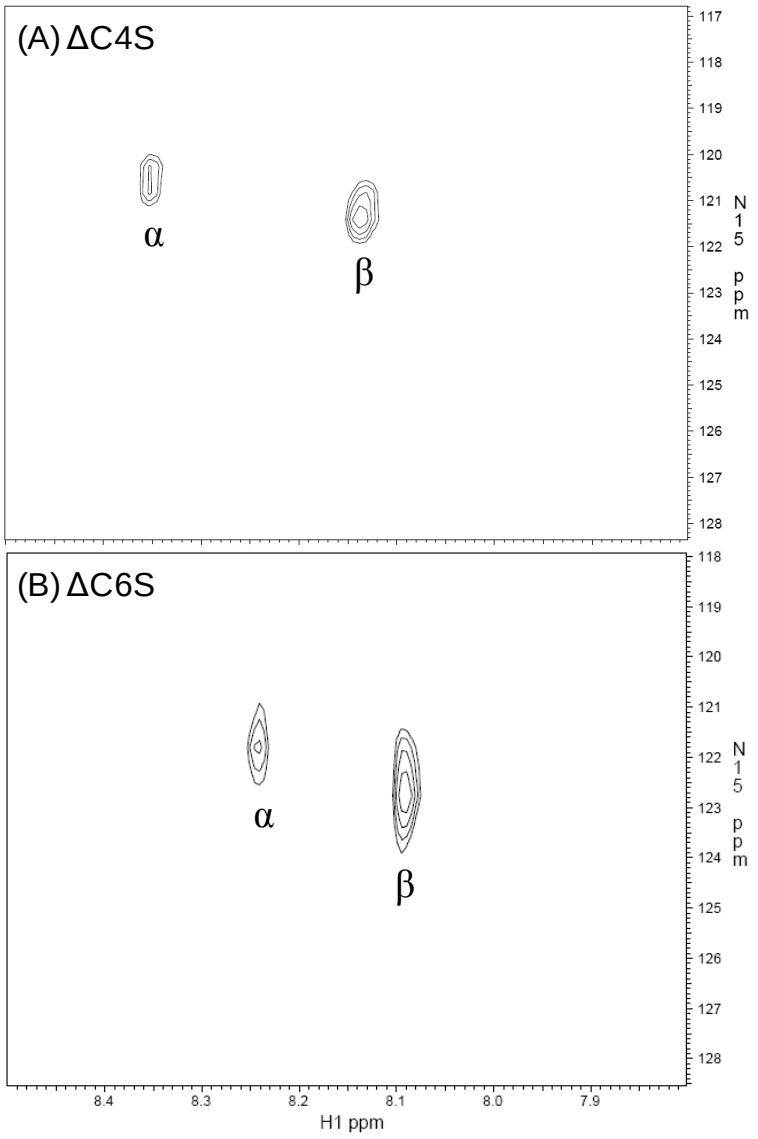

Figure 3.4. Comparative NMR analysis of α- and β-$^{1}H/^{15}N$-resonances of unreduced unsaturated 4- (A), and 6-sulfated (B) CS dimers obtained from ABC lyase digestion, using ^{1}H-^{15}N gHSQC spectra. The α-/β-signals arises from mutarotation of anomerics in aqueous solution, which the equilibrium ratio is 3.5/6.5.

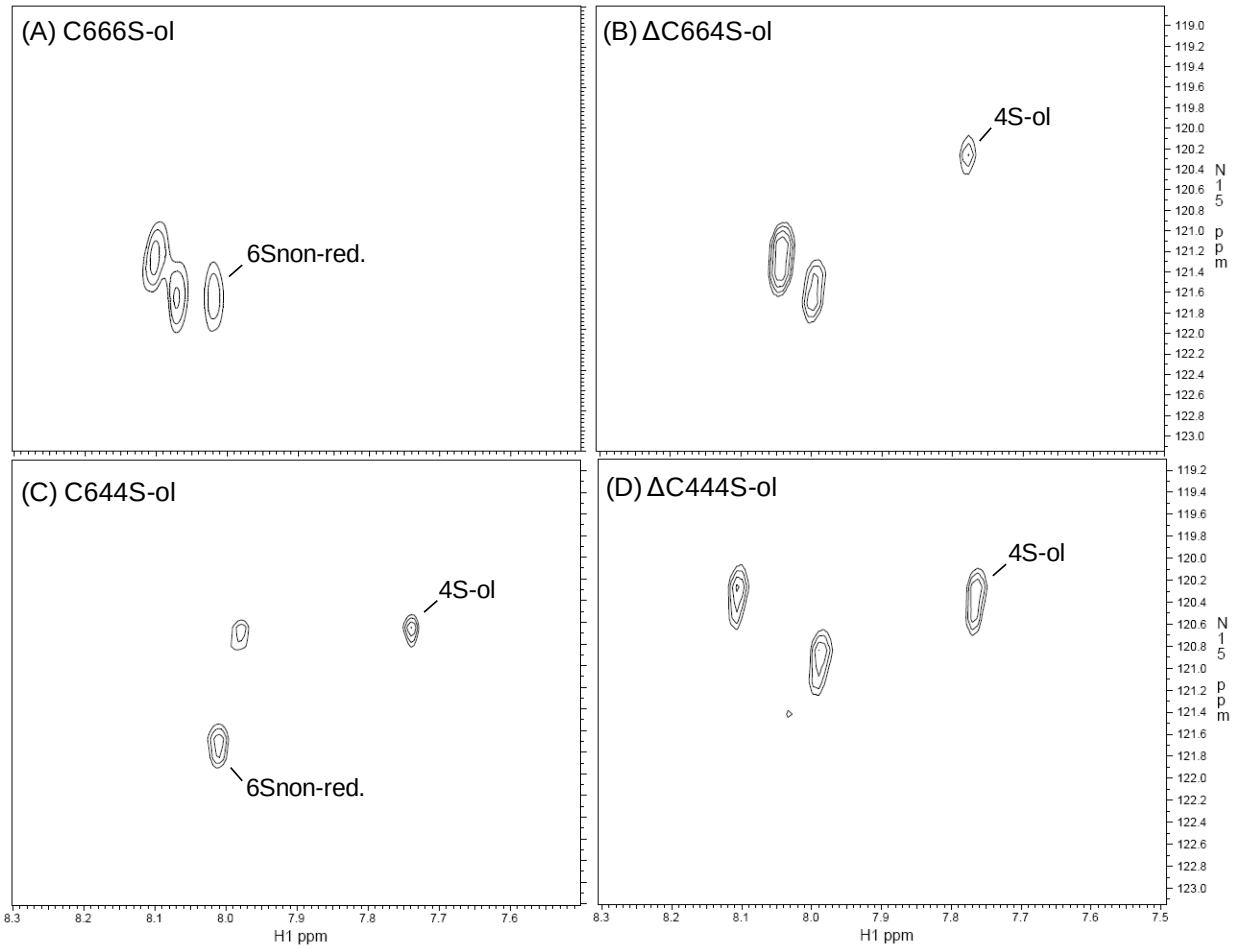

Figure 3.5. Comparative NMR analysis of reduced CS hexamers from ABC lyase (A,C), and hyaluronidase (B,D) digestions using ^{1}H-^{15}N gHSQC spectra. (A) C666S-ol, (B) ΔC664S-ol, (C) C644S-ol, and (D) ΔC444-ol. The peaks assigned as 6Snon-red., and 4S-ol belong to the 6-sulfated and 4-sulfated GalNAc units from non-reducing and reduced terminals respectively.

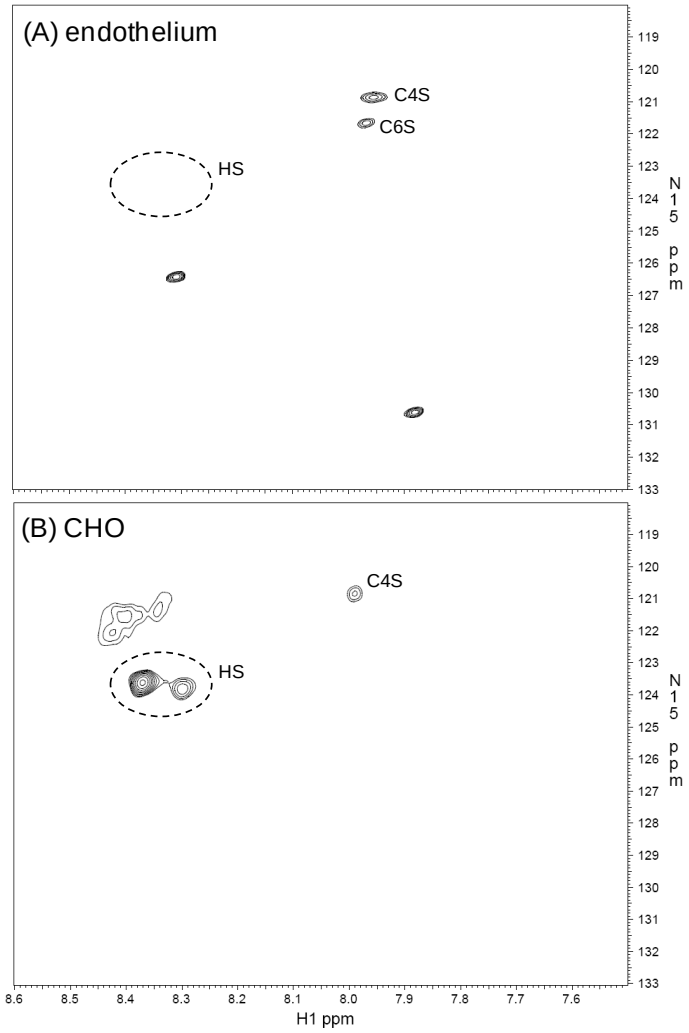

Figure 3.6. ^{1}H-^{15}N gHSQC spectra of ^{15}N-labeled negatively charged molecules extracted from the mouse lung endothelial cells (A), and (B) CHO cells.

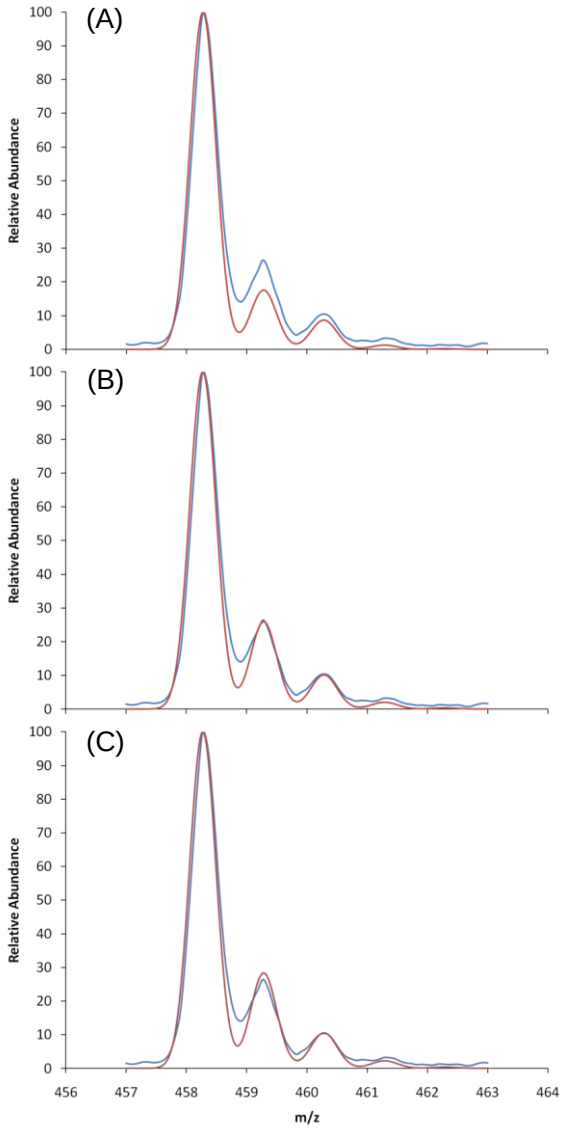

Figure 3.7. MS spectra of the endothelial ΔC4S dimers. The blue peaks represent the measured spectra while the red peaks represent the simulated ^{15}N-isotopic percentage in natural abundance of 0.37% (A), with 8% of ^{15}N incorporation (B), and with 10% ^{15}N incorporation (C).

Table 3.1. ^{1}H- and ^{15}N-chemical shifts (ppm) of amide protons of ^{15}N-acetylhexosamines from GAG types, unsaturated dimer derivatives, and commercial standards.

GAG types or derivatives	major amino sugar	figure	chemical shifts[a] (ppm)	
			^{1}H	^{15}N
CS-A	β-GalNAc-4(SO_3^-)	3A	7.963	120.91
CS-C	β-GalNAc-6(SO_3^-)	3B	7.942	121.61
OSCS	β-GalNAc-4,6di(SO_3^-)	3C	7.941	121.21
DS (CS-B)	β-GalNAc-4(SO_3^-)	3D	8.096	120.46
HS	α-GlcNAc-6(SO_3^-)	3E	8.361	123.62
ΔC4S dimer	α-GalNAc-4(SO_3^-)	4A	8.353	120.60
	β-GalNAc-4(SO_3^-)	4A	8.138	121.40
ΔC6S dimer	α-GalNAc-6(SO_3^-)	4B	8.241	121.80
	β-GalNAc-6(SO_3^-)	4B	8.092	122.75
GlcNAc (standard)	α-GlcNAc	S1A	8.138	122.95
	β-GlcNAc	S1A	8.039	123.72
GalNAc (standard)	α-GalNAc	S1B	8.080	122.61
	β-GalNAc	S1B	7.972	123.53

[a]Chemical shifts are relative to trimethylsilylpropionic acid at 0 ppm for ^{1}H and ^{13}C, and liquid ammonia for ^{15}N, obtained in experiments at 25 ^{o}C and pH 4.5.

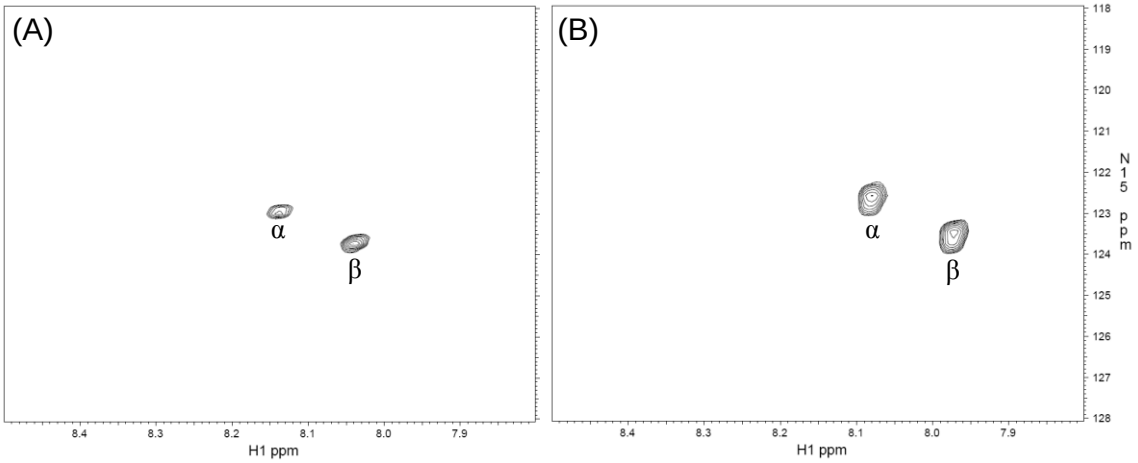

Figure 3.S1. ^{15}N-gHSQC spectra of the standard monomeric (A) GlcNAc, and (B) GalNAc.

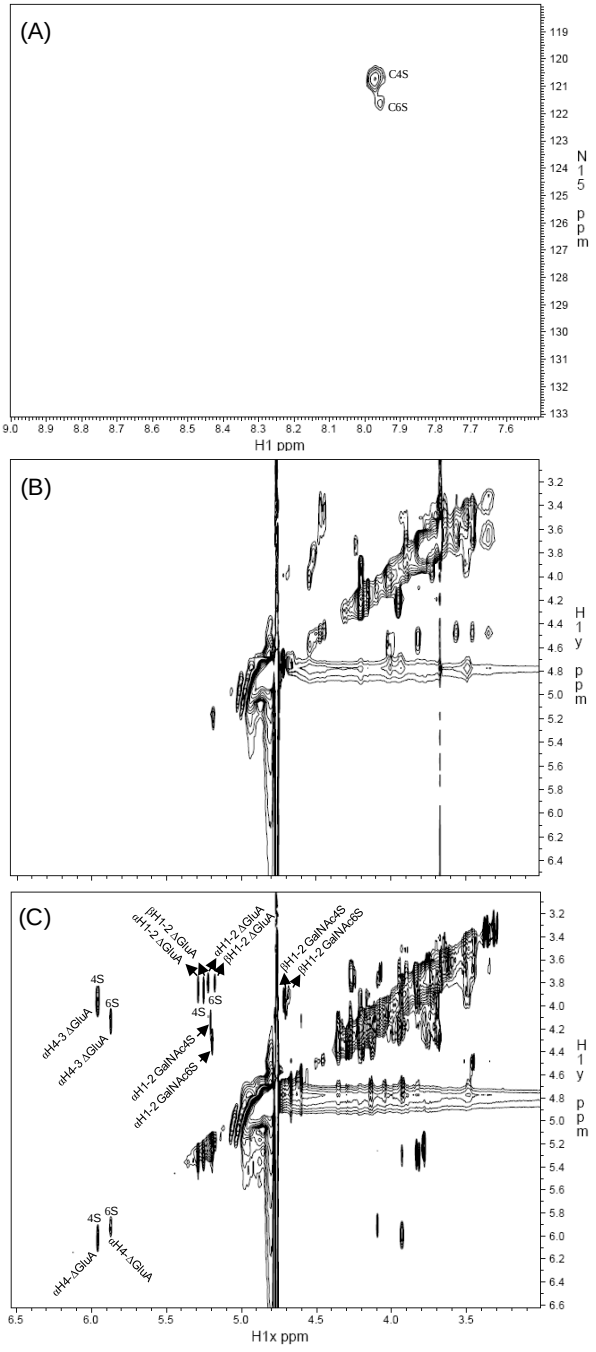

Figure 3.S2. ^{15}N-gHSQC spectrum (A), and TOCSY spectra (B,C) of the enzymatically treated endothelial negatively charged molecules: (A) Nuclease (DNAse/RNAse) treated, (B) ABC lyase digestion of the nuclease-untreated sample, and (C) ABC lyase digestion after nuclease-treated sample.

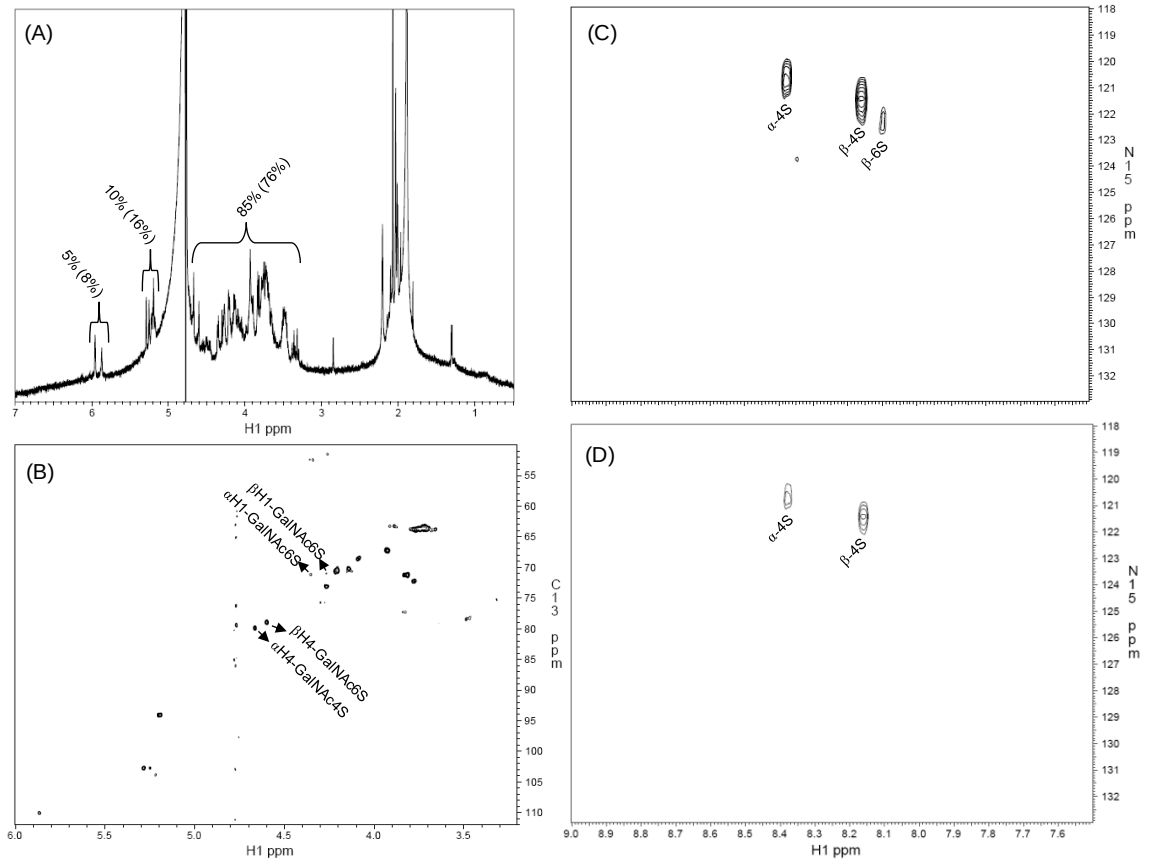

Figure 3.S3. NMR analysis of the endothelial nuclease/ABC lyase-treated sample (unsaturated CS low-molecular weight products) (A-C), and the purified ΔC4S dimer (D) obtained through SAX-HPLC chromatography. (A) 1D ^{1}H-spectrum, the percentage without parentheses represents the real integral values of the peaks, whereas the percentages with parentheses belong to theoretical values assuming a pure sample of dimers. (B) ^{13}C gHSQC and (C, D) ^{15}N gHSQC spectra.

CHAPTER 4: STEPWISE EVOLUTION OF TWO GIANT COMPOSITE LTR-RETROTRANSPOSON-LIKE ELEMENTS DA AND XIAO

Xuanyang Li, Jennifer Slife, Nail Patel, Shaying Zhao, BMC Evolutionary Biology, 2009. **9**(1): p. 1-10. Reprinted here with permission of publisher.

Abstract

Background

We recently discovered two composite long terminal repeat (LTR)-retrotransposon-like elements which we named DA (~300 kb) and Xiao (~30 kb), meaning big and small in Chinese respectively. Xiao and DA (three types of DA identified) were found to have been derived from several donor sites and have spread to 30 loci in the human genome, totaling to 5 Mb. Our bioinformatics analyses with the released human, chimp, rhesus macaque, orangutan, and marmoset genomic sequences indicate that DA and Xiao emerged ~25 million years (Myr) ago.

Results

To better understand the evolution of these two complex elements, we investigated various internal junctions of DA and Xiao as well as orthologous genomic sites of the 30 DA/Xiao loci in non-human primates including great apes, lesser apes, Old World monkeys, New World monkeys, and a prosimian. We found that Xiao and type I DA first emerged in the genome between 25 and 18 Myr ago, whereas type II and Type III DAs emerged between 14 and 7 Myr ago. Xiao and DA were most active in great apes, with their amplification peaking during 25-14 and 14-7 Myr ago, respectively. Neither DA nor Xiao seem to have been active in the human and chimp genomes during last 6 Myr.

Conclusion

The study has led to a more accurate age determination of the DA and Xiao elements than our previous bioinformatics analyses, and indicates that the amplification activity of the elements coincided with that of group I HERV-Es during evolution. It has also illustrated an evolutionary path with stepwise structural changes for the elements during past 25 Myr, and in doing so has shed more light on these two intriguing and complex elements that have reshaped our genome.

Background

Transposable elements (TEs) [1-6] are grouped into retrotransposons and DNA transposons, depending upon whether or not RNA intermediates are required for transposition. Simple DNA transposons such as insertion sequences (IS) encode a transposase and have an inverted repeat of usually 9–41 bp at each end [1,2]. Composite DNA transposons found in bacteria such as Tn10, Tn5, and Tn9 contain a middle region (often encoding a drug resistance gene) flanked by two IS elements. Owing to these flanking IS elements, the middle region of a composite DNA transposon becomes mobile as well. Retrotransposons can be divided further into two groups: one with a long terminal repeat (LTR) of a few hundred to over 1 kb long at each end (e.g., retroviruses) and the other without LTRs (e.g., long interspersed nuclear elements or LINEs) [2]. Retroviruses and LINEs encode reverse transcriptases that are essential for their amplification in the genome. In most cases, insertion of either a DNA transposon or a retrotransposon results in target site duplication (TSD) of usually 2–20 bp [1,2]. While composite DNA transposons such as those in the Tn family have been known for quite some time, a composite retrotransposon with a similar architecture has yet to be discovered.

The human genome contains significantly more recognizable retrotransposons (nearly 50%) than DNA transposons (only 3%) [6-8]. The already identified retrotransposons include LTR elements such as human endogenous retroviruses (HERVs), as well as non-LTR elements such as LINEs (e.g., L1s) and short interspersed nuclear elements (SINEs) (e.g., Alus). Although hundreds of thousands of copies of individual TEs have been identified [7,8], only a small number of composite elements are reported for the human genome including SVA that contains SINE, VNTR (variable numbers of tandem repeats), and Alu elements [9]. Additional examples are the

composite DNA transposon Ricksha, as well as Harlequin and HERV39 that have mostly simple repeats inserted into the relevant HERV elements.

Segmental duplications (SDs), another type of repeating DNA which differs from the traditional TEs described above, make up ~5% of the human genome [10]. SDs are low copy number repeats, with a size of at least 1 kb and ≥ 90% sequence identity among the copies. Although under extensive investigation in recent years, the origins and the duplication mechanisms of SDs remain largely unclear [11,12]. No possible linkages between SDs and retrotransposons had been reported until our recent discovery of two composite LTR-retrotransposon-like elements in the human genome [13].

While characterizing a genome-wide SD in the human genome, we discovered two new composite LTR retrotransposon-like elements, which we named DA and Xiao, meaning big and small in Chinese respectively. Complete DA/Xiao copies were found to have an architecture resembling bacterial composite DNA transposon Tn9, consisting of a middle region (the core) flanked by two elements that are direct repeats of each other. The only exception to this is that the flanking element is a modified HERV-E rather than a DNA transposon [13]. However, barring this structural resemblance, there is no experimental evidence that could determine whether DA and Xiao are indeed composite LTR-retrotransposons. Consequently, it is currently unclear whether they have propagated in the genome via retrotransposition or by other mechanisms.

Xiao, with a core of 10 kb, was found to originate from a region of chromosome 19p encoding olfactory receptor 7E members [13-15]. DA, with a core of ~260 kb, appears to have evolved from a Xiao that had an extra LTR5B element, which likely evolved from an ancestral Xiao via insertion of a HERV-K that later degenerated to a solo LTR [13]. The evolvement of DA,

according to our analyses [13], was accomplished by insertion of ~200 kb of chimeric sequence derived from chromosomes 16p and 21q into the Xiao core, followed by insertion of 56 kb of TEs and retrogenes. DA or Xiao elements were identified at 30 loci on 12 chromosomes, harboring a total of 20 copies of DA and 45 copies of Xiao[13]. Based on our reconstructed human-mouse-rat ancestral genome [13] and the rhesus macaque genome [16], only DAs mediated intra-chromosomal rearrangements.

Our previous bioinformatics analyses [13], with the published human, chimp and rhesus macaque genomic sequences [7,8,16,17] as well as the recently released orangutan and marmoset genomic contig sequences, indicated that DA and Xiao emerged in the genome after the human/apes diverged from Old World monkeys ~25 million years (Myr) ago [18]. In addition, structural analyses indicated three types of DA existing in the genome: type I DA is the most ancestral form (found in the human, chimp, and orangutan genomes); type II has an HERV-E inserted into an existing HERV-H, while type III has a sequence duplication of ~100 kb derived from chromosome 8p and is the most recently evolved (found in the chimp and human genomes only) [13]. To further refine this analysis, we conducted experiments to investigate the Xiao/DA orthologues in primates whose genomes have not yet been sequenced. This study greatly expanded the primate list under examination by including great apes, lesser apes, Old World Monkeys, New World Monkeys, and a prosimian (Fig. 4.1), covering an evolutionary span of 60 Myr. The analyses led to a more accurate age determination of DA and Xiao, indicating that their amplification activity coincided with that of group I HERV-E elements. It also illustrated an evolutionary path with stepwise structural changes for the elements. The study has shed more light on theses two intriguing and complex elements that have reshaped our genome.

Results

Age determination of Xiao as well as type I, type II and type III DAs by examining their internal junctions

Duplicon type-specific internal primers

As described previously [13], four types of duplicons exist in the human genome: Xiao, as well as type I, II and III DAs. Based on their architecture, we designed primers that are specific to each type of duplicon for polymerase chain reaction (PCR) analyses. As shown in Fig. 4.2a, "standalone Xiaos" (those that are not associated with DAs in the genome) do not have an LTR5B element (solo LTR of HERV-K). This is unlike the "Insertion-ready Xiao" which, based on our previous analyses [13], is likely to have evolved from a "standalone Xiao" by acquiring a HERV-K insertion (which later degenerates to a solo LTR), due to the fact that the donor sequence has neither LTR5B nor HERV-K at the corresponding position. We therefore used the pre-insertion site of LTR5B (HERV-K, to be more precise) to design primers that can only amplify the standalone Xiaos but cannot amplify those Xiao regions inside DAs. Type I DAs appear to have evolved from a LTR5B-containing Xiao via insertion of three sequence fragments derived from chromosomes 16p and 21q into the Xiao core [13] (which is why this Xiao is called "Insertion-ready Xiao" in Fig. 4.2). Consequently, we designed four pairs of primers flanking both insertion junctions, as well as the two 16p and 21q chimeric sequence fusion junctions (Fig. 4.2a), to amplify Type I DAs in primate genomes. Compared to type I DAs, type II DAs have an extra HERV-H/HERV-E/HERV-H element (formed by insertion of a HERV-E into an existing HERV-H). Thus, primers were designed flanking the right HERV-E/HERV-H junction, which we found to only exist inside DAs via comparison of the junction sequence with the entire human genome. Finally, given that type III DAs have an additional 100 kb sequence duplication

derived from chromosome 8p, primers were designed to span the 16p/8p chimeric sequence fusion junction (Fig. 4.2a). We also ensured that each primer was not copy-specific and that its sequence was common (with a few base mismatches/gaps allowed) to nearly all copies of a duplicon type.

Age of Xiao and three types of DA

With the primers described above, we performed PCR experiments with the primate species indicated in Fig. 4.1, with each experiment repeated multiple times. As shown in Fig.2b, Xiao and type I DA were amplified with the genomic DNA of apes but not with that of Old World monkeys, New World monkeys, or the lemur (in most cases, primers designed using the human genomic sequences are able to amplify the orthologous sequence fragments from the ape and Old World monkey genomic DNA, but are unable to achieve the same for the New World monkey and lemur genomic DNA due to larger sequence divergence. Thus, the PCR amplification results with the New World monkey and lemur DNA were expected to be negative for most of our primers. Thus, these species could serve as negative controls in our PCR experiments to a certain extent, while the human served as a positive control). However, type II and type III DAs could be amplified only with the human, chimp, bonobo and gorilla genomic DNA but not with that of other primates. These results indicate that Xiao and type I DA first emerged in the genome between 18 and 25 Myr ago (before the gibbon/siamang diverged from the great apes and after the apes diverged from Old World monkeys [18]), whereas type II and type III DAs emerged between 7 and 14 Myr ago (before the gorilla diverged from the human-chimp common ancestor and after the orangutan diverged from the gorilla-chimp-human common ancestor [18]). This study further refines the previous bioinformatics analyses that compared the released human, chimp, orangutan, rhesus macaque, and marmoset genomic sequences and concluded that Xiao

and type I DA emerged within the recent 25 Myr (after the human/ape – Old World monkey divergence [13]) and type II/III DA emerged within the recent 14 Myr (after the human/chimp – orangutan divergence [13]).

The 16p-21q junction primers amplified multiple bands with the human, chimp, bonobo, and gorilla (and possibly orangutan) genomic DNA but only a single band with that of the gibbon and the siamang (Fig. 4.2b). This implies that polymorphism of this junction is present in the human, chimp, bonobo, and gorilla genomes but absent in the gibbon and siamang genomes. Partial confirmation of this fact was obtained through in-silico PCR analyses (see Materials and Methods) with the published human and chimp genomic sequences, showing amplification of multiple PCR products of approximately 0.6 kb, 0.8 kb and 1.1 kb in size [see Additional file 1]. The only other ape whose genome has been sequenced is the orangutan. Unfortunately, however, the current orangutan release is a draft assembly from 6× whole genome shotgun sequences and contains gaps, which prevent accurate in-silico PCR results from being attained.

By examining the sequences of the in-silico PCR products, we found that the polymorphism is caused by either a 200 bp truncation of the chromosome 16p donor sequence at the fusion junction, or an AluY insertion (300 bp). We also performed in-silico PCR analyses with other primers (Fig. 4.2a) and found that, overall, the in-silico results agreed with the experimental analyses (Fig. 4.2b), yielding a single-sized product for Xiao and type II and III DAs but multiple-sized products for type I DAs for the human and chimp genomes [see Table 4.s2 in Additional file 1].

Age determination of Xiao as well as type I, type II and type III DAs by examining insertion junctions of individual DA/Xiao locus

To determine when each of the 30 DA/Xiao loci identified in the human genome emerged during the course of evolution, we tried to amplify either the two insertion junctions or the pre-insertion junction for a given locus from the genomic DNA of the 12 primate species (Fig. 4.1) as illustrated in Fig. 4.3a. We were able to design primers flanking the insertion sites for 25 of the 30 total loci [see Table 4.s1 in Additional file 1]. The remaining 6 loci were found to be located in repeat-rich regions (e.g., near the centromere or the telomere) and, as a consequence, we could not find primer pairs whose sequences were sufficiently unique (i.e., matching many places in the genome).

For loci that are not associated with large inversions (Xiao loci mostly, see reference 13), we performed three sets of PCR experiments to amplify the two insertion junctions and the pre-insertion junction as shown in Fig. 4.3. In contrast, for loci that are associated with large inversions (mostly DA loci), only the insertion junctions were examined. This is because it is not a straightforward task to pair the primers for amplification of the pre-insertion junction because at least two distinct loci were involved. Also, it is important to note that the inversion might have caused sequence deletions/duplications/insertions, thus complicating the pre-insertion site amplification analysis.

Each PCR experiment was repeated at least three times in order to confirm the results. In total, at least 2,500 PCR experiments were performed. As summarized in Table 4.1, the majority of the PCR experiments were conclusive. This required that the results from at least two separate PCR experiments agree with each other for a given PCR reaction, and the results from at least two junctions (out of two insertion junctions and sometimes one pre-insertion junction) agree with

each other for a given locus (except 3 loci where we were only able to design primers for one junction, see Table 4.s1 in Additional file 1). This analysis supports conclusions obtained with internal primers as described above. In addition, the results indicate that the Xiao amplification peak was between 25 and 14 Myr ago (after apes diverged from Old World monkeys and before the orangutan diverged from the human-chimp-gorilla common ancestor), whereas the DA amplification peak was between 14 and 7 Myr ago (after the orangutan diverged from the other great apes and before the gorilla diverged from the human-chimp common ancestor) (Fig. 4.4).

TSD identification

Using the strategy indicated in Fig. 4.3, we sequenced the PCR product of the pre-insertion junction amplified from either the pigtail macaque or the rhesus macaque. We then compared the resulting sequences to sequences flanking each of the two relevant insertion junctions in the human genome, which were determined by aligning the duplicon under study with all other duplicons. For all three Xiao loci that were sequenced, we successfully identified the TSDs [see Table 4.s3 in Additional file 1]. This was consistent with our previous bioinformatics analyses which found TSDs for a majority of Xiao and unrearranged DA loci [13]. These analyses suggest that DA and Xiao may, perhaps, be TEs and that they could have spread throughout the genome via transposition.

Structural polymorphisms of DA elements between the human and the chimp

At least 29 of the 30 total DA/Xiao loci identified in the human genome were also found in the chimp genome. Proof of this is given by the insertion junction amplification experiments described above (Table 4.1) and the previous bioinformatics analyses [13]. This means that DA and Xiao have been largely quiet in the human lineage during the last 6 Myr, after the human diverged from the chimp. However, we did find a few large structural variations present between

these two apes by comparing the corresponding genomic sequences. For instance, we found that the human 11q-67Mb DA (~280 kb) was degenerated to ~10 kb in the chimp genome, with 270 kb internal sequences deleted [see Fig. 4.s1 in Additional file 1]. On the other hand, the Xiao/DA locus at 15 Mb of chromosome 10 was found to be 252 kb in the chimp genome, but have degenerated to 45 kb in the human genome due to a 200 kb internal deletion of the DA copy [see Fig. 4.s2 in Additional file 1]. Additionally, we could not find the chimp homologues of the human DA/Xiao copies at 11–12 Mb of 8p in the current release of the chimp genome, but we did successfully amplify its external junctions with the chimp DNA sample in our PCR analyses (Table 4.1) [19]. At this point, we do not know if this is due to large internal deletions of DA/Xiao in the chimp lineage, or to the incompleteness of the current chimp genome release.

Discussion

Using the knowledge gained by our previous bioinformatics analyses [13] regarding the architecture and genomic locations of the recently discovered composite LTR-retrotransposon-like elements DA and Xiao, we designed experiments to investigate the homologues of the human DA/Xiao elements in primates whose genome has not yet been sequenced. The DA/Xiao pattern results, shown in Fig. 4.2 and Table 4.1, seemed to divide the apes into three groups. The first group; including the human, the chimp, the bonobo, and the gorilla; possesses a majority of the Xiao loci as well as DA loci of all three types in their genome. The lesser apes, including the gibbon and the siamang, belong to another group whose genome harbors only a fraction of the Xiao loci and Type I DA loci. The orangutan appears to be between the two groups, having most of the Xiao loci but only Type I DAs. The results indicate that DA and Xiao elements had been most active in great apes but seem to have been quiet in the human lineage during the past 7 Myr (after the human-gorilla divergence). Analysis of the released chimp genome, which did not

yield chimp-specific DA/Xiao loci either, supports these results by indicating that DA and Xiao have been most likely quiet in the chimp lineage as well during the past 6 Myr after the human-chimp divergence.

As this analysis only focused on the homologues of the human DA/Xiao loci, we do not know if DA and Xiao have also been quiet in other primate lineages or if they are still active today. To answer this question, it would be helpful to contrast closely related-primates such as the chimp and the bonobo on these elements. Regardless of whether or not these elements are still active today, it will always be informative to search for nonhuman primate-specific DA and Xiao loci, as well as to search for other types of DA and Xiao (i.e., with a different architecture than those shown in Fig. 4.2) in primates besides the chimp and the human. We did analyze the current orangutan genome release, and did not find orangutan-specific DA/Xiao copies except for one possible Xiao locus. However, this does not necessarily signify that no orangutan-specific DA/Xiao elements are present, because the current release of the orangutan genome is in draft state and some sequences could be missing (especially considering that recent sequence duplications such as DA and Xiao are particularly difficult to be correctly assembled and are usually underrepresented in the draft genome). We will continue this study with newer releases once they become available. Analyzing the gibbon and siamang genomes may provide interesting information, because DA and Xiao emerged immediately before these lesser apes diverged from the great apes. As an increased DA/Xiao activity was observed in the great ape lineages (Fig. 4.4), it would be useful to find out if amplification of DA/Xiao also peaked in these lesser apes. This would likely yield gibbon/siamang-specific DA/Xiao loci and/or DA/Xiao structures (a possibility indicated by the different amplification patterns between the lesser apes and most great apes with the Xiao-specific primers shown in Fig.2). We hope that these future

studies will shed more light on the nature, evolution, and function of these two intriguing elements.

Despite their structural resemblance to composite DNA transposon Tn9 (with a modified HERV-E, which is inactive, replacing the IS element [13]), we have no evidence demonstrating that DA and Xiao are indeed composite LTR-retrotransposons. However, considering the possibility of DA/Xiao being TEs raised by identification of TSDs at a majority of un-rearranged Xiao/DA loci (Table two in reference 13, some shown in Fig. 4.3and Table 4.s1), it may not be completely out of the question to hypothesize that DA and Xiao are composite LTR-retrotransposons. If so, we could also speculate that they have relied upon the retrotransposition machinery from active HERV-E elements to move around in the genome in a way that is analogous to a defective virus carrying an oncogene that depends on a helper virus to propagate.

A previous study [20] divided the >50 copies of HERV-E in the human genome into two groups, and reported that group I amplification peaked between 18 and 6–7 Myr ago (after the gibbon-great ape divergence and before the human-chimp divergence). This amplification peak overlapped with those of DA and Xiao (Fig. 4.4). In addition, similar to the DA and Xiao elements as well, no human-specific or chimp-specific copies of HERV-E were found [21,22], indicating that HERV-E had stopped its activity before the human-chimp divergence. These observations are consistent with the hypothesis described above, stating that DA and Xiao had depended upon the HERV-E machinery to proliferate in the genome. However, the enormous size of DA and Xiao (300 kb and 30 kb respectively) certainly raises questions regarding this hypothesis, as retroviruses including HERVs are below 12 kb and the longest known RNA viruses (corona viruses) are only ~30 kb. Even if the hypothesis is proven to indeed be true, some novel mechanisms which are different from that of HERVs must have been used. This is

especially so considering that TSDs identified at the DA/Xiao loci ranged from 4–9 bp with most being 6 bp [13], unlike those of HERVs which are usually 4 bp. Of course, only future studies can clarify these issues.

Conclusion

To better understand the evolution of the recently discovered composite LTR-retrotransposon-like elements DA and Xiao, we investigated their orthologues in non-human primates whose genomes have not yet been sequenced. These included great apes, lesser apes, Old World monkeys, New World monkeys, and a prosimian. By examining various internal junctions of DA and Xiao in these primate genomes, we found that Xiao and type I DA first emerged between 25 and 18 Myr ago (after the human/apes diverged from the Old Word monkeys and before the gibbon/siamang diverged from the great apes), whereas type II and Type III DAs emerged between 14 and 7 Myr ago (before the gorilla diverged from the human-chimp common ancestor and after the orangutan diverged from the gorilla-chimp-human common ancestor). After investigation of the orthologous sites of the 30 DA/Xiao loci in the human genome, we found that the Xiao amplification peak was between 25 and 14 Myr ago, whereas the DA amplification peak was between 14 and 7 Myr ago. Neither DA nor Xiao seemed to be active in the human and chimp genomes during last 6 Myr. Thus, the activity of DA and Xiao coincided with that of group I HERV-Es during the course of evolution.

The current study led to a more accurate determination of the age of the elements than our previous bioinformatics analyses comparing the released human, chimp, rhesus macaque, orangutan, and marmoset genomic sequences. This information illustrated an evolutionary path with stepwise structural changes for DA and Xiao during the past 25 Myr, and has shed more light on these two intriguing elements.

Methods

The human (hg18), chimp (panTro2), and rhesus macaque (rheMac2) genomic sequences were obtained from the genome site of the University of California Santa Cruz (UCSC) athttp://www.genome.ucsc.edu *webcite*. The orangutan contig sequences were obtained from the Washington University Genome Center at genome.wustl.edu. The primers were designed using the Primer3 program at frodo.wi.mit.edu. To ensure that the primer pairs were unique to the duplicons of interest, the primers were compared to the human genomic sequence using the blast program at the Ensemble site athttp://www.ensembl.org *webcite*. Usually 500 bp–2 kb amplicons were designed. All the primers used in this study are included in Table 4.s1 in Additional file 1. The non-human primate (Fig. 4.1) DNA samples were purchased from the Coriell Institute for Medical Research at http://www.coriell.org *webcite*. The human DNA sample was purified from human embryonic stem cells (BG01).

Each PCR experiment contained 500 nM primers and 5 ng genomic DNA templates that were amplified using the iQ™ Supermix (catalog number 170–8860) from Bio-Rad, which was found to give the most specific and sensitive results after trying various polymerases from several different companies. The PCR reactions were run using an annealing temperature range of 60–66 ℃ and an elongation temperature range of 72–78 ℃, depending on the primers and the PCR product. In-silico PCR analyses were conducted using the web tools at the UCSC site http://www.genome.ucsc.edu/cgi-bin/hgPcr*webcite*.

TSD finding: The PCR product of the pre-insertion site of a Xiao locus was cloned into the pGEM vector (Promega) using the AT cloning technology, which was then transformed into the *E. coli* strain Xblue-21 via electroporation. The colonies were screened by PCR analyses and the positive clones were sent to the campus facility for sequencing. The obtained sequences were

then compared to the two insertion junction sequences (500 bp flanking the junction that was determined by aligning with other duplicon copies) of the Xiao locus in the human genome using the FASTA sequence alignment program [23] for TSD identification.

Acknowledgements

We wish to thank Dr. Stephen Delton's lab for providing us the human ES cells, the UGA sequencing facility for the sequencing work, Mrs. Sudeep Patel, Hao Shen and Prafull Kaushik for their contribution to this study. The work was funded by the Georgia Cancer Coalition, American Cancer Society, and start up funds from the UGA.

References

1. Bailey, J., *Recent segmental duplications in the human genome.* Science, 2002. **297**: p. 1003 - 7.
2. Bailey, J., G. Liu, and E. Eichler, *An Alu transposition model for the origin and expansion of human segmental duplications.* Am J Hum Genet, 2003. **73**: p. 823 - 34.
3. Bennetzen, J., *Transposable elements, gene creation and genome rearrangement in flowering plants.* Curr Opin Genet Dev, 2005. **15**: p. 621 - 7.
4. Buzdin, A., *Human-specific endogenous retroviruses.* ScientificWorldJournal, 2007. **7**: p. 1848 - 68.
5. Consortium, I.H.G.S., *Initial sequencing and analysis of the human genome.* Nature, 2001. **409**: p. 860 - 921.
6. Craig, N., *Mobile DNA: an Introduction.* Mobile DNA II, 2002: p. 3 - 11.
7. Deininger, P. and M. Batzer, *Mammalian retroelements.* Genome Res, 2002. **12**: p. 1455 - 65.
8. Glusman, G., et al., *The complete human olfactory subgenome.* Genome Res, 2001. **11**: p. 685 - 702.
9. Ji, X. and S. Zhao, *DA and Xiao-two giant and composite LTR-retrotransposon-like elements identified in the human genome.* Genomics, 2008. **91**: p. 249 - 58.
10. Kazazian, H., *Mobile elements: drivers of genome evolution.* Science, 2004. **303**: p. 1626 - 32.
11. Lindeskog, M., et al., *Coamplification and dispersion of adjacent human endogenous retroviral HERV-H and HERV-E elements; presence of spliced hybrid transcripts in normal leukocytes.* Virology, 1998. **244**: p. 219 - 29.

12. Martin, S. and D. Garfinkel, *Survival strategies for transposons and genomes.* Genome Biol, 2003. **4**: p. 313.

13. Mills, R., et al., *Recently mobilized transposons in the human and chimpanzee genomes.* Am J Hum Genet, 2006. **78**: p. 671 - 9.

14. Newman, T. and B. Trask, *Complex evolution of 7E olfactory receptor genes in segmental duplications.* Genome Res, 2003. **13**: p. 781 - 93.

15. Pearson, W., *Flexible sequence similarity searching with the FASTA3 program package.* Methods Mol Biol, 2000. **132**: p. 185 - 219.

16. Samonte, R. and E. Eichler, *duplications and the evolution of the primate genome.* Nat Rev Genet, 2002. **3**: p. 65 - 72.

17. Sequencing, C. and A. Consortium, *Initial sequence of the chimpanzee genome and comparison with the human genome.* Nature, 2005. **437**: p. 69 - 87.

18. Sequencing, R.M.G. and A. Consortium, *Evolutionary and biomedical insights from the rhesus macaque genome.* Science, 2007. **316**: p. 222 - 34.

19. Stewart, C. and T. Disotell, *Primate evolution - in and out of Africa.* Curr Biol, 1998. **8**: p. R582 - 8.

20. Venter, J., *The Sequence of the Human Genome.* Science, 2001. **291**: p. 1304 - 1351.

21. Voytas, D. and J. Boeke, *Ty1 and Ty5 of Saccharomyces cerevisiae.* Mobile DNA II, 2002: p. 631 - 662.

22. Wang, H., *SVA elements: a hominid-specific retroposon family.* J Mol Biol, 2005. **354**: p. 994 - 1007.

23. Yi, J. and H. Kim, *Molecular evolution of the HERV-E family in primates.* Arch Virol, 2006. **151**: p. 1107 - 16.

Figure and tables

Table 4.1. PCR amplification for each of the DA/Xiao loci found in the human genome

Location (Mb)	Human	Chimp	Bonobo	Gorilla	Orangatan	Gibbon	Siamang	Rehsus	Pigtail	Tamarin	Spider	Lemur
2p-71,Xiao	Y	Y	Y	Y	Y	Y	Y	N	N	N	N	N
2q-159,Xiao	Y	Y	Y	Y?	Y	N?	N?	N	N	N	N	N
2q-95,Xiao	Y	Y	ND	ND	Y	ND	ND	N	ND	ND	ND	ND
3p-8, Xiao	Y	Y	Y	Y	Y	?	?	N	N	N	N	N
3q-113 Xiao	Y	Y	ND	ND	Y	ND	ND	N	ND	ND	ND	ND
8p-11,Xiao	Y	Y	Y	Y	Y	Y	Y	N	N	N	N	N
9q-92a,Xiao	Y	Y	Y	?	NC	?	?	N	N	N	N	N
9q-92b,Xiao	Y	Y	Y	Y	NC	N?	N?	N	N	N	N	N
10p-15,Xiao	Y	Y (DA)	Y	Y	Y	?	?	N	N	N	N	N
11p-17,Xiao	Y	N	ND	ND	Y	ND	ND	N	ND	ND	ND	ND
12q-50,Xiao	Y	Y	Y	Y	Y	Y	Y	N	N	N	N	N
13q-40,Xiao	Y	Y	Y	Y	Y	Y	Y	N	N	N	N	N
13q-45.9,Xiao	Y	N	ND	ND	N	ND	ND	N	ND	ND	ND	ND

13q-63,Xiao	Y	N	ND	ND	N	ND	ND	N	ND	ND	ND	ND
13q-67,Xiao	Y	Y	Y	Y	NC	N	N	N	N	N	N	N
14q-51,Xiao	Y	Y	N?	Y?	N	N	N	N	N	N	N	N
21q-32,Xiao	Y	Y	Y	Y	Y	Y	Y	N	N	N	N	N
3p-75 type I DA	Y	Y	Y	Y	Y	Y?	Y?	N	N	N	N	N
3q-126 Type I DA	Y	Y	Y	Y	Y	Y	Y	N	N	N	N	N
3q-131,Type IIDA	Y	Y	Y	Y	N	N	N	N	N	N	N	N
3p-15, TypeII DA	Y	Y	Y	Y	N	N	N	N	N	N	N	N
4p-4 Type II/I(?) DA	Y	Y	Y	Y	N	N	N	N	N	N	N	N
4p-9 type II/I(?)/III DA	Y	Y	Y	Y	N	N	N	N	N	N	N	N

7p/q-6.6/97												
TypeII DA	Y	Y	Y	Y	N	N	N	N	N	N	N	N
8p-7-8												
TypeII/IIIDAs	Y	Y	Y	Y	N	N	N	N	N	N	N	N
8p-11-12,												
TypeII/III DAs	Y	N?	?	?	N	N	N	N	N	N	N	N
11p-												
3,TypeIIDA	Y	Y	ND	ND	NC	ND	ND	N	ND	ND	ND	ND
		Y?										
11q-67,TypeII		Internal										
DA	Y	deletion	Y?	Y?	N	N	N	N	N	N	N	N
11q-												
71,TypeII/III												
DA	Y	Y	Y	Y	N	N	N	N	N	N	N	N
12p-												
8,TypeII/IIIDA	Y	Y	Y	Y	N	N	N	N	N	N	N	N

12p-8,TypeII/IIIDA	Y	Y	Y	Y	N	N	N	N	N	N	N	N

ND: not detemined

[1] Loci not examined (see text) included Xiaos at 2q-95Mb, 3q-113Mb, 11p-17Mb, 13q-45.9Mb and 13q-63Mb, as well as the 11p-3Mb DA. Bioinformatics analyses found all these loci in the chimp genome but not in the rhesus and marmoset genomes. Except for 11p-3Mb DA as well as 13q-45.9Mb and 63 Mb Xiaos, the rest of the loci were found in the current orangutan genome release [13].

[2] Others include Rhesus/pigtail/Tamerin/Spider Monkeys and Lemur. In a few cases, non-specific bands (usually not the right size based on the human genome) were amplified with the Old World Monkeys, New World monkeys, and the lemur.

[3] "?" indicates that the PCR results were inconclusive (see text), and further analyses are needed to confirm the existence or absence of the locus.

[4] This locus was found to be associated with a DA in the published chimp genome.

[5] Internal fissions occurred in these DAs and subsequent inversions dispatched broken pieces of DA to several distinct loci [13]. All loci involved were examined by the PCR experiments.

[6] We did not find a HERV-H/HERV-E/HERV-H element inside the 4p-4 Mb and -9 Mb DAs in the published human genome, but a previous study [22] found this element at both loci.

[7] Several DAs were found in the 8p 7–8 Mb and 11–12 Mb regions.

[8] We found a large internal deletion for this DA in the chimp genome (see text).

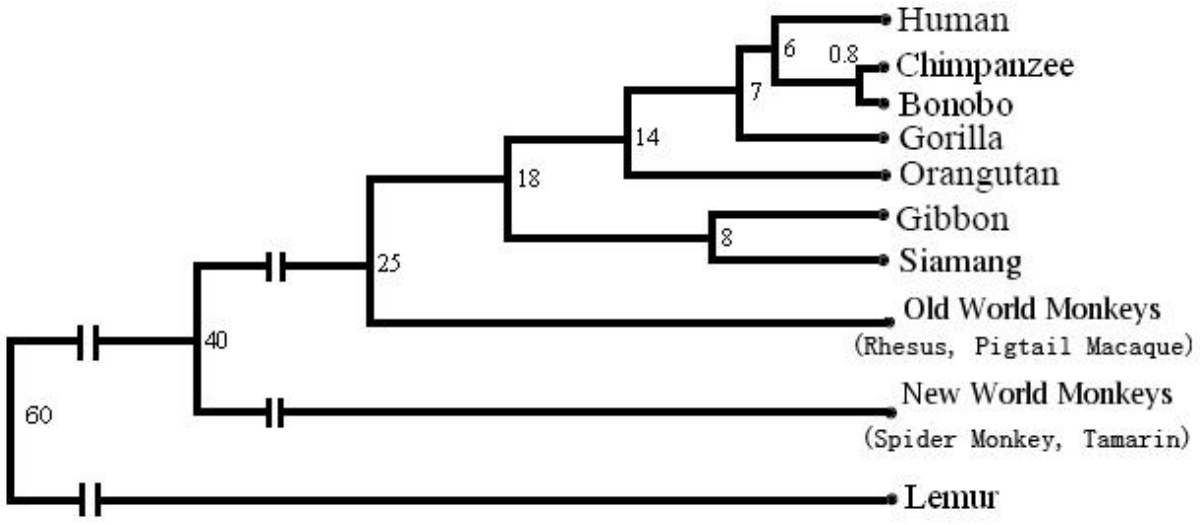

Fig. 4.1 Primates that were being investigated included great apes (the human, the chimp, the bonobo, the gorilla, and the orangutan), lesser apes (the gibbon and the siamang), Old World monkeys (the rhesus macaque and the pigtail macaque), New World monkeys (the spider monkey and the tamarin), and a prosimian (the lemur). The number near each node represents the divergence time in Myr. The scientific name of each species was listed in the legend of Fig. 4.2.

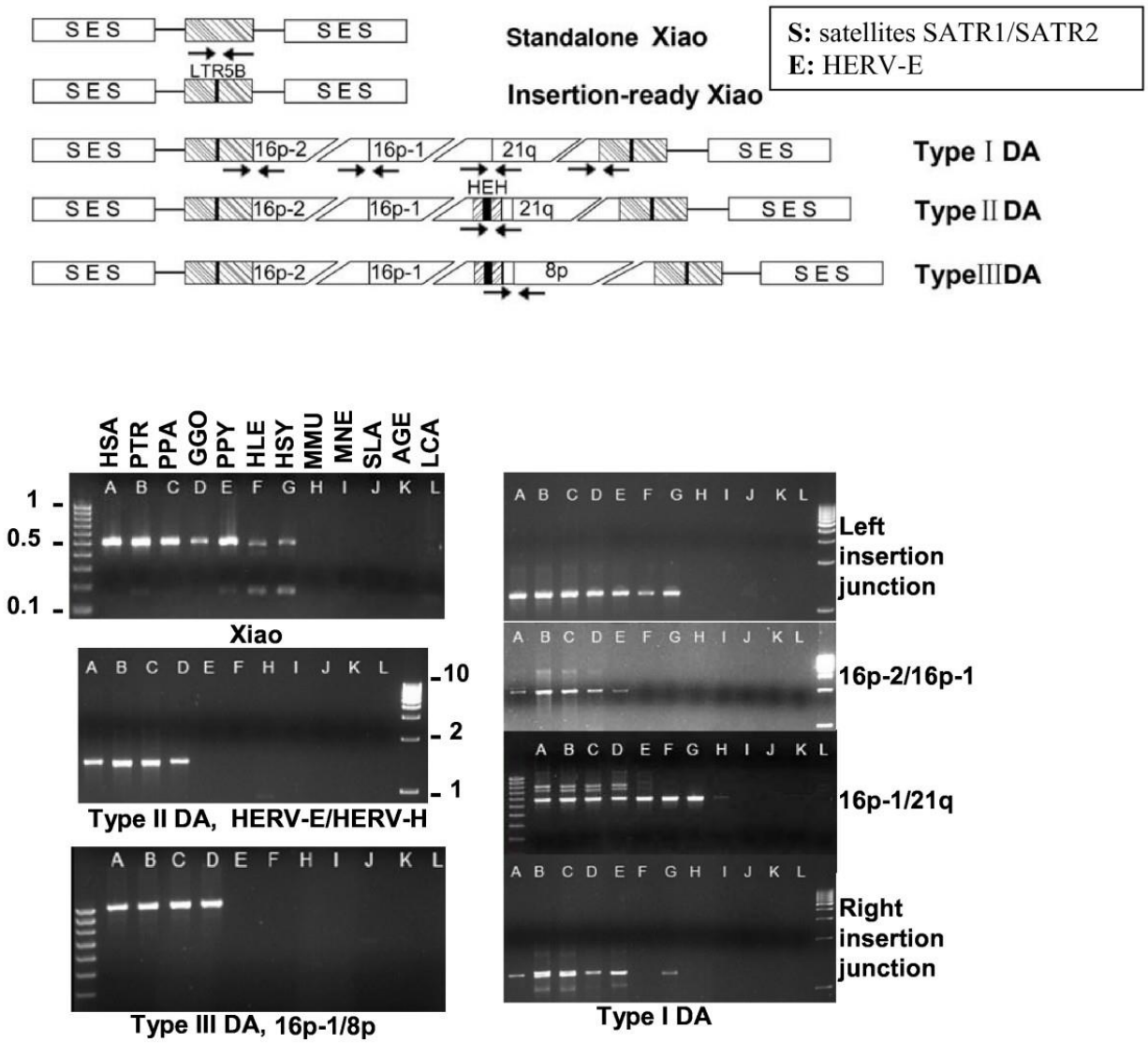

Figure 4.2 Age determination of Xiao, type I, type II, and type III DAs. Top: The primer pairs, indicated as paired arrows, flanked the junctions unique to each type of Xiao or DA as labeled (see the main text for details). "SES" represents the conserved flanking element of "SATR-HERVE-SATR", where SATR represents satellite sequences SATR1 and SATR2. "16p-1", "16p-2", "21q", and "8p" inside the changing core represent the four sequence fragments from the donor loci on chromosomes 16p, 21q, and 8p, respectively.Bottom: Using primers indicated above, each type of duplicon was amplified from genomic DNA samples of the 12 primates: A:

human or *Homo sapiens* (HSA); B: chimp or *Pan troglodytes* (PTR); C: bonobo or *Pan paniscus* (PPA); D: gorilla or *Gorilla gorilla* (GGO); E: orangutan or *Pongo pygmaeus* (PPY); F: gibbon or *Hylobates leucogenys* (HLE); G: siamang or *Hylobates syndactylus* (HSY); H: rhesus macaque or *Macaca mulatta* (MMU); I: pigtail macaque or *Macaca nemestrina* (MNE); J: tamarin or *Saguinus labiatus* (SLA); K: spider monkey or *Ateles geoffroyi* (AGE); and L: lemur or *Lemur catta* (LCA). The faint band for the 16p-1/21q junction in MMU (lane H of the 3rd gel image on the right) was likely due to nonspecific amplification because the result with another set of primers was negative (repeated multiple times). Additionally, we did not find this junction in the released rhesus macaque genomic sequences [13]. The leftmost and the rightmost lanes are 100 bp and 1 kb ladders.

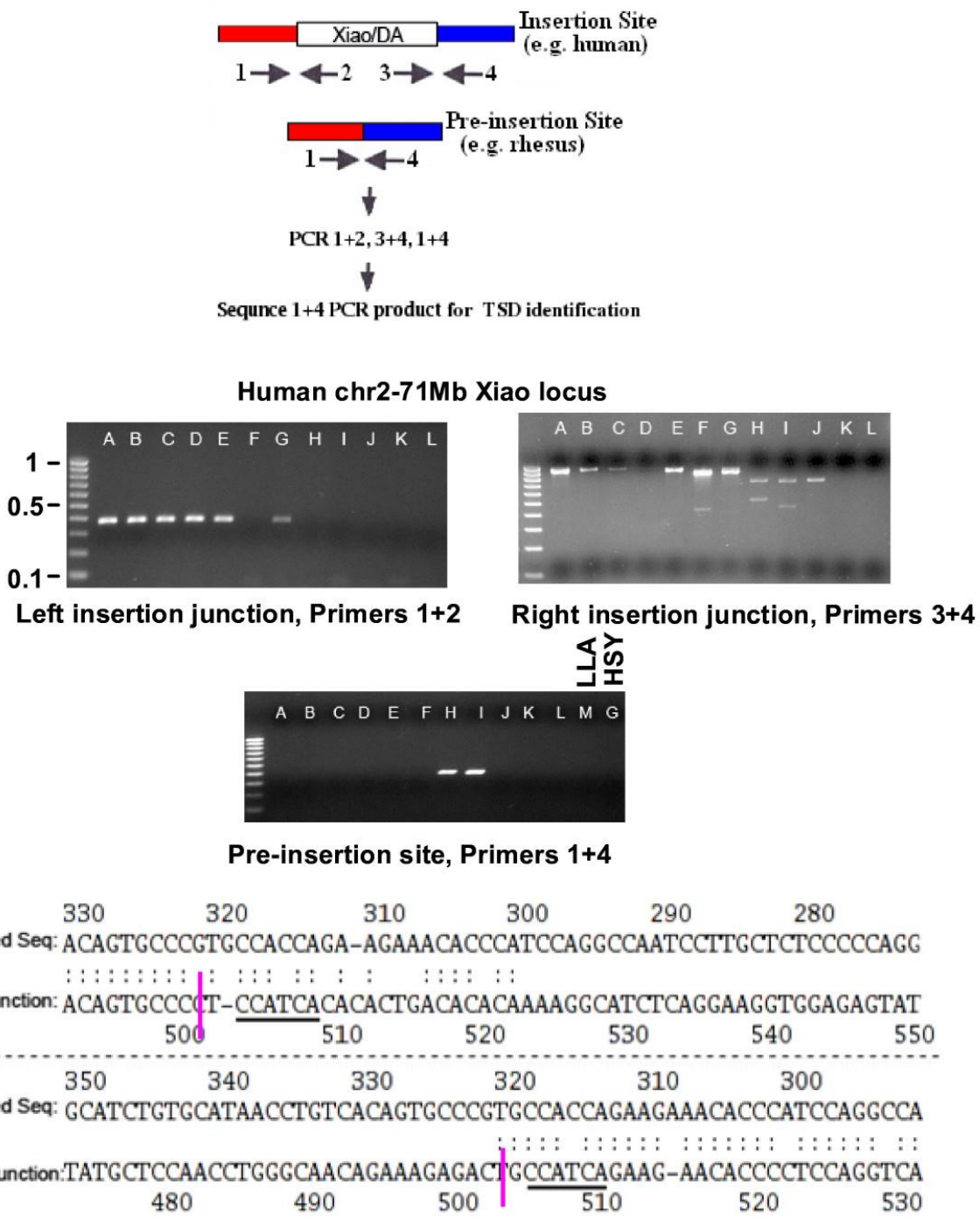

Figure 4.3 Copy-specific amplification and TSD determination. **Top**: For a Xiao or un-rearranged DA locus, three sets of PCR experiments were performed to amplify the insertion (primers 1+2 & 3+4) and pre-insertion (1+4) junctions with the 12 primates. The 1+4 PCR

product from humans' closest relatives was sequenced for TSD finding. **Bottom**: The images are the PCR products of the three junctions for chr2-71Mb Xiao. A-L represent primates as specified in Fig. 2, and M represents woolly monkey or *Lagothrix lagotricha*(LLA). The same 100 bp ladders were used as in Fig. 2. The reason that no products were amplified for the left insertion junction for the gibbon and for the right junction for the gorilla (lane F in the left- and D in the right top images) is likely due to variations between the human and the species involved (transposon insertions, sequence mutations, etc.). This is because the other insertion junction and the internal junction (Fig. 2) were amplified, and the pre-insertion junction was not amplified (the bottom image). The small bands in lanes H, I and J of the top right image are likely to be artifacts, because the pre-insertion junction was amplified for H and I. The pre-insertion junction for the siamang (HSY) was the last lane of the bottom image. The preinsertion site PCR product from the pigtail macaque was sequenced ("Cloned Seq") and compared to 500 bp sequences flanking each insertion junction (marked by a vertical pink bar) from the human genome, for TSD identification (CCATCA, underlined).

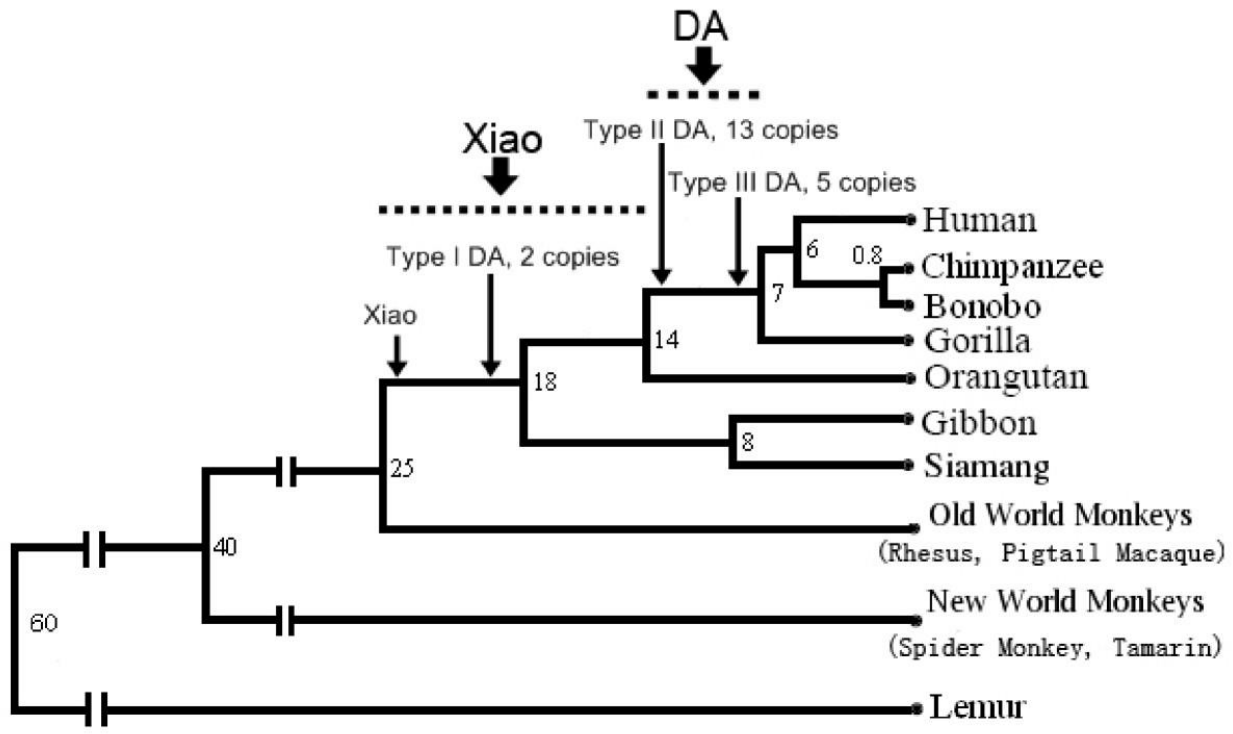

Figure 4.4 Age of the DA and Xiao elements. Thin arrows indicate that Xiao and type I DA first emerged 25-18 Myr ago, whereas Type II/III DA emerged 14-7 Myr ago. Thick arrows indicate that the amplification peak of Xiao and DA occurred during 25-14 and 14-7 Myr ago, respectively. There are a total of 45 copies of Xiao, 2 copies of type I DA, 13 copies of type II DA, and 5 copies of Type III DA. The evolutionary tree of the primates is presented the same way as in Fig. 4.1.

Table 4.s1: Primer sequences used in the study

DA/Xiao genomic location (Mb)	Forward	Reverse
H2-159L*	GAGTTCACGCCAACCTGAGT	AGGTCATCAACCTCGTGGAG
H2-159R*	TGGATGAGATTGCAGGTCTG	GTGAACAGGCTACGTGACCA
H2- 71L	TGCCCACGGATGTAGTGTAA	CAGCATGATTTCGAGAGCAG
H2-71R	CCAGCCACCACTTAGCATTT	ACTGAGATCCCGGACATGAG
H3-8R	GCGACTCTGGCTAATGAGGA	CCAGGATATCTAGCGGGATG
H3-15R	CCAGCTTTCAAGGACAGGAC	ACCACAACGAAACCTCCATC
H3-15L	TGTGCTAGTTGGAGGCCTTT	GACCCAAGCTCGACACTCTC
H3-131L	CCTGCAGTTGGGATGAATTT	CCCAGATGTCTCCAGATGCT
H3-131R	AAAGGTGCGAGTCATCAGGT	ATACCAGGGCATCCTTCCTC
H3-75L	CTCAATGCTGCGATTCTGAA	GGAGTATCACTGCCCTGGAA
H3-75R	GTGTTGAAGTCCGGAACAGC	GAACTCAAGCAGAATGGGAATT
H3-127R	CCCTAAAGCCCTGAGGAATC	TAATGAGAACCGCACATTGC
H3-127L	CGCAGGGTGAATACTCCTGT	GCGAGAAGCGGAAGATGTTA
H4-4L	CACAAAGAGGCGATGACAAA	TCCTCAACGATGTGATGGAA
H4-4R	TGACGCGGATCTCTACACAC	GGGTGTGAGTGGGACTGAGT
H4-9L	TGGAAGAGAAGAACGGTGCT	AAACACCACGTCGGATCAAT
H4-9R	TCAGTCTGCGTGGAACACTC	TCAAGCGTTTGGAGTCCTCT
H7-97L	TCCCGTAGCATCTTGCCTAT	TGCAAAGAACATCAGGCAAG
H7-6L	TAACAGGCCATGTGGAAACC	AGTATCACCGCCCTGGAATAT
H7-7R	TGCCATCTTCATCATTGCAT	CCCTGAGCCTGAGACTGAAG
H8-12DAL	GGGTCAAGCGCTGTTTAAGA	AGCATCTGCTGCAAACTGAA
H8-12DA-LastRightJunction	AATTTCATCGTGGGAGAGGA	TACACCCTCCGTGACATGAA
H8-11X-LJ	CTGATGACCAGGCACTGCTA	CAAGGTGGCAGTTAGGCATT
H8-11X-RJ	CGTAATGGCATCGTCTACCC	ATCTGCTGTTACGCCCATTC
H8-7-DR1	CCGTGTGACGTGGTTCTTAA	TTTGGATTGCCAACAAGTCA
H9-92aL	CCAGGCTGACCTGAAGAGAT	TTTCCGGTACACGCCATACT
H9-92aR	TGGATGAGATTGCAGGTCTG	AAATCACGAACCCAATCTCG
H9-92bR	ATTGCAACATGGGAGAGGAG	CATGGTGGTTTACCATTGCA

H9-92bL	AAAGCCCTTGTCTGCATTTG	TGTACATGCATTGCGACCTT
H10-15L	CTTAGGATTGCAGCCTCAGG	TGGAAGGACCCAGTTACCAG
H10-15R	GAGTCTCGCATTCGTTAGCC	CTTGTGCCTGTTGACATGCT
H11-71L	TGTGAGGTGGGTCCTAAAGG	GCAAGAGGTGCTGGCTCTTA
H11-71R1	CTGCGACCTTTGCTGTCATA	AGCTGCATTAGCCCTAACGA
H11-71R2	TTCCCCTGCACATTAGGAAG	CCCACTAGGAGGGTTGGAAT
H11-67L	CTCTAAGCAACACCCATGCA	TGGGACGCTACCTAATGGAC
H11-67R	TAAGCCACGAGGAGGTAAGC	ATGGGATAGCACCCACAGAG
H12-8L	TGGGCAAACATGTGAGTTGT	GGTGGTCTTTCGCTGTTGTT
H12-8R	AGGGATTGCGTGAAACAAAC	GACCCTATGGCAGAGAGCTG
H12-50L	ACATGGTGCTAGGTCCCAAG	ATATTGCAGGCTGTGTGCAG
H12-50R	TCAGGAGTATCATCCCGCTAA	ATGTGTGAACACCTCCTGTGA
H12-50R2	TCATGAAAGGCTTGCTGTTG	ACCATTGATCTCCCGAAGTG
H13-40L	ACAGCAGCCAACCAATCTCT	TTCCTGCAAGGTGGATAGCT
H13-40R	AGAGCACCGAATCCTAAGCA	CAGTGTCCACGGAGTAACGA
H13-67L	CCTCATCTAGCCGCCATTAC	GATACATGGACCGGGACAAC
H13-67R	CCTGCGATGCTGGAATTATT	TTCAAGTCTGCATGCCTTTG
H13-67R2	CCACATGCCAGTTAGGTCCT	ACGACTATGGTGGGACCAAG
H14-51L	TGAAGATCCATATCGCATGG	TTGTTCCCATAACCCTGGAG
H14-51R	GAGAGCCACAGGTAGCGAAG	ACATACCTCCTGCGATACGG
H21-32L	GGCGTCAGTCGCTGTTTATT	GAAATGTATACCCGCGCTGT
H21-32R	AGTATCACCGCCCTGGAATA	TTCCGGCGAGATAGACATTT

INTERNAL PRIMERS

H3-126XI (Xiao internal junction)	GCGACTCTGGCTAATGAGGA	CCTGCTATCGTGGGTGAGAC
H11-67-16-21 junction (Type I DA)	CCCACATGGACACAACTCAG	CACCCATGATAGCAGGGAAT
H3-127-16-16 Junction (Type I DA)	TTTGTGGCTTGAGACAGCAC	AGGGAGTGGGTCTCTTAGGG
H4-9-16-21 junction (Type I DA)	AGAGAAGGCAGCTGAGGATG	GTCTGCAGTTTGGGATTGGT
H11-67-21-21 junction (Type I DA)	CTGAGCCTGGGCATGTTTAT	CCATGCAGGAAAGATGGTTT

H12-8-HERVH/ER (Type II DA)	TCTGATGGCCACCCTACTTC	TGCCAATATCTCATCCCACA
H8-12-16-8 junction (Type III DA)	TCCACTGCTGACAGACGTTC	TGGTTAAGGCACCAATGACA

*H represents human; H2 represents human chromosome 2; H2-159L and H2-159R represent the left and right junction of the 159Mb Xiao on chromosome 2 respectively.

UCSC In-Silico PCR analyses: as shown below, the in-silico PCR analysis with the 16p-1/21q primers amplified multiple-sized products (578bp, 806bp, 810bp, and 1120bp) from the human genomic sequences. This is consistent with the experimental PCR analysis results shown in Fig. 4.2. However, for the chimp genome, only a single-sized product of ~810bp was obtained, which is likely due to the sequence divergence between the chimp and human genomes as well as the more stringent PCR condition in the in-silico analyses compared to the actual experiments.

16p-1/21q primers with the human genome:

>chr4:9321391+9322200 810bp AGAGAAGGCAGCTGAGGATG GTCTGCAGTTTGGGATTGGT
AGAGAAGGCAGCTGAGGATGggaggcctaccgggccctgaacagagagtg
tgtgctgcccagcttcatgaagagccagtgctgcaggtccagaggtgcct
ctttaaagaaagatgccggtttgtcgtagacggtcacagccctgcaatga
aatcatggcggggctattgggggtgctgaagaaaggcctcaggaatagag
gactcagaggctccaggaaaagaaggacgcttggggaatccaagtctcag
acgatgacaagaaaaagccttgcaattacttgggaatgcacagagagatg
tcctaggaccaaaactgcctggacccccctggctggctgggaaggaaactc
tgccccctcctctcccagcttccccaaattttcccataatgttgccaagc
attagtccagcgtgaaggctactttcttctcaaaccactcatttgggtcc
cgcgcccaatgtcacccatcctcagcaaaacaacctttatttccttcttc
ctgctttccagaaagttcccctaaagccctgagaaatcaccgaatgaaag
aggctttttacaaacaggaaacttaagtggagtgccaatacacaacatga
attgcaccaggctgggtctaagataaaaccagactgtggacaacaggaca
gataagacccccccacatggctctgcactgcctgggtctgttattatgtgg
aggaatgtcagtctgttgctcctgtgggtggagctgaagcatgaaccagg
agtcttcatccttagaaagcagttagacagacacctgagaACCAATCCCA
AACTGCAGAC

>chr8:8136192+8136769 578bp AGAGAAGGCAGCTGAGGATG
GTCTGCAGTTTGGGATTGGT
AGAGAAGGCAGCTGAGGATGggaggcctaccaggccctgaacagagagtg
cgtgctgcccaccttcatgaggagccggtgctgcaggtccagaggtgcct
ctttaaagaaagatgccagcttgtcgtagacggtcacagccctgcaatga
aatcatggcaggactattgcattagtccagcgtggaggctactttctgct
caaaccactcatttgggtcccgtgcccaacgtcacccatcctcagcaaaa
ccaccattatttccttctgcctggtttccagaaagttcccctaaagccct
gaggaatcaccgaatgaaaggggctttttacaaacaggaaacttaagtgg
agtgccaatacacaacatggattgcagcaggctcggtctaagataaaacc
agacggtggacaacaggccaggtaagacccacatggtctgcactccctgg
ttctgttattgtgtggaggaatgtcttagtctgttgctcctgtgggtgta
gctaaagcacaaaccaggagtcctcatccttagaaagcagttagacagac
atctgagaACCAATCCCAAACTGCAGcC
>chr11:67308341-67309460 1120bp AGAGAAGGCAGCTGAGGATG
GTCTGCAGTTTGGGATTGGT
AGAGAAGGCAGCTGAGGATGggaggcctaccgggccctgaacggagagtg
cgtgccgcccagcttcatgaagagccggtgctgcaggtccagaggtgtct
ctttaaagaaagatgccggcttgtcatagatggtcacagccctgcaatga
aatcatggcaggactattgggagggctgaagaaaggcctcaggaatagag
gactcagaggctccaggaaaagaaggacgcttggggaatccaagtctcag
acgatgacaagaagaagccttgcaatcacttgggaatgcacagagagaca
tcctaggaccaaaactgcctggacccccctggctggctgggaaagaaactc
tgccccctcctctccaggcttccccaaattttcccataatgttgccaagc
attagtccagtgtggaggctactttctgctcaaaccactcatttgggtcc
tgcacccaatgtcacccatcctcagtaaaacaacctttatttccttcttc
ctggtttccagaaagttcccctaaagccctgaggaatcaccgaataaaag
gggctttttacaaacaggaaacttaagtggagtgcctatatgcatcatcg
attgcaccaggctaggtctaagataaaaccagactgtggacaaaaggaca
gataagacccacatggctctgcactgcctgggtctgttattgtgtggagg
aatgtcttagtctgttgctcctgtggatgttgctaaagcacgaaccagga
gttttcatccttttttttttttttttttttgagacggagtcccactctg
tcgcccaggctggagtgcagtggagcgatctcggctcactgcaagccccg
cctctcgggttcataccattctccttcctcagcctctggagtagctggga
ctacaggcgcccaccaccatgccagctaatttttgtatttttagtagag
acgaggtttcaccgtgttaacaaggatggtctcgatctcctgacctcgtg
atccgcccgtcttggcctcccaaagtgctgggattataagagtaagccac
cgcgcccggcagtcttcatccttagaaagcagttagacagacacctgaga
ACCAATCCCAAACTGCAGcC
>chr11:3378898-3379703 806bp AGAGAAGGCAGCTGAGGATG
GTCTGCAGTTTGGGATTGGT
AGAGAAGGCAGCTGAGGATGggaggcctaccaggccctgaacggagagtg
cgtgccgcccagcttcatgaagagttggtgctgcaggtccagaggtctct
tgaaagaaagatgctggcttgtcatagacggtcacagccctgcaatgaaa
tcatggcagggctattgggagggctgaagaaaggcctcaggaatagagga
ctcagaggctccaggaaaagaaggatgcttggggaatccaagtctcagac

gatgacaagaagaagccttgcaattacttgggaatgcacagagagatgtt
ctaggaccaaaattgcctggacccccctggctggctgggaaagaaactctg
ccccctcctctcccagcttccccaaattttcccataatgttgccaagcat
tagtccagcgtggaggctacttttttgctcaaaccactcatttgggtccca
cgcccaatgtaacccatcctcagcaaaacaacctttatttccttcttcca
cgtttccagaaagttcccctaaagccctaggaatcaccaaatgaaagggg
ctttttacaaacaggaaacttaagtggagtgccaatacacaacatgaatt
gcaccaggctgggtctaagataaaaccagactgtggacagcaagacagat
aagacccacatggctctgcactgcctgggtctgttatggtgtggaggaat
gtcttagtctgttgctcctgtgggtgtagctaaagcacgaaccaggagtc
ttcatccttagaaagcagttagacagacacctgagaACCAATCCCAAACT
GCAGcC

16-1/21 primers with the chimp genome:

>chr4:9439299+9440108 810bp AGAGAAGGCAGCTGAGGATG
GTCTGCAGTTTGGGATTGGT
AGAGAAGGCAGCTGAGGATGggaggcctaccaggccctgaacagagagtg
tgtgctgcccagcttcatgaagagccagtgctgcaggtccagaggtgcct
ctttaaagaaagatgccggcttgtcgtagatggtcacagccctgcaatga
aatcatggcggggctattgggggtgctgaagaaaggcctcaggaatagag
gactcagaggctccaggaaaagaaggacgcttggggaatccaagtctcag
acgatgacaagaaggagccttgcaattacttgggaatgcacagagagatg
tcctaggaccaaaactgcctggacccccctggctggcttggaaggaaactc
tgccccctcctctcccagcttccccaaattttcccataatgttgccaagc
attagtccagcatgaaggctactttcctctcaaaccactcatttgggtcc
cgcgcccagtgtcacccatcctcagcaaaacaacctttatttccttcttc
ctgctttccagaaagttcccctaaagccctgaggaatcaccgaatgaaag
aggctttttacaaacgggaaacttaagtggagtgccaatacacaacatga
attgcatcaggctgggtctaagataaaaccagactgtggacaacaggaca
gataagacccccccacatggctctgcactgcctgggtctgttattatgtgg
aggaatgtcagtctgttgctcctgtgggtggagctgaagcatgaaccagg
agtcttcatccttagaaagcagttagacagacacctgagaACCAATCCCA
AACTGCAGcC
>chr11:3404621-3405427 807bp AGAGAAGGCAGCTGAGGATG
GTCTGCAGTTTGGGATTGGT
AGAGAAGGCAGCTGAGGATGggaggcctaccgggccctgaacggagagtg
cgtgccgcccagcttcatgaagagtcagtgctgcaggtccagaggtgtct
cgaaagaaagatgccggcttgtcatagacggtcacagccctgcaatgaaa
tcatggcagggctattgggagggctgaagaaaggcctcaggaatagagga
ctcagaggctccaggaaaagaaggacgcttggggaatccaagtctcagac
gatgacaagaagaagccttgcaattacttgggaatgcacagagagatgtt
ctaggaccaaaattgccttggacccccctggctggctgggaaagaaactct
gccccctcctctcccagcttccccaaattttcccataatgttgccaagca
ttagtccagcgtggaggctacttttttgctcaaaccactcatttgggtccc

acgcccaatgtaacccatcctcagcaaaacaacctttatttccttcttcc
tggtttccagaaagttcccctaaagccctaggaatcaccgaatgaaaggg
gctttttacaaactggaaacttaagtggagtgccaatacacaacatgaat
tgcaccaggctgggtctaagataaaaccagactgtggacaacaggacaga
gaagacccacatggctctgcactgcctgggtctgttattgtgtggaggaa
tgtcttagtctgttgctcctgtgggtgtagctaaagcacgaaccaggagt
ctttatccttagaaagcagttagacagacatctgagaACCAATCCCAAAC
TGCAGcC

Table 4.s2: In-silico PCR results of internal primers (Table s1) with the human, chimp and orangutan genomes.

Duplicon type	Primer	Human(bp)[1]	Chimp(bp)[1]	Orangutan(bp)[1]
Xiao	H3-126XI	498	494	***
	Left insertion junction H11-67-16-21	1177 1187 1189 1190 1191 1192 1193 1196	1189 1190 1191 1193 1194 1195 1196 1197 1199 1202 1203 1212 2568	1190 1194 1197
Type I DA	H3-127-16-16	1877	****	***
	H4-9-16-21	578 806 810 1120	807 810	1121 1125 2080
	Right insertion junction H11-67-21-21	1163 1197	1156 1213	***
Type II DA	H12-8-HERVH/ER	1404 1405	1373 1388	***
Type III DA	H8-12-16-8	1011	***	***

***: no PCR product obtained

[1]the numbers are the sizes of the amplified products by performing the in-silico PCR analyses with the primers shown in Table s1 on the human, chimp and orangutan genomic sequences, respectively.

Table 4.S3: TSD Identification*

Duplicon	Coordinate	Sequence alignment between cloned sequence and human duplicon junctions	TSD
chr14:51M Xiao	hg17 chr14:51280402-51311173 rheMac2 chr7:114792452-114792474	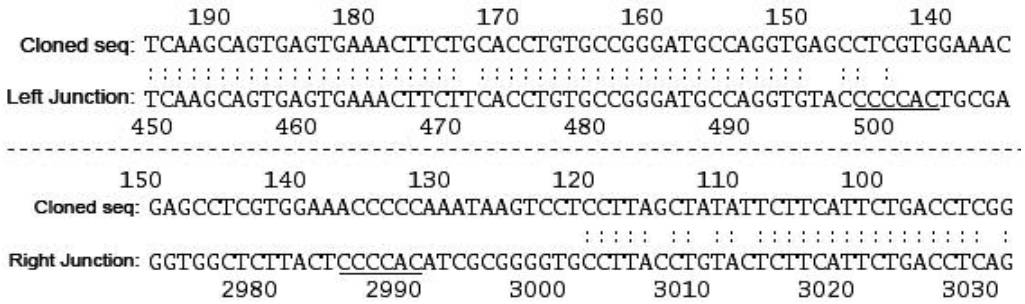	CCCCAC
chr2:71M Xiao	Hg17 chr2:71147690-71196795, Pigtail macaque	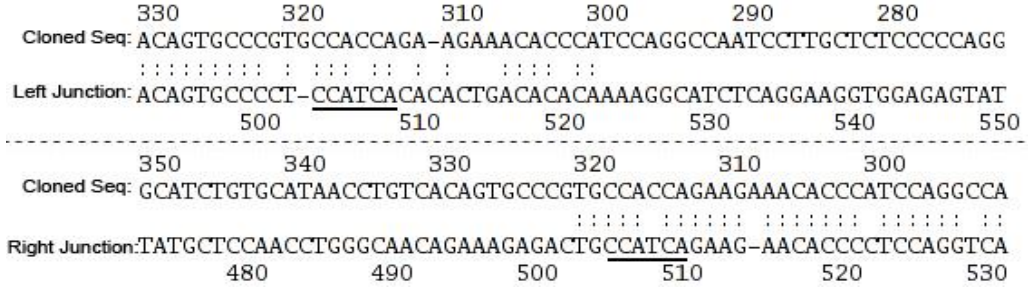	CCATCA
chr13:40M Xiao	Hg17 chr13:40892986-40928830, Rhesus Macaque		AAACTA

*The criteria for TSD determination are:

1. The left TSD was near the end of the alignment between the pre-insertion site sequence (PISS) from the non-human primate and the left insertion junction sequence (LIJS) from the human, whereas the right TSD was near the beginning of the alignment between the PISS and the right insertion junction sequence (RIJS). LIJS and RIJS from the human were obtained as described in the main text under "**TSD identification"** and Fig. 4.3.
2. In the ideal situation, the alignments of the PISS with LIJS and RIJS should overlap over the TSD region and be continuous within the PISS. Thus, the distance between the two alignments within the PISS should be 1bp if taking out the TSD sequence. However, due to changes such as transposon insertions, the distance could be big and we allowed a maximum of 1kb.
3. The right and left TSDs should be exact matches in the human genome; however, sequence mutations were allowed when comparing to the TSD sequence of the non-human primate.
4. TSD should be at least 4bp long.


chr11: 67250000 67300000 67350000 67400000 67450000 67500000
Chimp (Mar. 2006/panTro2) Alignment Net
Level 1
Level 2
Level 3
Level 4
Level 5
Level 6
Duplications of >1000 Bases of Non-RepeatMasked Sequence

Fig. 4.s1: The image of the human chromosome 11-67Mb DA locus (chr11:67,200,190-67,566,710bp) obtained from the UCSC site indicates a ~270kb internal deletion in the chimp homologous region. The top layer shows the sequence coordinate of this human locus in bp. The second layer shows the alignment of this locus with the chimp genomic sequences. The yellowish-green portions at both ends belong to the overall alignment between the human chr11:92549-134448572bp and the chimp chr11:142554-134194740bp. The red bars below indicate that the human chr11:67,252,246-67,507,210bp portion matches to the chimp chr4:9,231,827-9,501,946bp site where a DA copy locates. The third layer shows the alignments of this human DA copy with other DA/Xiao copies found in the human genome.

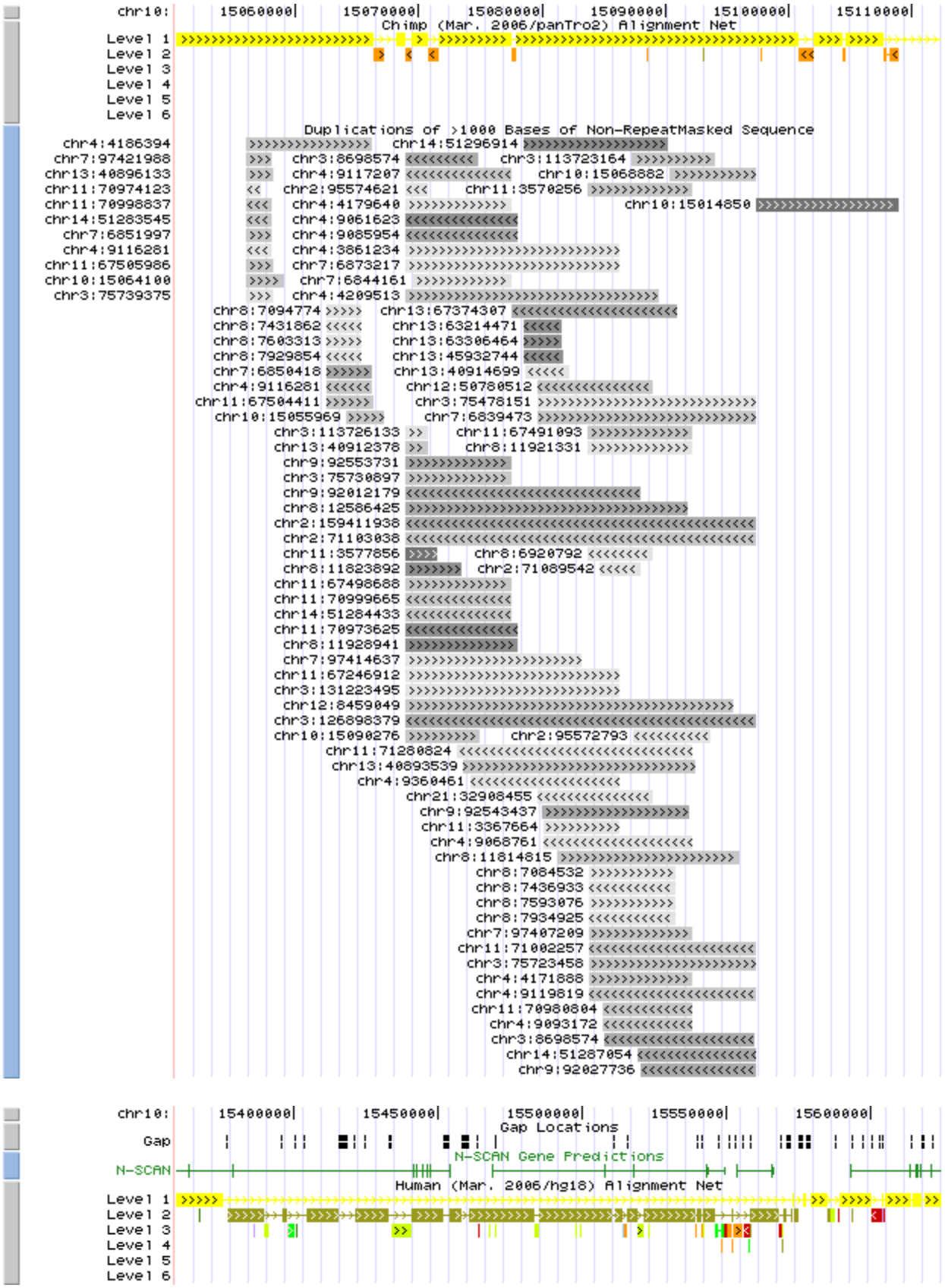
chr10: 15060000 15070000 15080000 15090000 15100000 15110000
Chimp (Mar. 2006/panTro2) Alignment Net
Level 1
Level 2
Level 3
Level 4
Level 5
Level 6
Duplications of >1000 Bases of Non-RepeatMasked Sequence
chr4:4186394 chr14:51296914
chr7:97421988 chr3:8698574 chr3:113723164
chr13:40896133 chr4:9117207 chr10:15068882
chr11:70974123 chr2:95574621 chr11:3570256
chr11:70998837 chr4:4179640 chr10:15014850
chr14:51283545 chr4:9061623
chr7:6851997 chr4:9085954
chr4:9116281 chr4:3861234
chr11:67505986 chr7:6873217
chr10:15064100 chr7:6844161
chr3:75739375 chr4:4209513
chr8:7094774 chr13:67374307
chr8:7431862 chr13:63214471
chr8:7603313 chr13:63306464
chr8:7929854 chr13:45932744
chr7:6850418 chr13:40914699
chr4:9116281 chr12:50780512
chr11:67504411 chr3:75478151
chr10:15055969 chr7:6839473
chr3:113726133 chr11:67491093
chr13:40912378 chr8:11921331
chr9:92553731
chr3:75730897
chr9:92012179
chr8:12586425
chr2:159411938
chr2:71103038
chr11:3577856 chr8:6920792
chr8:11823892 chr2:71089542
chr11:67498688
chr11:70999665
chr14:51284433
chr11:70973625
chr8:11928941
chr7:97414637
chr11:67246912
chr3:131223495
chr12:8459049
chr3:126898379
chr10:15090276 chr2:95572793
chr11:71280824
chr13:40893539
chr4:9360461
chr21:32908455
chr9:92543437
chr11:3367664
chr4:9068761
chr8:11814815
chr8:7084532
chr8:7436933
chr8:7593076
chr8:7934925
chr7:97407209
chr11:71002257
chr3:75723458
chr4:4171888
chr4:9119819
chr11:70980804
chr4:9093172
chr3:8698574
chr14:51287054
chr9:92027736
chr10: 15400000 15450000 15500000 15550000 15600000
Gap Locations
Gap
N-SCAN Gene Predictions
N-SCAN
Human (Mar. 2006/hg18) Alignment Net
Level 1
Level 2
Level 3
Level 4
Level 5
Level 6

Fig. 4.s2: The human chromosome 10-15Mb DA/Xiao locus obtained from the UCSC site is ~45kb (chr10: 15055931-15097361bp). However, the corresponding region in the chimp genome (the following image) is 252 kb (chr10:15,359,507-15,624,298), with the middle portion (chr10:15377512-15572555bp) matching to the human chr3:75478505-75728178bp which belongs to a DA. The images were obtained from the UCSC site and were drawn in the same way as explained in the legend of Fig. 4.s1.

Chapter 5: Discussion and Future Perspectives

The contribution of HS to the Pten-null PCa initiation, progression, and metastasis

This study reported that heparan sulfate is required to promote PCa tumorigenesis, invasion and metastasis. HS is a linear polysaccharide composed of glucuronic acid (GlcA) residues and iduronic acid residues (IdoA) as well as GlcNAc with various sulfation modifications, and is typically 50-200 disaccharides in length [1]. Heparan sulfate proteoglycans (HSPGs) are glycoconjugates composed of a core protein with one or more covalently attached heparan sulfate (HS) chains [2-4]. HSPGs present abundantly on the cell surface (including syndecans and glypicans) and in the ECM (including perlecan, agrin and others) where they interact with numerous growth factors, growth factor binding proteins, extracellular proteases, protease inhibitors, chemokines, morphogens, and adhesive proteins [2-5]. Pattern formation during development is controlled to a great extent by a small number of conserved signal transduction pathways that are activated by extracellular ligands such as FGFs, Hedgehog, Wingless or Decapentaplegic. Genetic experiments have identified HSPGs as important regulators of the tissue distribution of these extracellular signaling molecules [6]. It is frequently the case that pathways involved in embryonic development are reactivated in cancer. Gene expression studies have indicated that programs that regulate prostate development and growth are reactivated in PCa.

Cell surface HSPGs are reported to facilitate the formation and signaling of FGF2-FGF receptor complexes. Exogenous heparin or HS are also capable of forming complexes of FGF with FGF receptors. The HSPGs are considered as a coreceptor, because its function is to aid the formation

of ligand-receptor complexes either through conformational change of ligand and/or receptor or by acting as a template to approximate ligand and receptor [7].

There are four vertebrate FGFR genes: FGFR1-4. FGFRs consist of a single transmembrane region and an extracellular ligand-binding domain containing IgG-like domains. Located between IgG domains is a heparin-binding domain and a cell adhesion homology domain that are required for interactions with cell surface heparan sulfate proteoglycans and components of the extracellular matrix respectively [8, 9]. FGF signal transduction can occur via several pathways including the Ras/MAPK, PI3K/AKT and PLCγ/Ca^{2+} pathways [10].

In prostate, members of the FGF family and FGFRs are partitioned in the epithelium and mesenchyme, mediating directional and reciprocal communications between the two compartments. Ablation of these communications in mature prostates disrupts tissue homeostasis and leads to prostatic intraepithelial neoplasia (PIN) and more severe lesions. During prostatic organogenesis, messenger mRNAs for both FGF7 and FGF10 are localized in the mesenchyme, and the receptors for FGF7 or FGF10 are found in the epithelium of the urogenital sinus in embryos and in the distal signaling center of elongating and branching ducts in postnatal prostates. FGF7 and FGF10 regulate prostate development and prostate tissue homeostasis by signaling through the FGFR2 isoform [11]. Furthermore, changes in the expression of FGF1, FGF2, FGF6, FGF8, FGF9 and FGF17 have been observed to be associated with prostatic lesions [12-14].

In addition to the FGF signaling pathway, many pathways like TGF-β, EGF, IGF, PDGF, and SHH signaling pathways were identified to be the possible molecular events associated with prostate cancer initiation and progression in Pten-null mouse prostate cancer based on our IPA analysis of cDNA microarray data. It is reported that FGF, EGF, IGF, VEGF signaling through

Ras/MAPK pathway to stimulate cell growth and proliferation. It is also suggested that FGF, PDGF, VEGF, EGF, and IGF-1 can signaling through PI3K/AKT pathway to stimulate cell survival and suppress apoptosis [15-18].The TGF-β/Smad signaling pathway also plays an important role in cell proliferation, differentiation, promote survival and inhibit apoptosis [19]. Our studies have demonstrated that Pten homogeneous extinction led to progressively enlarged prostate glands. Gross anatomy of representative anterial prostates at 40 weeks of age shows that although C^{+}; Pten $^{loxP/loxP}$; Ext1 $^{loxP/loxP}$ prostates are larger than wild type, they are still significantly smaller than C^{+}; Pten $^{loxP/loxP}$ prostates (Figure 2.2B-C). Histological analyses show that simultaneously deleting Pten and Ext1 led to retarded prostate cancer tumorigenesis and invasion in contrast to the lesions observed in the C^{+}; Pten $^{loxP/loxP}$ prostates (Figure 2.2A). Conditionally knockout Ext1 in Pten null prostate can reduce proliferation rate and increase apoptosis rate of the prostate epithelial cells (Figure 2.3). These observations consolidate the results from cDNA microarray data IPA analyses (Figure 2.6). Prostate cancer cells are typically active in proliferation, upregulated in survival favored signalings and down-regulated in apoptosis pathways. The significant pathways found by microarray analyses are involved in stimulating cell growth and proliferation, promoting survival and inhibiting apoptosis. Therefore these significant pathways might be the molecular mechanisms associated to Pten-null mouse prostate cancer tumorigenesis, and indicate HS is necessary.

We also showed that conditional knockout Ext1 in Pten null mouse prostate can restore the diminishing expression of E-cadherin, marker of adherents junction formation, on Pten null prostates reveals higher metastatic potentials of C^{+}; Pten $^{loxP/loxP}$ prostates (Figure 2.7). Meanwhile it is observed that locally invasive in C^{+}; Pten $^{loxP/loxP}$; Ext1 $^{loxP/loxP}$ is rare (Figure 2.2A). The average weight of Pten, Ext1 double knockout anterial prostates at the age of 40

weeks is much lighter than C+; Pten $^{loxP/loxP}$ mouse's(Figure 2.2C), the mouse prostatic intraepithelial neoplasia or early stage of carcinoma are confined in the prostate organ, and never metastasis to adjacent organ, for example, seminal vesicle. It is reported that Pten conditional knockout mice age 12–29 weeks had found lymphovascular invasion by the prostatic cancer cells, and distance metastases lesions were also found in the lymph nodes and lung [20]. Considering all the evidence above HS may be also required for prostate cancer invasion and metastasis.

The role of HS in Pten-null prostate cancer stem cell maintenance and differentiation

Stem cells are found in all multicellular organisms. They can divide and differentiate into diverse specialized cell types and can self-renew to produce more stem cells. The generation, maintenance and repair of different tissues during development are regulated by stem cells that reside in defined microenvironments known as stem cell niches [21]. These niches are essential for protecting and perpetuating the undifferentiated, self-renewing state of the stem cells or to regulate differentiation of the stem cells into committed tissue specific progenitor cells. Heparan sulfate is one constituent of every niche and is a master regulator of mitogenic and adhesive molecule behavior with the ability to rapidly change its binding affinities on the cell surface [21]. Many of the signaling molecules involved in stem cell maintenance and differentiation, such as Wnts and FGFs, are regulated by HSPGs [22, 23]. Furthermore, HS structure was changed as the stem cells differentiate into specific lineages [24, 25].

It is reported that ablation of Ext1leads to HS deficiency of embryonic stem cells (ESCs), and Ext1-/- ESCs are incapable of transiting from self-renewal to differentiation on removal of leukemia inhibitory factor, which is caused by a defective response to FGF signaling [26]. These findings were confirmed by studies in Ndst1/2 deficient ESCs, which also cannot differentiate in

response to FGF signaling because of reduced N-sulfation [27]. Moreover, Ndst1/2 deficient ESCs were found to be unable to respond to VEGF signaling, preventing their differentiation into capillary vasculature [28]. Collectively, these evidences demonstrated the importance of HS in stem cell differentiation at least in vitro.

Cancer cells that are capable of self-renewal and differentiation, properties of normal tissue stem cells, have been shown to be the fundamental cause of both human acute myeloid and lymphoid leukemia [29, 30]. These cells have been termed "cancer stem cells" and there is increasing evidences that cells with stem cell characteristics are also the driving force behind tumor formation in many solid tissue cancers including cancers of brain, colon and breast [31, 32]. It has been reported that altered stem/ progenitor cell proliferation is directly associated with prostate tumor initiation and progression in the Pten-null murine model [33].

Recent studies suggest that p63 is required to maintain the commitment of the urogenital sinus endoderm to the prostate cell lineage and that the luminal secretory cells of the prostate originate from $p63^{+}$ basal progenitor cells [34]. Wang et al. reported that the initiation of differentiation in the Pten-null prostatic epithelium start from segregation of $P63^{+}$ basal cell and its $P63^{low}$; $CK5^{+}$ progeny, which usually exhibits an enlarged and elongated profile at an angle to the basement membrane [33]. In our study, we found that $P63^{+}$ basal cells form a discontinuous cell layer scattered along the basement membrane in all three genotypes of mouse prostates we investigated. Scattered $P63^{+}$ cells lie flat on the basement membrane of WT epithelium, while increased $P63^{+}$ cell number were observed in the Pten-null prostate epithelium, which is consistent with previous report [33]. However, there is no significant change in cell numbers and morphologies in Pten-/-; Ext1-/- prostates (Figure 2.7). Most of the BrdU-positive cells in Pten-null prostates were located in the proximal regions closed to basement membrane; BrdU-positive

prostatic epithelial cells in Pten-/-; Ext1-/- prostates are less than that in Pten-null prostates and they are also tend to locate close to basement membrane where we've shown $P63^+$ basal cells are closely located; BrdU-positive cells are rarely found in WT epithelium, indicating WT basal epithelial cells and/or their progenies are not active in proliferation, Pten-/-; Ext1-/- basal cells and/or their progenies are more proliferative than WT; Pten-null basal cells and/or their progenies are the most proliferative and might undergo morphology changes (Figure 2.3). There are also evidences shows that Pten deficiency negatively regulates $p63^+$ prostatic basal cell proliferation without blocking differentiation [33]. We also observed that CK5-positive basal epithelial cells were actively differentiated into CK5, CK8 double positive transient amplifying (TA)/intermediate progenitor cells in Pten-null prostates; WT prostate has no obvious differentiation, which is also consistent with previous studies. However, Pten-/-; Ext1-/- prostates with deficient HS in Pten-null prostate also exhibited repressed differentiation, no $CK5^+$ cells at an angle to the basal layer, and very few cells are CK5, CK8 double positive, implies that HS is required for CK5-positive basal epithelial cells differentiation into CK5, CK8 double positive transient amplifying (TA)/intermediate progenitor cells (Figure 2.5C).

The cell surface HSPGs can mediate FGFs and VEGF interactions with their receptors as a "coreceptor". Because FGF signal transduction can occur via several pathways such as the Ras/MAPK and PI3K/AKT, we tested Phosphorylation of Akt and Erk in the three different genotypes of mouse prostates. The results in Figure 2.4 C d-k demonstrate that Phosphorylation of Akt and Erk are both high in Pten-null but low in Pten-/-; Ext1-/- prostates. Faint phospho-Akt was detected in basal region of WT prostatic epithelium, but not in luminal cells; no phospho-Erk were detected in WT, indicates FGF signaling through PI3K/AKT might be the dominant pathway in WT mouse prostate epithelium stem cells to stimulate survival and self-renewal,

possibly via mTOR and β-Catenin respectively. Ras/MAPK downstream pathway of FGF is majorly responsible for cell growth and protein synthesis, and phospho-Erk is detected in the proximal region of Pten-null prostate, but not detected in both WT and Pten-/-; Ext1-/- prostates further confirmed that Pten-null prostates were more active in proliferation than both WT and Pten-/-; Ext1-/- prostates. Furthermore, these results also indicate HS deficient caused by conditional Knockout of Ext1 in Pten-null prostates inhibits FGF signaling through both Ras/MAPK and PI3K/AKT pathway.

Recent studies suggest that the activation of the SHH pathway may induce a transitory differentiation of prostatic stem/ progenitor cells into $CD44^{+}/P63^{-/+}$ hyperplasia basal cells with an intermediate phenotype (CK8/14), and this early transforming event may culminate in tumorigenesis by giving rise to CD44+ prostate cancer cells expressing PTCH1 and GLI[15]. IPA analysis of our cDNA microarray data and quantitative RT-PCR verification both validated that SHH pathway is upregulated in C^{+}; Pten $^{loxP/loxP}$ mouse prostates compared with C^{+}; Pten $^{loxP/loxP}$; $Ext1^{loxP/loxP}$ prostates (Figure 2.6B-C).

Future perspectives-Angiogenesis in Pten-null prostate cancer

Cancer progression is not only regulated by the interruption of oncogene and tumor suppressor pathways, but also based on the stromal compartment to create a more tumor promoting micro-environment. The stromal cell compartment of the prostate gland contains endothelial cells, which are the components of the capillary vascular. To date, primary xenografts of human prostate tissue SCID mouse model has been using to study angiogenesis induced by reactive stroma and found that androgen-modulated expression of VEGF-A appeared to be a causal regulator of angiogenesis [35]. Because angiogenesis is required for tumor growth and metastatic spread, strategies for inhibiting angiogenesis have been one of the most robust fields of cancer

investigation, focusing on the vascular endothelial growth factor (VEGF) family and its receptors.

Our IPA analyses of cDNA microarray data reveals VEGF as significant signaling pathway that different between Pten-null prostates and Pten-/-; Ext1-/- prostates. VEGF is a signal protein produced by cells that stimulates angiogenesis. Solid cancers cannot grow beyond a limited size without an adequate blood supply; VEGF induces endothelial cell proliferation, promotes cell migration, and inhibits apoptosis [36, 37]. Deregulated VEGF expression contributes to the development of solid tumors by promoting tumor angiogenesis. For instance overexpression of VEGF can cause vascular disease in the retina of the eye and other parts of the body [38]. HSPGs are coreceptor for VEGF. Suarez et al. found that a VEGF-A splice variant defective for heparan sulfate and neuropilin-1 binding shows attenuated signaling through VEGFR-2 [39]. Therefore, Investigation in the role of HS in angiogenesis of prostate cancer is needed. First, we can stain endothelial cell specific markers to visualize the vasculature structure on different genotypes of prostate tissues and to determine if HS deficient reduced the vascular distribution in Pten-null prostate.

To further study the role of HS in Pten-null mouse prostate cancer, cell lines of WT, Pten-null and Pten-/-; Ext1-/- prostate epithelial cells need to be established to test the inhibition of VEGF signaling pathway using chemical inhibitor sunitinib malate, axitinib, etc. in Pten-null cells, and the rescue effect of VEGF signaling pathway by adding heparin in Pten-/-; Ext1-/- prostate epithelial cell line. Now we've already obtained WT and Pten-null prostate epithelial cell lines. We can generate Pten-/-; Ext1-/- prostate epithelial cell line by using Znic Finger Nucleases (ZFNs) technique to knockout Ext1 in Pten-null prostate epithelial cell line.

The study of angiogenesis in Pten-null prostate cancer can shed lights on the molecular mechanism of prostate cancer invasion and metastasis, which are facilitated by angiogenesis, and on the following development of safe and effective pharmacological inhibitor for this process.

Hypoxia effects in Pten-null prostate cancer

It is part of the system that restores the oxygen supply to tissues when blood circulation is inadequate. Therefore, the expression of VEGF is potentiated in response to hypoxia. Tumor cell hypoxia is an innate environmental factor encountered during the development of many types of human tumors, including malignant prostate tumors. Recent studies suggest that androgenic steroids are important regulators of blood flow to prostate tumors and suppressors of tumor cell hypoxia [40]. Besides, prostate cancer cells respond to hypoxic conditions with excessive changes in gene expression mediated by the upregulation of a unique transcription factor, hypoxia inducible factor 1 α (HIF1α). This response increases metabolic resistance to hypoxia, and also enhances the ability of prostate cancer cells to attract a more strong blood supply by upregulating the expression of pro-angiogenic factors.

Ingenuity knowledge-based signaling pathway analysis the C^{+}; Pten $^{loxP/loxP}$ and C^{+}; Pten $^{loxP/loxP}$; Ext1 $^{loxP/loxP}$ prostate transcriptome shows significant difference in several cell growth, proliferation and tumor-related metabolism signaling pathways. The HIF1α is known to be detectable as adaptive metabolic response to hypoxia. However, HIF1α pathway is also activated to eliminate toxic metabolic waste products generated by the tumor-specific metabolism under normoxic conditions. Figure 2.6C shows HIF1α pathway is the most significantly different pathway between Pten null and Pten and Ext1 double knockout prostates, indicates tumor-specific metabolism is more active in the higher grade of mPIN prostates, the Pten null prostates [41].

ΔExt1ΔPten prostate epithelial cell line establishment and characterization

In previous sections the Znic Finger Nucleases (ZFNs) technique has been mentioned in generation of a Pten-/-; Ext1-/- prostate epithelial cell line. ZFNs is a class of engineered DNA binding proteins, facilitate targeted genome editing by binding to a user-specified locus and causing a double-strand break (DSB). The cell then employs endogenous DNA repair processes, either non-homologous end joining (NHEJ) or homology-directed repair (HDR), to heal this targeted DSB. These repair processes can be channeled to generate precisely targeted genomic edits resulting in an organism or cell lines with specific gene disruptions (knockouts), integrations, or modifications. To make a *ΔExt1ΔPten* prostate epithelial cell line, Ext1 will be targeted by ZFNs, a homologous DNA donor containing puromycin resistance gene will be designed and co-transfected with ZFNs. Antibiotic screening and following FACS sorting will be employed to isolate the homogenous knockout of Ext1.

After establishing an viable cell line, it is necessary to determine the tumor related characterizations of the *ΔExt1ΔPten* mouse prostate epithelial cell line, such as cell proliferation, migration, invasion, and colony formation in soft agar, etc. All these experiments will be carried out for WT, Pten-null and *ΔExt1ΔPten* mouse prostate epithelial cell lines. And the results will tell us how aggressive the *ΔExt1ΔPten* mouse prostate epithelial cells are.

Determine possible molecular mechanism for HS to facilitate prostate cancer initiation and progression in mouse prostate epithelial cell lines

Based on our IPA analysis of cDNA microarray data, many pathways like FGF, TGF-β, EGF, VEGF, IGF-1, PDGF, and SHH signaling pathways were identified to be the possible molecular events associated with prostate cancer initiation and progression, stimulation of cell survival and suppression of apoptosis in Pten-null mouse prostate cancer. However, there are few methods for

studying molecular signaling can be applied to tissue sections. The establishment of *ΔExt1ΔPten* mouse prostate epithelial cell line and maintaining the WT and Pten-null cell lines can enrich our experimental methods for signaling studies. For instance, using signaling molecules, like FGFs, to activate signaling pathways and using chemical inhibitor to block the signaling pathways will greatly improve our understanding of certain pathways in prostate cancer initiation and progression.

Re-administrate heparan sulfate to rescue the HS deficiency prostate cancer stem cells in basal layer of epithelium to differentiate into transit amplifying/intermediate cells (TA/IC)

Previous study showed that the LSC^{high} subpopulation or its derived sphere cells isolated from Pten-null primary cancers could reconstitute adenocarcinoma when subject to the prostate regeneration assay [42]. Therefore, I propose that the LSC^{high} subpopulation of ΔExt1ΔPten mouse prostate epithelial cell line is incapable of reconstitute adenocarcinoma when subject to the prostate regeneration assay; but re-administration of heparan sulfate will generate a prostatic sphere with adenocarcinoma. This experiment will further confirm role of HS in regulation of prostate cancer stem cell differentiation and maintaining the tumorigenic properties.

HS structure analysis

We've demonstrated that HS is required for prostate cancer tumorigenesis in Pten-null mouse. Recent evidence shows that SULF2 acts on heparan sulfate proteoglycans (HSPGs) in the tumor microenvironment to release ligands critical for oncogenic signaling [43]. Ferguson et al. demonstrated that Heparan sulfate 2-O-sulfotransferase (2OST), which transfers sulfate to the 2 position of the iduronic acid residue of heparan sulfate, is essential for maximal proliferation and invasion of prostate cancer cells in the LNCaP-C4-2B model [44]. These findings suggest that modifications of sulfation status of HS in tumor microenvironments are important for HS to

regulating the tumorigenic properties of Pten-null prostate cancer cells. Carbazole assay and disaccharide analysis will be performed to determine distinct structure of HS produced by prostate epithelial cells.

Altogether, this study has made valuable contributions to the understanding of HS in Pten-null prostate cancer tumorigenesis and progression in mice. We also observed that HS is dispensable for prostate development and function (figure 2.9), and will likely lead to valuable applications of HS in development of new target for anti-prostate cancer drugs.

Reference

1. Sugahara, K. and H. Kitagawa, *Heparin and Heparan Sulfate Biosynthesis.* IUBMB Life, 2002. **54**(4): p. 163-175.
2. Bernfield, M., et al., *FUNCTIONS OF CELL SURFACE HEPARAN SULFATE PROTEOGLYCANS.* Annual Review of Biochemistry, 1999. **68**(1): p. 729-777.
3. Esko, J.D. and S.B. Selleck, *Order out of chaos: assembly of ligand binding sites in heparan sulfate.* Annu Rev Biochem, 2002. **71**: p. 435-71.
4. Bishop, J.R., M. Schuksz, and J.D. Esko, *Heparan sulphate proteoglycans fine-tune mammalian physiology.* Nature, 2007. **446**(7139): p. 1030-7.
5. Forsberg, E. and L. Kjellen, *Heparan sulfate: lessons from knockout mice.* J Clin Invest, 2001. **108**(2): p. 175-80.
6. Häcker, U., K. Nybakken, and N. Perrimon, *Heparan sulphate proteoglycans: the sweet side of development.* Nature Reviews. Molecular Cell Biology, 2005. **6**(7): p. 530-541.
7. Sarrazin, S., W.C. Lamanna, and J.D. Esko, *Heparan Sulfate Proteoglycans.* Cold Spring Harbor Perspectives in Biology, 2011. **3**(7).
8. Ornitz, D.M., *FGFs, heparan sulfate and FGFRs: complex interactions essential for development.* BioEssays, 2000. **22**(2): p. 108-112.
9. Pellegrini, L., *Role of heparan sulfate in fibroblast growth factor signalling: a structural view.* Current Opinion in Structural Biology, 2001. **11**(5): p. 629-634.
10. Böttcher, R.T. and C. Niehrs, *Fibroblast Growth Factor Signaling during Early Vertebrate Development.* Endocrine Reviews, 2005. **26**(1): p. 63-77.
11. Lin, Y., et al., *Fibroblast growth factor receptor 2 tyrosine kinase is required for prostatic morphogenesis and the acquisition of strict androgen dependency for adult tissue homeostasis.* Development, 2007. **134**(4): p. 723-734.
12. Giri, D., F. Ropiquet, and M. Ittmann, *Alterations in Expression of Basic Fibroblast Growth Factor (FGF) 2 and Its Receptor FGFR-1 in Human Prostate Cancer.* Clinical Cancer Research, 1999. **5**(5): p. 1063-1071.

13. Giri, D., F. Ropiquet, and M. Ittmann, *FGF9 is an autocrine and paracrine prostatic growth factor expressed by prostatic stromal cells.* Journal of Cellular Physiology, 1999. **180**(1): p. 53-60.
14. Ropiquet, F., et al., *Increased Expression of Fibroblast Growth Factor 6 in Human Prostatic Intraepithelial Neoplasia and Prostate Cancer.* Cancer Research, 2000. **60**(15): p. 4245-4250.
15. Chen, B.-Y., et al., *Hedgehog is involved in prostate basal cell hyperplasia formation and its progressing towards tumorigenesis.* Biochemical and Biophysical Research Communications, 2007. **357**(4): p. 1084-1089.
16. Mimeault, M. and S.K. Batra, *Frequent Gene Products and Molecular Pathways Altered in Prostate Cancer– and Metastasis-Initiating Cells and Their Progenies and Novel Promising Multitargeted Therapies.* Mol Med., 2011. **17**(9-10): p. 949–964.
17. Putz, T., et al., *Epidermal Growth Factor (EGF) Receptor Blockade Inhibits the Action of EGF, Insulin-like Growth Factor I, and a Protein Kinase A Activator on the Mitogen-activated Protein Kinase Pathway in Prostate Cancer Cell Lines.* Cancer Research, 1999. **59**(1): p. 227-233.
18. Conley-LaComb, M.K., et al., *PTEN Regulates PDGF Ligand Switch for β-PDGFR Signaling in Prostate Cancer.* The American Journal of Pathology, 2012. **180**(3): p. 1017-1027.
19. Hany Kayed, J.K., Shereen Keleg, Xiaohua Jiang, Roland Penzel, Thomas Giese, Hanswalter Zentgraf, Markus W. Büchler, Murray Korc, Helmut Friess, *Correlation of glypican-1 expression with TGF-β, BMP, and activin receptors in pancreatic ductal adenocarcinoma.* International Journal of Oncology, 2006. **29**(5): p. 1139-1148.
20. Wang, S., et al., *Prostate-specific deletion of the murine Pten tumor suppressor gene leads to metastatic prostate cancer.* Cancer Cell, 2003. **4**(3): p. 209-221.
21. Nurcombe, V. and S.M. Cool, *Heparan sulfate control of proliferation and differentiation in the stem cell niche.* Critical reviews in eukaryotic gene expression, 2007. **17**(2): p. 159-171.
22. Noboru, S., et al., *Maintenance of pluripotency in human and mouse embryonic stem cells through activation of Wnt signaling by a pharmacological GSK-3-specific inhibitor,* 2003, Nature Publishing Group.
23. Xu, C., et al., *Basic Fibroblast Growth Factor Supports Undifferentiated Human Embryonic Stem Cell Growth Without Conditioned Medium.* STEM CELLS, 2005. **23**(3): p. 315-323.
24. Baldwin, R.J., et al., *A Developmentally Regulated Heparan Sulfate Epitope Defines a Subpopulation with Increased Blood Potential During Mesodermal Differentiation.* STEM CELLS, 2008. **26**(12): p. 3108-3118.
25. Johnson, C.E., et al., *Essential Alterations of Heparan Sulfate During the Differentiation of Embryonic Stem Cells to Sox1-Enhanced Green Fluorescent Protein-Expressing Neural Progenitor Cells.* STEM CELLS, 2007. **25**(8): p. 1913-1923.
26. Kraushaar, D.C., Y. Yamaguchi, and L. Wang, *Heparan Sulfate Is Required for Embryonic Stem Cells to Exit from Self-renewal.* Journal of Biological Chemistry, 2010. **285**(8): p. 5907-5916.
27. Lanner, F., et al., *Heparan Sulfation–Dependent Fibroblast Growth Factor Signaling Maintains Embryonic Stem Cells Primed for Differentiation in a Heterogeneous State.* STEM CELLS, 2010. **28**(2): p. 191-200.

28. Jakobsson, L., et al., *Heparan Sulfate in trans Potentiates VEGFR-Mediated Angiogenesis.* Developmental Cell, 2006. **10**(5): p. 625-634.
29. Bonnet, D. and J.E. Dick, *Human acute myeloid leukemia is organized as a hierarchy that originates from a primitive hematopoietic cell.* Nat Med, 1997. **3**(7): p. 730-737.
30. George, A.A., et al., *Detection of leukemic cells in the CD34+CD38− bone marrow progenitor population in children with acute lymphoblastic leukemia.* Blood, 2001. **97**(12): p. 3925-3930.
31. Al-Hajj, M., et al., *Prospective identification of tumorigenic breast cancer cells.* Proceedings of the National Academy of Sciences, 2003. **100**(7): p. 3983-3988.
32. Singh, S.K., et al., *Identification of a Cancer Stem Cell in Human Brain Tumors.* Cancer Research, 2003. **63**(18): p. 5821-5828.
33. Wang, S., et al., *Pten deletion leads to the expansion of a prostatic stem/progenitor cell subpopulation and tumor initiation.* Proceedings of the National Academy of Sciences of the United States of America, 2006. **103**(5): p. 1480-1485.
34. Signoretti, S., et al., *p63 regulates commitment to the prostate cell lineage.* Proceedings of the National Academy of Sciences of the United States of America, 2005. **102**(32): p. 11355-11360.
35. Montecinos, V.P., et al., *Primary Xenografts of Human Prostate Tissue as a Model to Study Angiogenesis Induced by Reactive Stroma.* PLoS ONE, 2012. **7**(1): p. e29623.
36. Ebos, J.M.L., et al., *Accelerated Metastasis after Short-Term Treatment with a Potent Inhibitor of Tumor Angiogenesis.* Cancer cell, 2009. **15**(3): p. 232-239.
37. Pàez-Ribes, M., et al., *Antiangiogenic Therapy Elicits Malignant Progression of Tumors to Increased Local Invasion and Distant Metastasis.* Cancer cell, 2009. **15**(3): p. 220-231.
38. Adamis, A.P., et al., *Inhibition of vascular endothelial growth factor prevents retinal ischemia-associated iris neovascularization in a nonhuman primate.* Archives of ophthalmology, 1996. **114**(1): p. 66-71.
39. Cébe Suarez, S., et al., *A VEGF-A splice variant defective for heparan sulfate and neuropilin-1 binding shows attenuated signaling through VEGFR-2.* Cellular and Molecular Life Sciences CMLS, 2006. **63**(17): p. 2067-2077.
40. Shabisgh, A., et al., *Early Effects of Castration on the Vascular System of the Rat Ventral Prostate Gland.* Endocrinology, 1999. **140**(4): p. 1920-1926.
41. Matthias Kappler, H.T., Johannes Schubert, Dirk Vordermark and Alexander W. Eckert *The real face of HIF1α in the tumor process.* Cell Cycle, 2012. **11**(21): p. 1-5.
42. Mulholland, D.J., et al., *Lin−Sca-1+CD49fhigh Stem/Progenitors Are Tumor-Initiating Cells in the Pten-Null Prostate Cancer Model.* Cancer Research, 2009. **69**(22): p. 8555-8562.
43. Phillips, J.J., et al., *Heparan sulfate sulfatase SULF2 regulates PDGFRα signaling and growth in human and mouse malignant glioma.* The Journal of Clinical Investigation, 2012. **122**(3): p. 911-922.
44. *Role of Heparan Sulfate 2-O-Sulfotransferase in Prostate Cancer Cell Proliferation, Invasion, and Growth Factor Signaling.* Prostate Cancer, 2011. **2011**.